Dissertation

submitted to the
Combined Faculty of Natural Sciences and Mathematics
of the Ruperto Carola University Heidelberg, Germany
for the degree of
Doctor of Natural Sciences

Presented by
Santosh Kumar Lomada, M.Sc Biochemistry
born in: Kadiri, India
Oral examination: 16th November 2021

Investigations on inhibitors of nucleoside diphosphate kinases as putative novel therapeutics for the treatment of heart failure

Referees: Prof. Dr. Thomas Wieland

Prof. Dr. Marc Freichel

Acknowledgement

I am delighted to grab this excellent opportunity to thank my saviors who have given their time, support and energy.

I honestly express my deep sense of thanks and gratitude to my supervisor, Prof. Thomas Wieland, for bringing the weight of his considerable experience and knowledge to this project. I sincerely thank him for providing support, innovative ideas, motivation, and for his patience. His high standards have made me better at what I do. Indeed, I am incredibly grateful to him for the opportunity he has given me to be a part of his research family.

There is an extensive list of people whom I would like to thank. I am always grateful to all of them for their kind help.

I owe my profound gratitude to Dr. Christiane Vettel for her immense support during the whole project. She invested her time and never hesitated in guiding me. I am very thankful for her being very patient with me.

I want to extend my sincere gratitude to Prof. Dr. Marc Freichel, Dr. Aimo Kannt for their support and encouragement during the project's progress.

I am very thankful to all the collaborators who supported this project: Prof. Paul Attwood; Dr. Kathryn Perez, Dr. Wieland Steinchen, Prof. Gert Bange, Dr. Marcel Bermudez, Prof. Dr. Gerhard Wolber, Dr. Aimo Kannt, Dr. Hagen Gegner, Dr. Karin Hammer, Dr. Felix Trogisch**,** Prof. Klaus Scheffzek, who provided material, knowledge and technical support to this project. Without their cooperation, this project wouldn't have come this far.

My heartfelt thanks to Dr. Yuxi Feng for the great support during my project work. I thank our technicians Heinz, Tina, Sabine, and Heike for their support for the smooth running of the lab. I thank Irene for her generous support, who I could always reach out for help. My special and heartfelt thanks to Doris for her helping hands in the lab and Geman bureaucratic works. I want to thank all my fellow labmates, Pan, Rachana, Anu, Joost, Yohanes, Hong Peng, Nan, Atif, Magdolna, and Sepp, who became a wonderful part of my project journey. I am so glad to have you as my workmates.

I honestly thank my previous supervisor Prof. Rohini Kuner, who gave me a significant opportunity to be a part of her lab. Her trust and kind support motivated me to step into new prospects. I extend my thankfulness to my mentor Dr. Subhadeep Chatterjee for his encouragement, patience. I realized my strengths during my project work in his lab. I also thank Dr. Nagender for his gracious support in inspiring me to pursue a career in research.

This acknowledgement would be incomplete without mentioning the support and involvement of Jagdeesh, who backed me to come here from India. I sincerely thank him and his wife Deepthi for their outstanding help. I am very thankful to Dr. Kiran Bali for his advice in reviewing my thesis. I would also like to mention my gratefulness to all my friends, Shanmukha, Gowrinadh, Venkat, Venu, Mahesh, Priyanka, Jidnyasa, Revathi; without them, my PhD life wouldn't have been fun.

I am indebted to my parents, Rameswara Rao and Prameela, for their support in every aspect of my life. I thank my sister Sireesha for her encouragement and for shaping me into what I am now. Last but not least, I thank my wife, Lavanya, for her patience in dealing with me. Her cooperation during my journey is unforgettable.

Table of contents

Summary

Impaired cAMP signaling and dysfunctional calcium handling in cardiomyocytes are both characteristics associated with heart failure. So far, therapeutic attempts to improve contractile function by globally increasing cAMP levels failed clinically due to higher arrhythmia susceptibility and increased risk of sudden cardiac death. Novel strategies aiming to modulate distinct cAMP pools in cardiomyocytes may improve contraction force without detrimental effects. Nucleoside diphosphate kinase (NDPK), an enzyme with transphosphorylase activity, contributes to heterotrimeric G protein activation by GTP formation from ATP and GDP. Moreover, oligomers consisting of the isoforms NDPK B and C form a complex with heterotrimeric G proteins and act as protein histidine kinase on the Gβ subunit leading to direct activation of the G protein. NDPK C is upregulated in end-stage human heart failure, where it promotes the complex formation of NDPKs with G_i proteins and enhances their activity. This likely contributes to the suppression of cAMP formation. Therefore, this project aims to identify compounds that inhibit NDPK B and C and investigate the consequences of NDPK inhibition in heart muscle.

To screen for potential inhibitors of NDPK activity, recombinantly expressed human NDPK A, B, and C were purified. An ATP-dependent, firefly luciferase-based luminescence assay was used to quantify the amount of ATP formed from GTP+ADP, monitoring the NDPK transphosphorylase activity. Out of the tested library, one small molecule compound (SanWie3) preferentially reduced the activity of NDPK C > NDPK B >> NDPK A. Further in vitro studies revealed that SanWie3 is an allosteric inhibitor of the transphosphorylase activity of NDPK C (IC_{50} ~ 3 µM). Biophysical protein analyses confirmed that binding of SanWie3 mediates small structural changes in the NDPK C protein. Preliminary studies on the binding of SanWie3, using HDX-mass spectrometry and *in silico* protein modeling, identified a putative binding pocket near the catalytically active site. The potential off-target binding of SanWie3 on other enzymes, channels, and receptors was studied using *in vitro* screens, which did not suggest any additional SanWie3 targets so far. Previously, we reported that the knockdown of NDPK C reduced the isoproterenol-induced cAMP in neonatal rat cardiomyocytes (NRCM). Therefore, cAMP formation and PKA-dependent protein phosphorylation were analyzed in NRCM and adult mouse ventricular cardiomyocytes (AMVCM), stimulated with isoproterenol (ISO). SanWie3 attenuated the ISO-induced cAMP formation in NRCM, consistent with the reported complex formation of NDPK C with G_s proteins. In accordance, the SanWie3-induced deprivation of cAMP reduced the phosphorylation of the cAMP/PKA downstream target phospholamban (PLN). Surprisingly SanWie3 treatment of AMVCM and measuring cAMP pools by differentially targeted cAMP-Förster resonance energy transfer (FRET) suggested a different function in AMVCM. Here, SanWie3 caused an increase of ISO-induced cAMP levels in the PLN/SERCA2a subdomain and the PKA-dependent PLN phosphorylation. The ISO-

induced cAMP formation and PKA-dependent phosphorylation of other targets in other cellular domains (cytosol, plasma membrane, and ryanodine receptor-2-subdomain) were unchanged. Consistently, the influence of SanWie3 on calcium handling in AMVCM showed an accelerated basal Ca^{2+} reuptake, an increase in the basal sarcoplasmic reticulum (SR) Ca^{2+} load, and an increase in Ca^{2+} transients and spontaneous Ca^{2+} spark frequency. To analyze the effect of SanWie3 on ISO-induced ventricular contraction, cardiac muscle stripes from rats were isolated, and force development was measured in an organ bath. This significant increase in ISO-induced contractility was associated with an increase in PLN phosphorylation. As in AMVCM, the effect of SanWie3 on ISO-induced PLN phosphorylation was mimicked by the inhibition of G_i activity by pertussis toxin treatment; the results suggest a constitutive activation of G_i by NDPK C in a signalosome controlling PLN/SERCA2a activity, thereby modulating Ca^{2+} load and cardiomyocyte contractility.

The results demonstrate that the identified small molecular inhibitor SanWie3, which preferentially attenuates the enzymatic activity of NDPK C, modulates cAMP-dependent signaling in NRCM and AMVCM preferentially in the PLN/SERCA2a subdomain. Therefore, SanWie3 may be a lead compound in designing small molecules able to relieve the detrimental suppression of cAMP signaling in specific cellular compartments in cardiomyocytes occurring in heart failure.

Zusammenfassung

Beeinträchtigte cAMP-abhängige Signaltransduktion und dysfunktionales Calcium-Handling in Kardiomyozyten sind zwei mit der Herzinsuffizienz verbundene, charakteristische Merkmale. Bisherige therapeutische Versuche zur Verbesserung der kontraktilen Funktion durch globale Erhöhung der cAMP-Spiegel scheiterten klinisch aufgrund einer höheren Anfälligkeit für Herzrhythmusstörungen und eines erhöhten Risikos für plötzlichen Herztod. Neue Strategien, die darauf abzielen, distinkte cAMP-Pools in Kardiomyozyten zu modulieren, könnten jedoch eine Verbesserung der Kontraktionskraft ohne nachteilige Auswirkungen ermöglichen. Nukleosiddiphosphatkinase (NDPK), ein Enzym mit Transphosphorylase-Aktivität, trägt zur heterotrimeren G Protein Aktivierung durch GTP-Bildung aus ATP und GDP bei. Darüber hinaus bilden Oligomere aus den Isoformen NDPK B und C einen Komplex mit heterotrimeren G Proteinen und wirken als Protein-Histidin-Kinase an der Gβ-Untereinheit, was zu einer direkten Aktivierung des G Proteins führt. NDPK C wird bei höhergradiger, menschlicher Herzinsuffizienz hochreguliert, wobei das Protein die Komplexbildung von NDPKs mit G_i Proteinen und damit eine Steigerung der G_i Aktivität fördert. Dies trägt wahrscheinlich zu einer verstärkten Unterdrückung der cAMP-Bildung bei. Daher zielt dieses Projekt darauf ab, Verbindungen zu identifizieren, die NDPK B und C hemmen und die Folgen einer Hemmung der NDPK-Aktivität im Herzmuskel zu untersuchen.

Um potenzielle Inhibitoren der NDPK Aktivität zu identifizieren, wurden die humanen Isoformen NDPK A, B und C rekombinant exprimiert und aufgereinigt. Ein ATP-abhängiger Lumineszenz-Assay auf Luziferase-Basis wurde verwendet, um die Menge von aus GTP + ADP gebildetem ATP zu quantifizieren und damit die NDPK-Transphosphorylase-Aktivität zu bestimmen. Aus der getesteten Substanz-Bibliothek wurde eine niedermolekulare Verbindung (SanWie3) identifiziert, die bevorzugt die Aktivität von NDPK C > NDPK B >> NDPK A reduzierte. Weitere *in vitro* Studien zeigten, dass SanWie3 ein allosterischer Inhibitor der Transphosphorylase-Aktivität der NDPK C (IC_{50} ~ 3 µM) ist. Biophysikalische Proteinanalysen bestätigten, dass die Bindung von SanWie3 kleine strukturelle Veränderungen im NDPK C-Protein hervorrufen. Vorstudien zur Bindung von SanWie3 mit HDX-Massenspektrometrie und *in silico* Proteinmodellierung identifizierten eine mutmaßliche Bindungstasche in der Nähe des katalytisch aktiven Zentrums. Potenzielle Off-Target-Effekte von SanWie3 auf andere Enzyme, Kanäle und Rezeptoren wurde in weiteren *in vitro* Screenings untersucht, die bisher keine Hinweise auf weitere SanWie3-Targets ergaben. Publizierte Ergebnisse zeigten, dass der Knockdown von NDPK C Isoproterenol (ISO)-induzierte Bildung von cAMP in Kardiomyozyten aus neonatalen Ratten (NRCM) reduzierte. Daher wurden die cAMP-Bildung sowie die PKA-abhängige Proteinphosphorylierung in NRCM und adulten ventrikulären Kardiomyozyten der Maus (AMVCM) unter ISO-Stimulation untersucht. SanWie3 schwächte die ISO-induzierte cAMP-Bildung und cAMP/PKA-abhängige Phosphorylierung von Phospholamban (PLN) in

NRCM ab, was mit der berichteten Komplexbildung von NDPK C mit G_s-Proteinen in NRCM übereinstimmte.

Überraschenderweise wurde in SanWie3 behandelten: AMVCM durch Messung von cAMP-Pools mittels differenziell gerichteten cAMP-Förster-Resonanzenergietransfer (FRET) eine andere Regulation beobachtet, die auf eine andere Kopplung der NDPK C deutet. Hier verursachte SanWie3 einen Anstieg der ISO-induzierten cAMP-Spiegel in der SERCA/PLN-Subdomäne und entsprechend eine Verstärkung der PKA-abhängigen PLN-Phosphorylierung. Die ISO-induzierte cAMP-Bildung und PKA-abhängige Phosphorylierung anderer Ziele in anderen zellulären Domänen (Cytosol, Plasmamembran und Ryanodin-Rezeptor-2-Subdomäne) waren unverändert. Konsequenterweise zeigte der Einfluss von SanWie3 auf das Calcium-Handling bei AMVCM eine beschleunigte basale Ca^{2+}-Wiederaufnahme, eine Erhöhung der basalen sarkoplasmatischen Retikulum (SR) Ca^{2+}-Beladung, eine Erhöhung der Ca^{2+}-Transienten und der spontanen Ca^{2+}-Freisetzung. Um die Wirkung von SanWie3 auf ISO-induzierte ventrikuläre Kontraktion zu analysieren, wurden Herzmuskelstreifen von Ratten isoliert und die Kraftentwicklung im Organbad gemessen. Hier zeigte sich ein signifikanter Anstieg der ISO-induzierten Kontraktilität, der mit einem Anstieg der PLN-Phosphorylierung assoziiert war.

Interessanter Weise, wurde die Wirkung von SanWie3 auf die ISO-induzierte PLN-Phosphorylierung durch die Hemmung der G_i Aktivität mittels Pertussis-toxin imitiert. Diese Ergebnisse deuten daher auf eine konstitutive Aktivierung von G_i durch NDPK C in einem Signalosom hin, dass die PLN/SERCA2a-Aktivität und damit indirekt die Kontraktilität der Kardiomyozyten kontrolliert.

Zusammenfassend zeigen die Daten, dass der niedermolekulare NDPK C Inhibitor SanWie3, die cAMP-abhängige Signalgebung bei NRCM und AMVCM vorzugsweise in der PLN/SERCA2a-Subdomäne moduliert. SanWie3 kann daher eine chemische Leitstruktur zum Design von Molekülen sein, die in der Lage sind, die konstitutive, kontraproduktiveUnterdrückung der cAMP-Signaltransduktion in bestimmten zellulären Kompartimenten von Kardiomyozyten in der Herzinsuffizienz abzuschwächen.

Abbreviations

%	Percent
°C	Degree Celcius
AC	Adenylyl cyclase
AMP	Adenosine monophosphate
ADP	Adenosine diphosphate
ANOVA	Analysis Of Variance
APS	Ammonium Peroxide Sulphate
ATP	Adenosine triphosphate
bp	Base pair
BSA	Bovine Serum Albumin
Ca^{2+}	Calcium
CamKII	Calmodulin-dependent protein kinase II
cAMP	Cyclic AMP
CO_2	Carbon Dioxide
CoIP	Co-Immunoprecipitation
dH2O	Distilled Water
DMEM	Dulbecco´s Modified Eagles Medium
DMSO	Dimethyl Sulphoxide
DNA	Deoxyribonucleic Acid
FCS	Fetal Calf Serum
GDP	Guanine diphosphate
GPCR	G protein Coupled receptor
GTP	Guanine triphosphate
HCl	Hydrochloric Acid

HRP	Horseradish peroxidase
IP	Immunoprecipitation
KCl	Potassium chloride
KH_2PO_4	Potassium dihydrogen phosphate
NaCl	Sodium chloride
NaOH	Sodium hydroxide
NDP	Nucleoside DiPhosphate
NTP	Nucleoside TriPhosphate
PAGE	Poly Acrylamide Gel Electrophoresis
PCR	Polymerase Chain Reaction
RT	Room Temperature
SDS	Sodium Dodecyl Sulphate
PCR	Polymerase Chain reaction
SW3	SanWie3
UDP	Uridine DiPhosphate
WB	Western Blot

Units

µl	Microliter
g	Gram
mg	Milligram
M	Molar
Mdeg	Millidegree
mM	Millimolar
mol	Mole
µmol	Micromole
nmol	Nanomole
pmol	Picomole
cm	Centimeter
µM	Micrometer
cm^2	Centimeter Squared
h	Hour
min	Minute
kDa	KiloDalton
V	Volt
Rpm	revolutions per minute

1. Introduction

1.1 Importance of Nucleotides

Nucleotides play a crucial role in all living organisms. They are the building blocks of deoxy- and ribonucleic acids and provide the chemical energy necessary for biological processes such as DNA replication, RNA and protein synthesis, and cell motility. Moreover, nucleotides function as cofactors of enzymes and are central mediators of cellular signal transduction (Lane & Fan, 2015). The two main categories of nucleotides based on nitrogen base are purines (adenine and guanine) and pyrimidines (cytosine and thymine), attached to a sugar moiety and phosphate group. Other nucleotide forms include cofactors of enzymatic reactions such as coenzyme A, NAD, and FAD. Based on the number of phosphate groups bound to the sugar molecule, nucleotides are termed nucleoside mono-, di-, and triphosphate. Adenosine triphosphate (ATP), a purine nucleotide, provides the energy for many cellular processes, including synaptic signaling, active transport, and muscle contraction. ATP is used as the substrate by most protein kinases, and therefore critical to the pleiotropy of signaling cascades involving the phosphorylation of downstream effector proteins (Mishra et al., 2006). ATP is also used by adenylate cyclase to produce the second messenger cyclic adenosine monophosphate (cAMP). cAMP regulates intracellular signaling, including hormone signaling cascades, protein kinase activation, and ion channel regulation (Kamenetsky et al., 2006). ATP is a requisite in muscle contraction, which is required to generate force against adjoining actin filaments through the cycling of myosin cross-bridges.

Additionally, it is necessary for maintaining ion gradients across cell membranes through active transport, driven by ATP hydrolysis (Barclay, 2015). Guanosine triphosphate (GTP) derived cyclic guanosine monophosphate (cGMP) is another second messenger molecule. It is involved in modulating various effectors, including cGMP-dependent protein kinases and ion channels. GTP also provides energy in processes such as protein synthesis and gluconeogenesis. GTP plays a vital role during signal transduction by activating GTP binding proteins, often named G Proteins. G proteins are a large family of GTP hydrolyzing enzymes (GTPases) that act as molecular switches. In their GTP-bound form, they interact with effector proteins, thereby regulating fundamental cellular processes. By the hydrolysis of GTP, they return to an inactive GDP-bound state, thereby acting as biochemical clocks for cellular activation (Ma & Karplus, 1997).

1.2 Nucleoside diphosphate kinases

Nucleoside diphosphate kinases (NDPKs) are enzymes ubiquitously expressed in all living organisms, except mycoplasma, *L. lactis*, and *E. faecalis* (Kilstrup et al., 2005; Pollack et al., 2002). In humans, ten paralogous genes encoding the NDPK family proteins are known to date (Boissan et al., 2009). Nine of these genes are named *nme1–9* (NME stands for the non-

metastatic enzyme), whereas the 10th gene encodes a truncated form called *RP2* (Fig. 1A) (Boissan et al., 2009; Desvignes et al., 2009). NME/NDPK enzymes are categorized into two groups based on the homology in the amino acid sequences (Lacombe et al., 2000). Group I includes NDPK A-D, which exhibits 58-88% amino acid identity. All gene products show NDPK activity in humans (Wieland et al., 2010). They are localized in the cytosol, nuclei, and plasma membrane except for the NDPK D isoform, which is located in mitochondria by a specific mitochondrial targeting sequence (Milon et al., 2000). The rest of the *nme* gene products comprises group II, which share only 22-44% homology, with low or no NDPK activity. They are primarily confined to ciliated structures except for the *NME6* enzyme, which is ubiquitously expressed (Boissan et al., 2018).

NDPKs form tetrameric and hexameric multi-subunit complexes in prokaryotic cells and eukaryotic cells, respectively (Fig. 1B) (Gilles et al., 1991). The molecular mass of a monomer varies between 17 to 23 kDa. NDPK A, NDPK B are the predominantly expressed NDPK isoforms encoded by the 17th chromosome at locus 17q21.3, with a molecular mass of ~17 kDa. The 16th chromosome encodes NDPK C and NDPK D at locus 16p13.3. NDPK C, with a molecular mass of 19 kDa, shares 55% homology with NDPK A and NDPK B. In contrast to NDPK A/B, NDPK C contains a 17 amino acid hydrophobic peptide at the N-terminus, possibly involved in membrane targeting. NDPK D, with a molecular mass of 23 kDa, possesses a mitochondrial targeting motif (Milon et al., 2000). NDPK isoforms in different species such as rats, mice, and even zebrafish are highly homologous to the human NDPKs.

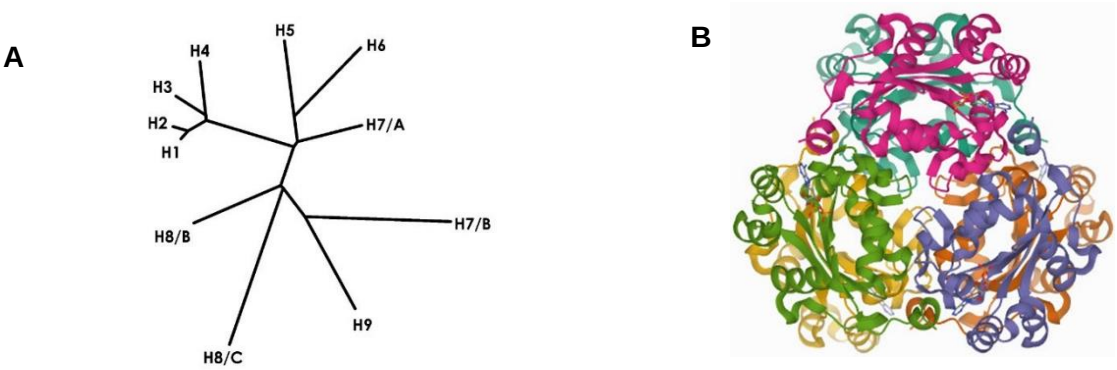

Figure 1: A. Phylogenetic tree of human NDPK isoforms indicated as H1 to H9, obtained from ClustalW alignment of the homologous sequences. The domain A for NME8 and the 10th isoform XRP2 are not included **(adapted from (Boissan et al., 2009))**. B. Hexameric structure of NDPK, each monomer is shown in a different color **(adapted from (Dexheimer et al., 2009))**.

1.3 Enzymatic activity of the NDPKs

NDPKs catalyzes the transfer of a high-energy terminal phosphate from nucleoside triphosphates (NTPs) to nucleoside diphosphates (NDPs) through a phosphohistidine intermediate by a ping-pong mechanism (Fig. 2). Magnesium (Mg^{2+}) is an essential cofactor for many reactions in cell metabolism, which involves Mg^{2+} chelation to nucleotides such as ADP, ATP, and GTP (Kleczkowski & Igamberdiev, 2021). Many enzymes can use ATP only in its Mg^{2+} chelated form, MgATP, as substrate or cofactor. Likewise, NDPKs utilize Mg^{2+} chelated nucleotides as substrates. The primary function of NDPKs is to maintain nucleotide homeostasis (Hippe et al., 2003) and based on their enzymatic activity, NDPKs have to be correctly named NDP/NTP transphosphorylases. The NDPK active site (H118 for NDPK A/B, H135 for NDPK C) contains the motif NXXHG/ASDS with the catalytically active histidine at position 118 (Schaertl et al., 1998). This histidine can undergo autophosphorylation from any bound MgNTP, e. g. MgATP in the course of the enzymatic reaction, forming a phosphohistidine intermediate (Attwood & Muimo, 2018). In the second part of the reaction, this high energetic phosphate group is transferred on a newly bound MgNDP, e.g. MgGDP.

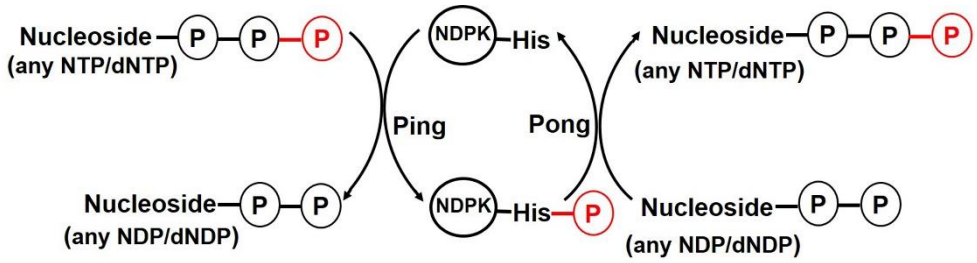

Figure 2: Scheme explaining the phosphotransfer activity of NDPKs through a ping-pong mechanism.

The monomeric subunits of the different NDPK isoforms contain 152 residues with a similar secondary structure fold. An alpha-helix hairpin and Kpn loop make up the nucleotide-binding pocket unique for NDPKs and different from other kinases or ATPases (Janin et al., 2000). One of the first reports on NDPKs demonstrated that NDPK A and NDPK B are highly homologous, and the monomers of the two proteins can associate to form heterohexamers (Gilles et al., 1991). Subsequently, most likely, all group I NDPKs can form heterohexamers along with homohexamers (Abu-Taha et al., 2018). NDPKs are involved in numerous intracellular processes such as cell proliferation, differentiation, development, signal transduction, G protein activation, endocytosis, and gene expression (Lascu & Gonin, 2000; Palacios et al., 2002; Postel & Abramczyk, 2003).

1.4 NDPKs as protein histidine kinases

Based on the amino acid residues involved, there are three major classes of kinases. Serine/ threonine and tyrosine protein kinases are highly investigated. In contrast, histidine kinases are relatively less studied because of the difficulty to detect phosphohistidines due to their heat and acid-labile nature (Kee et al., 2010). Serine/threonine kinases possess uncharged

nonpolar amino acid residues at the active site. However, histidine kinases are positively charged because of the aromatic imidazole ring at the active histidine residue. So, the nature of the chemical bond formed (phosphoramide) by histidine residues is different with higher energy when compared to the phosphoester bond formed by serine/threonine kinases (Besant & Attwood, 2009). In response to environmental cues, most prokaryotes use a conserved two-component phosphotransfer mechanism for signal transduction. The two-component system is comprised of a histidine protein kinase and a response regulator protein. The histidine protein kinase autophosphorylates at a histidine residue, generating a high-energy phosphoryl group. The phosphate group is subsequently transferred to an aspartate residue in the response regulator protein through the histidine-aspartate transfer mechanism (Stock et al., 2000).

Some eukaryotes, including plants, utilize a similar two-component phosphotransfer mechanism in signal transduction cascades (Schaller et al., 2011). In mammals, proteins such as eukaryotic elongation factor-2 kinase and pyruvate dehydrogenase kinase have structural similarities to bacterial two-component histidine kinases, suggesting an evolutionary relationship (Besant & Attwood, 2005). In mammals, NDPKs are the only well-characterized protein histidine kinases so far. It has been shown that NDPKs can phosphorylate a histidine residue in the ATP citrate lyase of rat liver (Wagner & Vu, 2000). The anti-metastatic activity of NDPK A was demonstrated in human breast carcinoma cell motility through the overexpression of wild-type (WT) and site-directed mutant forms (P96S and S120G). These mutant forms maintained their ability to autophosphorylate; however, they failed to exhibit protein kinase activity and could not suppress metastasis compared to the WT NDPK A (Freije et al., 1997). NDPK A facilitates genomic stability in melanoma through direct interactions in DNA repair pathways such as nucleotide excision repair and double-strand break repair, potentially through its nucleoside diphosphate kinase and 3′-5′exonuclease activities (Kaetzel et al., 2006). In addition, NDPK A, through its phosphotransfer activity, promotes the activity of the GTPase dynamin, thereby being involved in the regulation of cytoskeletal dynamics (Snider et al., 2015).

It is well established that ligand-bound G protein-coupled receptors (GPCR) activate heterotrimeric G proteins by promoting a conformational change that allows a GDP/GTP exchange at the G protein α-subunit. Our group reported that in addition to the GPCR induced GDP/GTP exchange, G protein activation could occur via intermediate histidine phosphorylation on the Gβ subunit mediated by NDPK B (Cuello et al., 2003; Hippe et al., 2003; Wieland et al., 1992). NDPK B forms a complex with Gβγ dimers and, through its kinase activity, facilitates the transfer of high-energy phosphate from ATP onto the His266 residue on the Gβ subunit. This high-energy phosphate is further transferred specifically onto GDP, forming GTP locally. In turn, this GTP binds to potentially empty guanine nucleotide-binding

site within the G protein α-subunit and thereby activates it (Wieland, 2007). Such a receptor-independent NDPK B/Gβ axis was shown to promote the activation of the G_s-protein subfamily in cardiomyocytes, thereby contributing to the G_s/cAMP-mediated increase in contractility (Hippe et al., 2007; Wieland, 2007). In lymphocytes, the direct interaction of NDPK B with another substrate, the Ca^{2+}-activated K^+ channel (KCa3.1), was reported. The phosphorylation of KCa3.1 at His358 by NDPK B kinase activity increases the channel's open probability, which is counteracted by the protein histidine phosphatase, PHPT1 (Srivastava et al., 2006). In canine renal epithelial cells, the phosphorylation of the transient receptor potential vanilloid-5 (TRPV5) channel on His771 by NDPK B increased the channel open probability and thus regulates Ca^{2+} reabsorption in the distal convoluted tubule of the kidney (Cai et al., 2014).

In contrast to NDPK A/B, little is known about the cellular function of the isoform NDPK C. In mammals, it was recently demonstrated that NDPK C, through its phosphotransferase activity, provides GTP to dynamin-like protein 1 (DLP1), a GTPase required for peroxisomal constriction. Conversely, the loss of NDPK C resulted in elongated peroxisomes (Honsho et al., 2020). In a patient with congenital hypotonia, NDPK C was reported to be involved in maintaining mitochondrial integrity and cell viability under glucose starvation through its kinase activity (Chen et al., 2019). Recent findings from our group showed that NDPK C regulates G_i/G_s modulated cAMP signaling in the human heart and is essential for the interaction of NDPK B with G proteins (Abu-Taha et al., 2017). Whether NDPK C acts as a protein histidine kinase in one of these processes still needs to be shown.

1.5 G protein-coupled receptors

G protein-coupled receptors (GPCRs) are also often referred to as seven transmembrane receptors (TMRs). They are the largest and most diverse group of plasma membrane receptors in eukaryotic cells, making up ~4% of all encoded genes in the human genome (Fredriksson et al., 2003). GPCRs play a significant role in maintaining various physiological processes such as metabolism, cell growth, and hormonal homeostasis (Lefkowitz et al., 2000). Consequently, they are the most prominent family of proteins targeted by approved drugs. Many extracellular ligands, such as amines, ions, peptides, etc., mediate their response by interacting with GPCRs and stabilizing their active conformation. This active state enables the GPCRs to interact with a heterotrimeric (Gα, Gβ, and Gγ) G protein on the cytoplasmic side, thereby promoting the exchange of GDP for GTP in the Gα subunit and the activation of the G protein. Upon activation, the heterotrimeric Gαβγ dissociates into the active Gα and Gβγ subunits, which can independently interact with a variety of signaling effectors such as ion channels, or enzymes that in turn produce second messengers, converting the stimulus to a specific cellular response. After the signal transduction, GTP is hydrolyzed to GDP on the Gα subunit, promoting its re-association with Gβγ to complete a G protein cycle (Fig. 3) (Wang et al., 2018; Weis & Kobilka, 2018).

Meanwhile, structural evidence has been obtained of how an activated GPCR interacts with the coupled G protein and thereby induces the release of the GDP bound in the Gα subunit (for review see (Weis & Kobilka, 2018)). As an activated GPCR can stimulate more than one G protein and a given G protein can run through its activation cycle for several rounds, the local supply of GTP might become a limiting factor for signal transduction. Replenishing GTP from GDP and ATP by NDPKs at the site of G protein activation (Fig. 3) has already been postulated since the 1990s (for a recent review, see (Aktories et al., 2019).

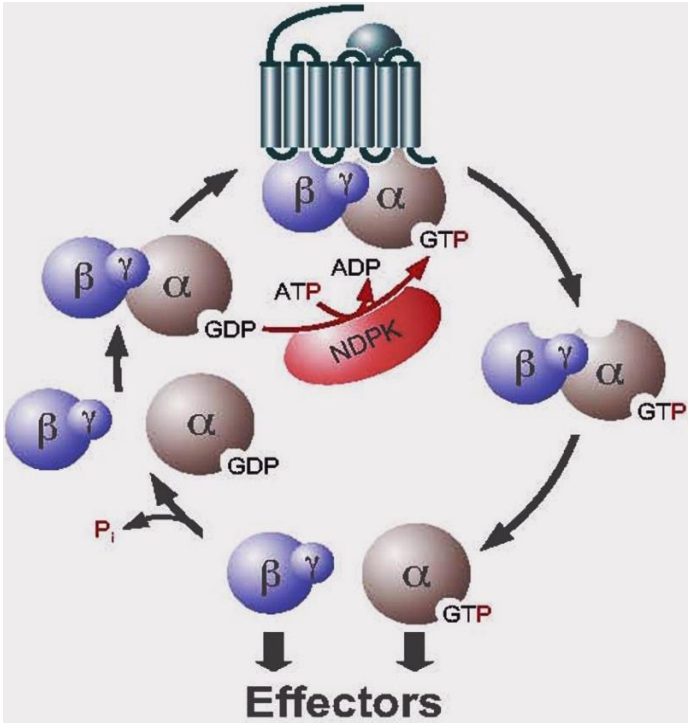

Figure 3: Activation cycle of heterotrimeric G proteins NDPKs, which can contribute the required GTP from ATP and GDP by the phosphotransfer activity **(adapted from (Aktories et al., 2019))**

In mammals, the G protein family is encoded by sixteen genes for Gα subunits, six encoding for Gβ subunits, and twelve genes for Gγ subunits. The interaction of these subunits allows for approximately 700 different potential Gαβγ heterotrimer compositions (Simon et al., 1991). This diversity contributes to the selectivity and specificity of both GPCRs and effector systems, although it has become evident that not all potential combinations are formed in vivo. Based on the primary sequence similarity of Gα subunits involved, heterotrimeric G proteins are divided into four main families, G_s, $G_{i/o}$, $G_{q/11}$, and $G_{12/13}$. The G_s family includes two isoforms G_s and G_{olf}, whereas the $G_{i/o}$ and $G_{q/11}$ family proteins are subdivided into several isoforms (Duc et al., 2017).

Transducin (G_t) belongs to the G_i family of proteins. It is mainly for phototransduction in vertebrates. In contrast to the other membrane-bound family members, G_t can be released from rod outer segment membranes and thus be obtained in more significant amounts as pure protein, which can be used in protein-protein interaction studies. Based on these characteristics, a direct interaction of NDPK C with NDPK B and purified heterotrimeric

transducin ($G_t\alpha\beta\gamma$) was recently demonstrated (Abu-Taha et al., 2017), identifying NDPK C as the missing component allowing for complex formation of Gβγ dimers with NDPK B, which is already known since the early 2000s (Cuello et al., 2003).

GPCRs are widely expressed in the mammalian heart in different cell types, such as cardiomyocytes, fibroblasts, endothelial cells, and vascular smooth muscle cells. Among them, the β-adrenergic receptors (β_1AR and β_2AR) are the predominant GPCR subtypes in many mammalian species (Wang et al., 2018). Other well-described cardiac GPCRs include α-adrenergic receptors (αAR), angiotensin II (AT1) - muscarinic acetylcholine (M_2), endothelin (ET_A), and adenosine receptors (A_{2A}), as well as a variety of other less expressed GPCRs such as histamine H_2 receptors. (Wang et al., 2018).

1.6 β-adrenoceptors

βAR signaling plays a critical role in regulating cardiac function in response to the activation of the sympathetic nervous system (SNS). The SNS releases noradrenaline as a neurotransmitter acting on SNS-innervated cardiac tissues and releases adrenaline from the adrenal gland into the bloodstream. Both catecholamines (CA) can act as agonists on βARs to adapt cardiac output and metabolism during acute and chronic stress (Madamanchi, 2007). The human heart primarily expresses β_1ARs (75-80%), to a lesser extent β_2ARs (20-25%), and very few β_3ARs. Each subtype possesses different affinities towards its ligands; for instance, noradrenaline and adrenaline activate β_1AR and β_2AR, respectively (Kaumann & Molenaar, 1997). It has been confirmed that all cardiomyocytes express β_1AR, whereas it was reported that only ~5% of the cells express β_2AR and β_3AR (de Lucia et al., 2018). In cell types other than cardiomyocytes, such as smooth muscle cells, endothelial cells, and fibroblasts, βAR expression is restricted to β_2AR and relatively low levels of β_3AR, with endothelial cells as the predominant cell type. (Bristow et al., 1986; Myagmar et al., 2017). The spatial segregation and subcellular localization of βARs and G proteins forming signalosomes (association of different effector proteins) is now an established concept, which mediates subtype-specific responses in distinct compartments (Lohse et al., 2003).

The nature of the cellular response is determined by the βAR subtype that is activated and the pathophysiological setting regarding effector molecule expression and abundance. All the βAR subtypes are associated with G_s proteins, whereas β_1AR specifically activates G_s, β_2AR, and β_3AR can additionally couple to G_i proteins. However, even though all the three βAR isoforms can activate G_s, the downstream activated signaling cascades are specific to each subtype. For instance, both β_1AR and β_2AR activate G_s signaling in cardiomyocytes, but only β_1AR hyperactivity is associated with maladaptive hypertrophic growth. On the other hand, only the β_2AR in cardiomyocytes can also activate the non-canonical G_i protein signaling pathways, which are sensitive to pertussis toxin (PTX). PTX modifies G_i through nicotinamide adenine

dinucleotide dependent ADP-ribosylation on a cysteine residue in position 351 of the c-terminus of the $G\alpha_i$ subunit (Engelhardt et al., 1999; Feldman et al., 1988). Therefore, $G\alpha_i$ signaling can no longer inhibit AC, resulting in increased cAMP levels in specific signaling compartments (Mangmool & Kurose, 2011).

1.7 Role of calcium and βAR signaling in cardiac contractility

Tight regulation of calcium homeostasis is critical for cardiac muscle function (Sejersted, 2011). An imbalance in Ca^{2+} handling, altered Ca^{2+} sensitivity, and enhanced Ca^{2+} leak, or reduced Ca^{2+} sequestration can cause the mechanical and electrical dysfunction observed in end-stage human heart failure (Sipido & Vangheluwe, 2010).

Cardiac muscle contraction and relaxation are central events in the systolic and diastolic function of the heart. As the contraction is initiated by electrical excitation through action potential, causing membrane (sarcolemma) depolarization by Na^+ influx, the process is known as excitation-contraction (EC) coupling. The depolarization of the sarcolemma triggers the opening of L-type Ca^{2+} channels (LTCC) localized in the transverse tubule (t-tubule), allowing for the entry of extracellular Ca^{2+}. The elevated cytosolic Ca^{2+} level induces an additional Ca^{2+} release from the sarcoplasmic reticulum (SR) through the ryanodine receptor 2 (RYR2) channels, a process called Ca^{2+} induced Ca^{2+} release. The increased cytosolic Ca^{2+} interacts with sarcomeric proteins, like troponin-C, a component of the thin filaments, which are bound to the actin. Ca^{2+} binding causes a shape change in the troponin, which exposes areas on the actin to which the head of the myosin filaments can bind. The binding of the myosin head to actin is called a cross-bridge. The energy provided by ATP hydrolysis is used to move the myosin head, carrying the actin. As a result, actin slides across the myosin filament, shortening the muscle. To initiate relaxation, the binding of Ca^{2+} to the sarcomeric proteins has to be lowered. As cytosolic Ca^{2+} is actively transported back into the SR through the sarcoplasmic reticulum Ca^{2+}-ATPase (SERCA) and to the extracellular space via the Na^+/Ca^{2+} exchanger (NCX), the cytosolic Ca^{2+} concentration drops and Ca^{2+} dissociates from the sarcomeric proteins. The amount of Ca^{2+} delivered to the cytoplasm, and the rate of Ca^{2+} removal from the cytoplasm are the crucial factors determining the contraction's duration, intensity, and pace (Eisner et al., 2017; Huser et al., 2000; Liu et al., 2021).

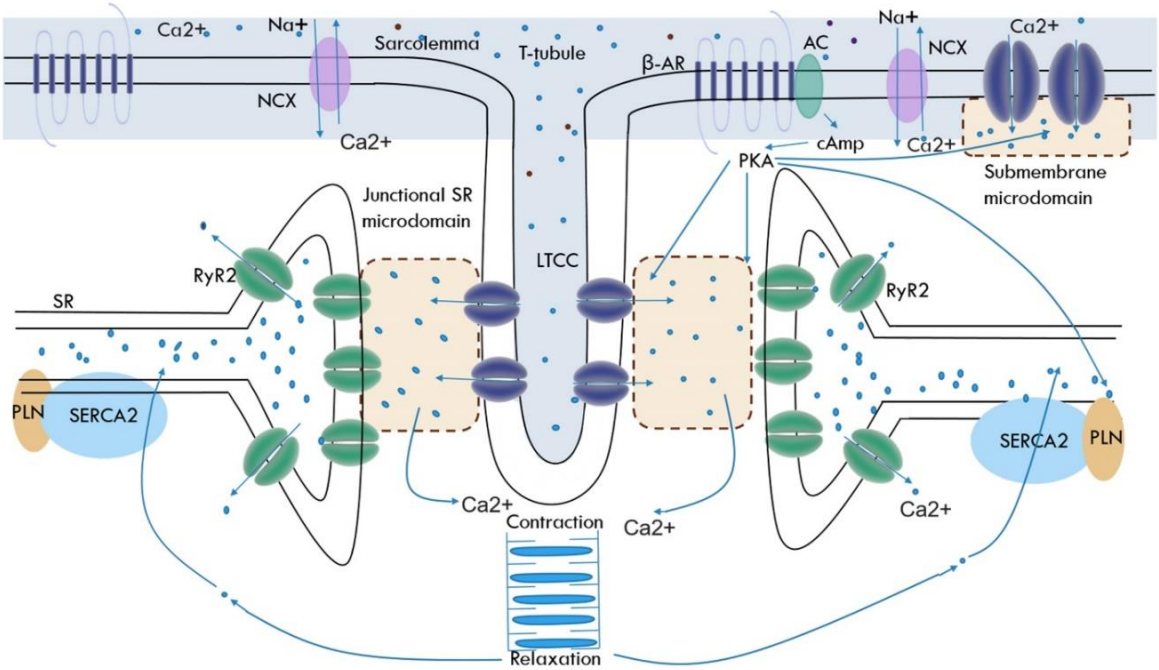

Figure 4: Sarcolemmal depolarization leads to Ca^{2+} entry into the cytoplasm through the opening of Ca^{2+} channels (LTCC, shown in blue). Ca^{2+} then binds to the Ca^{2+}-release channels, RyRs (shown in green), to allow a further Ca^{2+} release from the SR thereby, initiating contraction by binding to troponin. Ca^{2+} is removed from the cytoplasm by the Na^{+}/Ca^{2+} (NC) exchanger, located in the plasma membrane, or by SERCA2a, located in the SR. The activity of SERCA2a, which is negatively regulated by phospholamban (PLN), is a PKA target downstream of the βAR/AC/cAMP cascade.

In addition to EC coupling, SNS/catecholamine-mediated activation of the βAR/cAMP axis markedly increases the heart rate, contractility, relaxation, and conduction velocity (Fig. 4). Activated $G\alpha_s$ in response to βAR activation stimulates adenylyl cyclase (AC) to produce the second messenger cAMP. ACs form a family of several isoforms (AC1-10), of which AC5 and AC6 are the dominant isoforms in cardiomyocytes. While the isoforms localize to distinct cellular compartments and differ regarding their regulatory mechanisms, AC5 and AC6 are closely related and share a similar regulatory mechanism, i.e. activation by $G\alpha_s$ and inhibition by $G\alpha_i$ (Zaccolo, 2009). cAMP, either increased globally or at a specific compartment, based on the spatial organization, activates cAMP-dependent effectors like protein kinase A (PKA), exchange proteins activated by cAMP (EPAC), and cyclic nucleotide-gated, hyperpolarization-activated cation channels (HCN) (Fischmeister et al., 2006). The balance between the enzymatic activities of ACs and cyclic nucleotide phosphodiesterases (PDEs), hydrolyzing cAMP to 5'-AMP, determines the cellular cAMP signal amplitude, distribution, and duration (Liu et al., 2021). PKA is the principal mediator of βAR signaling through the phosphorylation of distinct target proteins. Active PKA phosphorylates the proteins involved in the Ca^{2+} clock of pacemaker cells and proteins involved in the different steps of the contraction cycle. These targets comprise; LTCC to enhance opening and Ca^{2+}-influx, RyR2 to increase Ca^{2+}-release from the SR during systole, contractile proteins such as troponin I (TnI), and myosin-binding

protein C (MyBP-C) for force development and relaxation velocity. In its dephosphorylated state, phospholamban (PLN) binds to SERCA2a and inhibits its Ca^{2+} pump activity. Phosphorylation of PLN by PKA diminishes the PLN–SERCA2a interaction, thereby relieving Ca^{2+}-pump inhibition to enhance relaxation rates and contractility (Bers, 2014; de Lucia et al., 2018; Leroy et al., 2018; MacLennan & Kranias, 2003) (Fig. 4).

1.8 Compartmentalized cAMP signaling

An immense amount of work demonstrated the compartmentalization of cAMP in cardiomyocytes (Leroy et al., 2018). Differential localization of the respective signaling cascade constituents often called a signalosome, and transverse tubules (Fig. 5) creates various cAMP production sites in discrete domains. This signalosome formation leads to the activation of the specific cAMP effectors in the vicinity. Compartmentalized signaling enables different GPCRs to generate specific, spatially confined cAMP pools, which activate defined subsets of localized PKA (Fig. 5) (Zaccolo & Pozzan, 2002). The distribution of cAMP signaling through different micro subcellular compartments has been extensively characterized in cardiomyocytes during the last decade. A wide variety of signal transducers regulate various signalosomes through cAMP to generate distinct functional responses (Delaunay et al., 2019; Surdo et al., 2017). The signalosome complex's key players that regulate cardiac contractility are A-Kinase anchoring proteins (AKAPs), cAMP-degrading phosphodiesterases (PDEs), AC, and PKA. This complex formation promotes spatiotemporal regulation of the cellular signal and thus orchestrates the subsequent physiological response (Cheepala et al., 2013; Houslay, 2010). AKAPs provide the structural basis for a tight regulation of the cAMP-dependent phosphorylation events by controlling the localization of PKA, tethering PKA to specific subcellular compartments (Ghigo & Mika, 2019; Zaccolo, 2009). PDEs play a vital role in the spatial regulation of cAMP propagation and define the boundaries of individual cAMP pools (Beavo & Brunton, 2002). AC isoforms have been shown to localize at different compartments, have distinct roles, and selectively interact with specific receptors. For example, AC6 promotes Ca^{2+} cycling and contractile function with a beneficial effect on cardiac performance (Lompre et al., 2010). However, AC5 depletion had a beneficial impact in preserving cardiac function against pressure overload (Okumura et al., 2003) and preventing myocardial apoptosis without functional deterioration (Iwatsubo et al., 2004).

The cAMP pools maintained at different cellular compartments can be monitored through Fluorescence resonance energy transfer (FRET) measurements, using microdomain-specific fluorescent cAMP biosensors (Perera & Nikolaev, 2013). FRET assays have been established to monitor the cAMP levels at various microdomains, such as the plasma membrane, sarcoplasm, and the nuclear/perinuclear region (Borner et al., 2011).

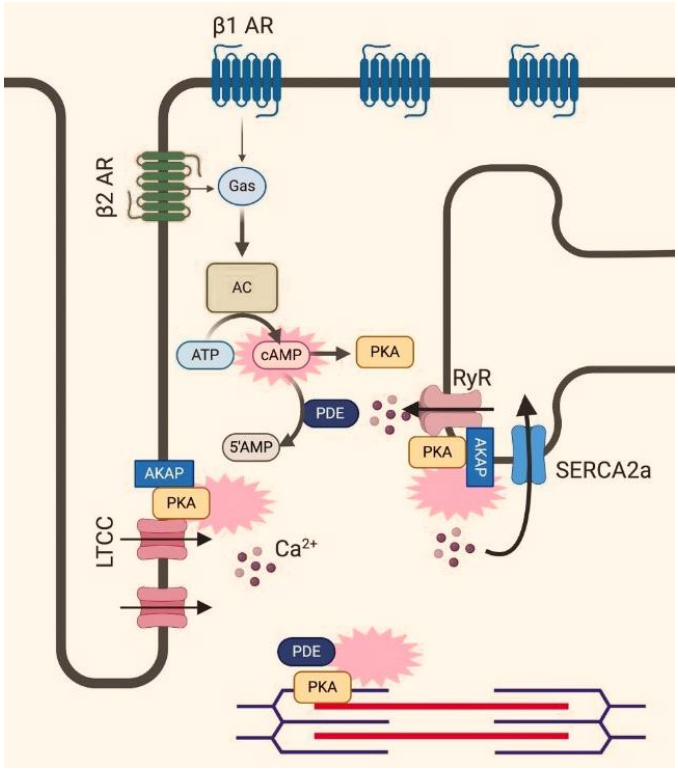

Figure 5: Differential cAMP signaling pathways and the localization of several signalosomes in the cardiomyocytes. Various components of the signalosomes with cAMP pools (shown in pink) in the vicinity of T-tubule (LTCC), SERCA2a (PLN), contractile filaments (cytosolic), and βARs (plasma membrane) are indicated **(Adapted from (McCabe & Rangamani, 2021))**.

1.9 Heart failure

Heart failure (HF) is a disease characterized by an unstable or insufficient cardiac output resulting from the alteration of the heart's systolic or diastolic function, or both. Diseases or injuries that promote the development of heart failure include ischemic heart disease, dilated cardiomyopathy, arterial hypertension, valvular heart disease, anemia, and toxic damage (Guellich et al., 2014). During HF, several neurohormonal mechanisms are activated to maintain cardiac output. The early stages of HF are often asymptomatic. In contrast, the progression of the disease is characterized by hyperactivation of the SNS, which leads to a chronic increase in circulating catecholamines, and over time promotes maladaptive molecular and structural changes in the heart (de Lucia et al., 2018). Moreover, the renin-angiotensin-aldosterone system (RAAS), another potent diver of cardiac remodeling, is activated in parallel, along with increases in vasopressin and natriuretic peptide concentrations (McFarlane et al., 2003)

Short-term stimulation of βARs is essential to adapt the cardiac performance to changing demand physiologically. Initially, a long-lasting activation of the SNS can compensate for the insufficient output of a heart in transition to heart failure. However, the persistent catecholamine stimulation becomes detrimental and results in altered Ca^{2+} signaling causing arrhythmia, cardiac hypertrophy, and fibrosis, further promoting a decrease in cardiac

contractility (Lohse et al., 2003). Moreover, a long-term elevation of catecholamines alters the responsiveness of the βAR signaling cascades, characterized by the downregulation of β_1AR at the plasma membrane and the G protein-coupled receptor kinase (GRK)/β-arrestin mediated uncoupling of β_1ARs and β_2ARs from G proteins, finally resulting in functional desensitization and receptor internalization during HF. Especially the upregulation of the GRK2 isoform is responsible for lowering the cardiac βAR density and responsiveness, causing a depletion in inotropic reserve (Lymperopoulos et al., 2013). Other changes contributing to cAMP signaling desensitization include the upregulation of PDEs, such as PDE1, constitutively lowering cAMP levels (Kim and Kass, 2017), and the increase in the catalytic activity of a serine/threonine phosphatase, Protein phosphatase 1, counteracting PKA-mediated phosphorylation (Chiang et al., 2018). Another desensitization mechanism is an enhanced $G\alpha_i$ coupling resulting from increased G_i protein levels at the plasma membrane, further lowering cAMP production in end-stage HF (Abu-Taha et al., 2017; El-Armouche et al., 2003).

Moreover, altered cAMP/PKA compartmentalization leads to abnormal signaling of second messengers, cAMP, and its guanosine analog, cGMP (Preedy, 2020; Wang et al., 2018). Although the β_1AR expression is downregulated in failing hearts, impairing contractility and adaptational responses to cardiac output, a chronic increase in catecholamine levels still promote structural and molecular changes in cardiomyocytes, further deteriorating cardiac function. Therefore, chronic β_1AR antagonist treatment is a widely accepted measure to counter the cardiotoxic hyperadrenergic state by blocking circulatory catecholamines, leading to resensitization of the system and decreasing the high metabolic demands of the heart (Bristow, 2011; Guellich et al., 2014).

1.10 NDPK B/C in heart physiology and failure

In contrast to the findings in healthy hearts, evidence showed that NDPKs might participate in a receptor-independent activation of $G\alpha_i$ proteins in human heart failure (Zhou & Artman, 2001). Explants from severe congestive heart failure patients showed a four-fold higher amount of NDPK A, B, and C and a three-fold higher NDPK activity on the sarcolemmal membranes than the non-failing hearts (Lutz et al., 2001). In contrast, the amount of NDPKs and the resulting enzymatic activity was not altered in the homogenate, cytosol, or other fractions obtained from cardiomyocytes. The increased amount and activity of NDPKs at plasma membranes, together with the corresponding increase in G_i protein levels (Abu-Taha et al., 2018; Feldman et al., 1988), correlated to a reduced AC activity. In line with these reports, chronic treatment of rats with isoproterenol-induced the translocation of NDPKs to the plasma membrane, which were prevented by a non-selective βAR antagonist, propranolol (Lutz et al., 2003). Conversely, in the healthy heart, the loss of NDPK B significantly reduced membranous G protein content and caveolae formation, leading to a severe loss of cardiac contractility and pump function in the zebrafish. As the formation of signalosomes often occurs

in caveolae, these findings indicate that not only the catalytic activity but also the complex formation of NDPKs with G proteins itself regulate cAMP signaling in the heart by modulating G protein levels in the signalosomes (Hippe et al., 2011; Hippe et al., 2009).

Recently, our lab reported that NDPK C is essential in forming the NDPK B/NDPK C/G protein complexes and targets these complexes to the plasma membrane in cardiomyocytes (Abu-Taha et al., 2017). Interestingly, the prevalence of NDPK C for its interaction with G_s or G_i depended on the G protein's relative expression. In end-stage heart failure patients, a higher expression of G_i has been already documented in the 1990s (Eschenhagen et al., 1992). Consistently, the formation of NDPK C-G_i complexes prevailed over NDPK C-G_s complexes, whereas the opposite was found in healthy controls. Based on these data, we hypothesized that increased amounts of NDPK B/C at the plasma membrane contribute to the G_i dependent cAMP suppression in cardiomyocytes of heart failure patients through its direct interaction with G_i (providing sufficient GTP for the activation of G_i and Gβ), shifting the prevalence from G_s-mediated AC stimulation to G_i mediated inhibition (Abu-Taha et al., 2017).

1.11 Potential use of NDPK inhibitors to treat cardiovascular diseases

Early investigations on inhibiting NDPKs enzymatic activity demonstrated that cAMP analogs such as M-mbcAMP, 8-Chloro-cAMP, and 8-Bromo-cAMP inhibited the transphosphorylase activity of NDPKs (NDPK A and NDPK B) in rat glioma cells (Anciaux et al., 1997; Schwede, Maronde, et al., 2000). Accordingly, 8-Bromo-cAMP was used to counteract the NDPK-mediated G_i activation observed in plasma membranes of heart failure patients, which corrected the reduced cAMP formation (Lutz et al., 2001). Although cAMP analogs like 8-Bromo-cAMP are cell-permeable and thus could be used as NDPK inhibitors, they contribute to various other biological effects such as activating PKA and therefore are too unspecific (Schwede, Christensen, et al., 2000). The same holds up for ellagic acid, which besides its inhibitory effects on NDPK (Buxton, 2008), also interferes with tyrosine kinase receptor signaling (Kowshik et al., 2014). As recent findings from our lab position NDPK C as a novel critical determinant of βAR/cAMP signaling that could contribute to impaired cardiac function and remodeling in human HF (Abu-Taha et al., 2017), a rather specific small-molecule inhibitor could provide a new therapeutic option. As NDPK B is also part of the complex with G proteins, an inhibitor targeting both isoforms might be an alternative. As NDPK B specifically mediates the activation of the KCa3.1 channel in pathological vascular smooth muscle cell proliferation and neointima formation (Zhou et al., 2015), a specific inhibitor of this isoform might be of interest, too. Together, all these data warrant the search for novel NDPK inhibitors that might offer therapeutic potential.

2. Aims of the study

Abnormalities in cAMP signaling and Ca^{2+} handling and homeostasis are vital features that contribute to contractile dysfunction in heart failure. Prior research provided evidence that both the protein levels and the activity of NDPKs are significantly increased in human heart failure (Lutz et al., 2001). Additionally, recent findings indicated that in end-stage human heart failure, NDPK C forms complexes with NDPK B/G_i proteins and reduces the cAMP levels, which may further compromise contractile performance (Abu-Taha et al., 2017). The underlying molecular mechanisms of NDPK B/C mediated changes in cAMP are still not understood. The present study aimed to identify a small molecule inhibitor specific for NDPK C to decipher its function in cardiomyocytes. The specific aims included:

1. To identify small-molecule compounds that can potentially inhibit NDPKs, and validate their binding site and mode of inhibition.

2. To analyze the effects of the identified compound under basal conditions and within the b-adrenergic signaling cascade in cellular models.

3. To validate the effects of the inhibitors on *ex vivo* on heart tissue and *in vivo* in animal models.

3. Materials & Methods

3.1 Materials

3.1.1 Cell culture

3.1.1a Cell culture media

Components (500ml)	Catalog number
DMEM (1000 mg/ml glucose)	D-5546; Sigma-Aldrich
DMEM (4500 mg/ml glucose)	D-6546; Sigma-Aldrich
FCS	F7524; Sigma

3.1.1b Cell isolations and cell lines

Cell type	Catalog number
AMVCMs	Self-isolated from adult mouse hearts (Section 3.2.7)
NRCMs	Self-isolated from neonatal rat hearts (Section 3.2.8)

3.1.1c Cell culture reagents and enzymes

Reagents	Company	Catalog number and details
Liberase Mix	Roche	5401089001
EDTA Trypsin 0.05%	Sigma-Aldrich	T3924
Dispase II	Roche	04942078001
Puromycin	Sigma	P7255
DNaseI	Sigma-Aldrich	11284932001
Rat-tail Collagen type I	Corning	354236
Penicillin/Streptomycin	Sigma	P4333

3.1.2 Buffers and chemicals

3.1.2a Cell culture buffers

Buffer	Catalog number
DMEM for adult cardiomyocyte isolation (a-DMEM)	0.2% BSA, 1% Pen-Strep, 1% Glutamine (200 mM), 0.1% BDM and 0.08% Taurin, 0.22% HEPES
Buffer-F	144 mM NaCl, 5.4 mM KCl, 1 mM MgCl2 , 2 mM CaCl2 and 10 mM HEPES (pH-7.3)
Hank's balanced salts	H6136; Sigma-Aldrich
Perfusion buffer	113 mM NaCl, 4.7 mM KCl, 600 µM KH_2PO_4, 600 µM $NaH_2PO_4.2\ H_2O$, 1.2 mM $MgSO_4.7\ H_2O$, 12 mM $NaHCO_3$, 10 mM $KHCO_3$, 10 mM HEPES, 30 mM Taurin, 5.5 mM Glucose, 10 mM BDM-adjusted with KOH to pH 7.4
PBS	D-5652; Sigma-Aldrich
Relaxing solution	118.3 mM NaCl, 3 mM KCl 0.5 mM CaCl2, 4 mM $MgSO_4$, 2.4 mM KH2PO4, 24.9 mM $NaHCO_3$, 10 mM Glucose, 2.2 mM Mannitol-adjusted to pH-7.4
0.5% trypsin EDTA (10x)	59427C; Sigma-Aldrich
Tyrode buffer	1mM Ca^{2+}, 140mM NaCl, 4mM KCl, 1mM $CaCl_2$, 1mM $MgCl_2$, 5mM HEPES, 10mM Glucose-adjusted to pH 7.4 with NaOH

3.1.2b Protein analysis buffers

Buffer	Contents
ADS buffer (10x)	116 mM NaCl, 20 mM HEPES, 12.5 mM NaH_2PO_4, 5.6 mM Glucose, 5.4 mM KCl, 0.8 mM $MgSO_4$, adjusted with NaOH to pH 7.35

Buffer A	20 mM Tris-HCl (pH-8.0), 2 mM $MgCl_2$, 150 mM NaCl, 3-5 % Glycerol
Buffer B	50mM Tris-HCl, pH 7.5, 2 mM MgCl2, 1 mM DTT, and 0.01 % BSA
Ponceau S (100 ml)	5 ml acetic acid; 95 ml H_2O; 0.2 g Ponceau
Laemmli buffer (4x) (50 ml)	25 ml 50% Glycerol; 10 ml 1 M Tris-HCl, pH 6.8; 5 ml 10% 2- Mercaptoethanol; 0.4% Bromophenol Blue; 10 ml H_2O
RIPA buffer	150 mM NaCl; 1.0% Triton X-100; 0.5% sodium deoxycholate; 0.1%SDS; 50 mMTris, pH 8.0
Cell lysis buffer	RIPA buffer; Protease inhibitor (Roche) (1tablet/10 ml)
Phosphotransfer assay buffer	50 mM Tris-HCl pH 7.5; 2 mM MgCl2; 1 mM DTT; 0.01% BSA
SDS-PAGE Electrophoresis buffer (5X SDS)	0.2 M Tris-HCl; 1.25 M Glycine; 0.5% SDS; 500 ml H_2O
SYPRO-fix solution	50% methanol, 7% acetic acid, 43% ultra-pure water
SYPRO-wash solution	10% methanol, 7% acetic acid, and 83% ultra-pure
TAE buffer (50X)	2 M Tris; 5.7% Acetic acid; 0.05 M EDTA pH 8.0 in 1 L H_2O
TBS (10x) TBST (1000 ml)	100 mM Tris; pH: 7.4; 1.5 M NaCl 100 ml 10x TBS; 890 ml H_2O, 10 ml; 1 ml Tween 20

Tris Buffer for stacking gel	1 M Tris, pH: 6.8
Tris Buffer for separating gel	1.5 M Tris, pH: 8.8
Western Blot transfer buffer (WB) (10x)	32.5 g Tris; 144 g Glycine; 1000 ml H_2O

3.1.3 Chemicals

Chemicals	Company	Catalog number
1,2-Propanol	Sigma-Aldrich	134368
2-Mercaptoethanol	Serva	28625
5-BrdU	Sigma	B9285
Absolute ethanol	Riedel-de Äen	32205
APS	Merck	1.012.010.100
Bromophenol Blue	Chroma-Gesellschaft	4F057
BSA	Sigma-Aldrich	A9418-5G
BSA	Sigma-Aldrich	B-4287
Chloroform	Merck	2447
Coomassie R250	ThermoFischer	20278
DMSO	Sigma-Aldrich	D8418
DAPI	Life Technologies	1603428
D-(+)-Glucose	Sigma-Aldrich	SLBF1738V
Ethanol	Richter Chemie	V-126
EDTA	Roth	8040.1
FURA 2 AM	Merckmillipore	344905
Gelatin from porcine skin	BD	214340

Glycerol	Sigma-Aldrich	G9012
HEPES	Sigma-Aldrich	H4034
HCl	Sigma-Aldrich	H1758
His60-Ni Superflow Resin	Takara	635660
Imidazole	Merck	1047160250
IPTG	Roth	CN08.02
KCl	Sigma-Aldrich	P9333
Laminin	Sigma-Aldrich	L2020
Luciferase (ATP-dependent)	Promega-Kinase-GLo	V6711
Methanol	Roth	4627.5
NaCl	Sigma-Aldrich	M7439
$NaHCO_3$	Sigma-Aldrich	S5761
NaOH	Merck	106498
Isofluorane	Piramal	09714675
PhosSTOP™	Sigma-Aldrich	4906845001
Ponceau S	Sigma-Aldrich	P-3564
Protease inhibitor	Roche	5892970001
Protein marker (uncolored)	ROTH	T8512
Protein marker (colored)	Biorad-Precision plus	1610374
Protein A/G beads	Santa Cruz	sc-2003

Roti-Block	Roth	A151.1
Rotiphorese Gel 30	Roth	3029.1
SDS	Sigma-Aldrich	74255
TEMED	Roth	T7024
Tetracaine hydrochloride	Sigma-Aldrich	136-47-0
Tris	Serva	37181
Triton-X-100	Merck	1.080.031.000
Tween 20	Sigma-Aldrich	P-7949

3.1.4 Antibodies

3.1.4a Primary antibodies for western blot

Antibody	**Catalog number; Company**	**Dilution**
Calsequestrin	PA1-913; Thermo Scientific	1:1000
$G\alpha_{i2}$	Prof. Bernd Nuernberg	1:5000
$G\alpha_{t1}$	Sc-389; Santa Cruz	1:200
Gβ	Sc-378; Santa Cruz	1:200
N1-phospho-histidine	MABS1330; Millipore	1:1000
NDPK C	Prof. Ioan Lascu	1:1000
p-ACC	3662; Cell Signaling	1:1000
p-AMPK	50081; Cell Signaling	1:1000
p-MyBP-C	ALX-215-057-R050; Enzo	1:1000
p-ser16-PLN (WB)	A010-12; Badrilla	1:5000
p-TnI	4004; Cell Signaling	1:1000

3.1.4b Secondary antibodies

Table 8: Secondary antibodies

Antibody	**Catalog number; Company**	**Dilution**
Rabbit anti-mouse peroxidase	A-9044; Sigma-Aldrich	1:20000
Goat anti-rabbit peroxidase	7074; Cell Signaling	1:2000
Goat anti-rabbit peroxidase	A-9169; Sigma-Aldrich	1:40000

3.1.5 Consumables

Consumables	Company	Catalog number
Cell counting chamber	Marienfeld	0640010
Cell culture plate (24 well, 12 well, 6 well)	Sarstedt	83.3922, 83.3921, 83.3920
Cell culture dish (6 cm, 10 cm, 15 cm)	Sarstedt	83.3901, 83.3902, 83.3903
Cell trap	Corning	CLS431750
Cell scraper	Sarstedt	83.1830
GentleMACS-C tube	Miltenyi Biotec	130-093-237
Glass bottomed dishes for IonOpix	MatTek	P35G-1.5-20-C
Gel combs	Bio-rad	1653359
Cryotube	Sarstedt	72.377
Eppendorf tubes (1.5 ml, 2 ml)	Eppendorf	0030 120.086
Eppendorf tips (1000 µl, 200 µl, 10 µl)	Eppendorf	70.760.002, 70.1130, 70.762
Conical centrifuge tubes (15 ml, 50 ml)	Sarstedt	62.554.502, 62.547.254
Nitrocellulose membrane	Amersham-Protran	10600000
Oak ridge tubes	Nalgene	T1793

Pipettes (5 ml, 10 ml, 25 ml)	Sarstedt	86.1253.001, 86.1254.001, 86.1685.001
Parafilm	Parafilm'M'	PM-996
Whatman paper	VWR	514-8013
Filtropur S 0.2	Sarstedt	31046103
Stirrup-shaped blade	Carl Roth	CK07.1
Syringe	Seidel Medipool	301229
Syringe needle 30G	BD Microlance	30400

3.1.6 Primers used for PCR

Primers	Sequence
NDPK A H118A Forward	TAACATCATCgccGGTAGCGACTCTGTTGAGAGC
NDPK A H118A Reverse	CGGCCGACCTGGATGCAG
NDPK B H118A Forward	TAACATCATCgccGGTAGCGACTCTGTTGAGAGC
NDPK B H118A Reverse	CGGCCGACCTGGATGCAG
NDPK C H135A Forward	GAACTTGATTgctGGTAGCGATAGCG
NDPK C H135A Reverse	TTGCCGACTTCGATGCAA

3.1.7 Kits

Kits	Catalog number; Company
Bacterial transformation kit	Z3001; Zymo-Mix & Go
Bio-Rad turbo blotting supplements	10026938; Bio-Rad
cAMP assay	K019-H; Arbor assays
Lumi-Light Western Blotting	12015200001; Roche
Neonatal Cardiomyocyte Isolation Kit, mouse	130-100-825; Miltenyi Biotech
Plasmid isolation kit	11754785001; Roche T1010S, NEB
Site-directed mutagenesis kit	E0554, NEB
Super Signal West Femto Maximum Sensitivity Substrate	34095; Thermo Scientific
SYPRO™ Ruby Protein Gel Stain	S12000; Thermo Scientific

3.1.8 Apparatus

Apparatus	Company
Centrifuge	Eppendorf/Hettich/Thermo Scientific
Electrophoresis chamber and apparatus	Bio-Rad
Incubator (37 °C, 5% CO_2)	Memmert
gentleMACS dissociator	Miltenyi biotec; 130-093-235
Laminar flow bench	Herasafe, Heraeus
Pipettor	Eppendorf
Multi-pipettor	Eppendorf
Microprocessor pH meter	WTW
Heating block	Thermomix comfort, Eppendorf
Bio-Rad turbo blotter	1704150
Mini-PROTEAN casting module	Bio-Rad; 1658015
Roller	Phoenix instrument-RS-TR-05
Shaker	Neolab
Sonicator	Bandelin Sonoplus; GM70
Sonicator Probe	Bandelin electronic; UW70
Spectrophotometer	Thermolabsystems Multiscan EX
Voltmeter	Biometra
Vortexer	Janke & Kunkel

Water bath	ThermoScientific
Weighing machine	Sartorius
Stereomicroscope	Eschenbach
Fluorescence microscope	Olympus
Double-distilled water system	Milli-QR; Millipore
High-temperature sterilizer	Systec
-20 °C freezer	Bosch/ Liebherr
-80 °C freezer	Hera
ELISA plate reader	AlphaImager® Innotech
Envision 2102 multilabel reader	Perkin-Elmer
Chemiluminescence imager	Vilber Fusion FX
UV transilluminator	Vilber Fusion FX

3.1.9 Software

Software	**Company**
CD analysis software	OriginLab
Excel document	Microsoft
Fluorescence microscope software	Leica
Image J	NCBI
Nanotemper	PR.ThermControl
Powerpoint document	Microsoft
References	Endnote V4
Statistics	Graph Pad Prism 6 software
Sanger sequencer	Eurofins
Word document	Microsoft

3.2 Methods

3.2.1 Competent cell preparation and transformation

BL21 (DE3), a bacterial strain deficient in protease expression, is commonly used in transforming plasmids with the T7 promoter for recombinant protein expression. The bacteria transformation kit (Zymo) containing wash buffer and competent buffer were used as per the user's manual to prepare BL21 (DE3) competent cells and stored at -80°C. The NDPK plasmids containing T7 promoter were transformed into BL21 (DE3) competent cells, prepared using the Zymo transformation method. The competent cells containing microcentrifuge tubes, stored at -80°C, were thawed on ice for ~15 minutes, and 100 pg-1 ng plasmid was added to them. The tubes were gently tapped to homogeneously mix the plasmid with the cells and incubated on ice for 5-10 minutes. After incubation, the mixture from the tubes was evenly spread in the respective antibiotic containing LB-agarose plates, using a glass spreader. These plates were incubated overnight at 37°C in an inverted position. The next day, the agarose plates with bacterial colonies were stored at 4°C, until used beforeinoculation.

A single colony, picked from a transformed LB plate, was inoculated into 10 ml 2x Yeast-tryptone (2x YT) broth, incubated overnight at 37°C, shaking at 180 rpm. The next day, the overnight grown culture, called primary culture, was again inoculated into 1000 ml 2x YT media, giving a dilution of 1:100 of the primary culture into the new media, called secondary culture. The secondary culture was incubated in a shaking incubator at 37°C for about 3-4 hours, intermittently, measuring the optical density (OD) until 0.6. At this OD, a final concentration of 0.5 mM IPTG was added to the secondary culture to induce the over-expression of NDPKs. After adding IPTG, the culture was grown for about 4 hours. Later, the cells were harvested by centrifugation at 4°C, 6000 rpm, for 10 minutes (the pellet was stored at -80°C, until the start of the protein purification process).

3.2.2 Generation of catalytically inactive NDPK mutants

A site-directed mutagenesis kit was used to replace the catalytically active histidine amino acid with alanine in all the NDPK isoforms. The respective primers for point mutant generation were dissolved in ultra-pure water to give a final stock concentration of 10 µM. A reaction mixture of 25 µl containing 12.5 µl each of forward and reverse primers, 1 µl of NDPK plasmid (1-25 ng/µl), 12.5 µl high fidelity polymerase, and 9 µl nuclease-free water was used to amplify the NDPK plasmids. For amplification, an initial denaturation temperature of 98°C for 30 seconds, followed by 25 cycles of denaturation at 98°C for 10 seconds, annealing at 65°C for 30 seconds, and extension at 72°C for 2 minutes. The last extension cycle at 72°C for 5 minutes was used to ensure the completion of plasmid amplification. The methylated adenine (^{m}A) cleavage reaction was prepared by mixing 1 µl of the PCR product, 5 µl of 2X KLD reaction buffer, 1 µl of KLD enzyme mix, and 3 µl of nuclease-free water, by mixing them well by

pipetting up and down and incubated at room temperature for five minutes. This mixture was transformed into Top-10 competent cells using the Zymo transformation method and plated onto ampicillin (100 µg/ml) containing agarose plates. The next day, positive colonies were picked, and the respective plasmids were isolated using a plasmid miniprep kit, strictly following the manufacturer's instructions. The isolated plasmids were sequenced to confirm the amino acid change at the active site.

3.2.3 Purification of NDPK isoforms

The bacterial cell pellet from 1000 ml culture was dissolved in 80 ml of 'buffer A' with added protease inhibitors. The cells were gently dissolved in buffer A to obtain a homogenous suspension. The bacterial cells were lysed using a sonicator probe, with a 30 second on/off pulsing and 12-15 cycles. The cell lysate was centrifuged at 14000 rpm in 30 ml Oak Ridge centrifuge tubes for 20 minutes at 4°C to pellet down the unlysed cells. The supernatant thus obtained was eventually treated with 10 mM imidazole to reduce non-specific interactions and applied onto 1-2 ml bed volume of His60-Ni Superflow Resin and further incubated at 4°C on a roller for 30 minutes. An empty column with a frit was used to trap the overexpressed protein bound to Ni-NTA beads. The flow-through was collected to test the binding efficiency; a fraction of this was stored to run on an SDS- PAGE. The trapped beads were washed with a gradient of imidazole (10-30 mM) and NaCl (50-200 mM) in 'buffer A' with 5-6 washes. Wash fractions were also collected to further analyze them on SDS-PAGE for the presence of purified protein if washed away. To elute the protein bound to the beads, around 50 ml of elution buffer (300 mM imidazole in buffer A) was applied to the beads after washes and incubated for about 2-5 minutes. The flow-through was collected in 3 different eluates, each with 2 ml, the rest in 15 ml tubes. The flow-through from the lysate, wash fractions, and elution fractions were run on an SDS-PAGE and coomassie stained to detect the proteins.

3.2.4 Autophosphorylation Assay

The autophosphorylation of NDPKs was analyzed with ATP as a substrate in the presence of $MgCl_2$. 50ng of stock NDPKs were incubated with and without 1mM ATP for 5 minutes at room temperature in 30 µl buffer A. Reaction was stopped by adding 5 mM EDTA for Mg^{2+} chelation. 10 µl of 4X Laemmli buffer was added, and the samples were stored overnight at 4°C. Proteins were separated without heat denaturation on two 15% SDS-PAGE in replicates: one gel was stained with SYPRO Ruby Protein Gel Stain as described later. Proteins from the second gel were transferred onto a 0.2 µm nitrocellulose membrane and probed overnight at 4°C with a 1:1000 αN1-Phosphohistidine (1-pHis) antibody clone SC1-1, followed by 1:80,000 horseradish peroxidase (hrp)-conjugated secondary antibody at room temperature for 60 minutes. The blots were developed using SuperSignal West Femto Maximum Sensitivity Substrate and visualized with a chemiluminescence imaging system.

3.2.5 SYPRO Ruby staining

SYPRO Ruby Protein Gel Stain is a highly sensitive, ready-to-use fluorescent stain to detect total proteins separated by PAGE. After electrophoresis, the gels were placed into a clean container with 20 ml of SYPRO-fix solution and agitated on an orbital shaker for 30 minutes. This step was repeated once more with the new SYPRO-fix solution. The fix solution was discarded, and 20 ml of SYPRO Ruby gel stain was added to the container and agitated on an orbital shaker overnight. The next day, the gels were washed by transferring them into a clean container with 30 ml of SYPRO-wash solution and incubated for 30 minutes at RT. The wash buffer was discarded and replaced with ultrapure water at least two times for 5 minutes each to prevent possible corrosive damage to the imager. The stained proteins were visualized under a UV transilluminator.

3.2.6 Phosphotransfer assay

The phosphotransfer activity of the NDPKs was measured in a reaction mixture containing buffer B. The three distinct inhibitors (SanWie1/2/3) were serially diluted; thus, 3x stock concentrations were pipetted in replicates on a 384 well plate. To these wells, one volume of the respective NDPK protein solution (NDPK A/B/C) was added from stock proteins (diluted in buffer A to a concentration of 300 pM) and incubated at RT for 30 minutes. The substrate mixture (300 µM GTP and 30 µM ADP in buffer A) was added to the protein-inhibitor incubated wells. This mixture was incubated at room temperature for 30 minutes, and two volumes of the Kinase-GLO reagent containing an ATP-dependent firefly luciferase were added. The luminescence was measured using a plate reader. Six different concentrations of ATP (0 - 10 µM) were used as standards for a calibration curve to calculate the amount of ATP produced by the different NDPKs. All readings were obtained under conditions where the ATP formation was still linear with time and enzyme concentration.

3.2.7 SDS-polyacrylamide gel electrophoresis (SDS-PAGE)

SDS-PAGE is used to separate polypeptides based on their size. By applying an electricity gradient, the polypeptides are resolved based on their mass by charge ratio. SDS added as a component of the gel and SDS in the protein samples from Laemmli buffer provides a negative charge to the peptides. Consequently, all the peptides are negatively charged; the lower molecular mass containing peptides moves faster, followed by the peptides with increasing molecular mass. SDS-PAGE comprises a stacking gel and a resolving gel. The protein samples are loaded onto the stacking gel, which later runs into resolving gel, where the proteins are resolved.

3.2.8 Immunoblot assay

The protein samples were loaded into the SDS-PAGE gels along with the prestained protein marker. Initially, the gels were run at 90 volts for 15-20 minutes, later increased to 120-140

volts in the resolving gel until the dye-front reaches the bottom of the gel. The proteins from the gel were transferred onto a nitrocellulose membrane at room temperature using a pre-listed protocol (standard, 2.5 amp, up to 25 volts for 30 minutes) in a semi-dry transfer apparatus, Trans blot turbo. After the transfer, the blots were transferred to a box with Ponceau stain. They were cut according to the molecular weight of the respective proteins and incubated in a blocking buffer for 60 min at room temperature. These blots were then washed with 1x TBST and incubated overnight at 4°C with the respective primary antibodies in the dilutions prescribed by the manufacturer, dissolved in 1x TBST. The blots were washed with 1x TBST three times, 10 minutes each, and incubated with 1:40000 dilution of anti-rabbit hrp or 1:20000 dilution of anti-mouse hrp antibodies, respectively at room temperature for 1 hour. Again, the blots were washed with 1xTBST three times, each for 10 minutes. Eventually, the blots were developed using SuperSignal West Femto Maximum Sensitivity Substrate and visualized with a chemiluminescence imager.

3.2.9 Circular Dichroism

Circular Dichroism (CD) is an ideal biophysical method used to rapidly determine the secondary structure and folding properties of proteins. CD is defined as dissimilar absorption of left-handed and right-handed circularly polarized lights. Whenever asymmetric molecules such as protein molecules interact with light, they can absorb the two different circularly polarized light in different extents with varying indices of refraction for the two waves. Thus, the difference in absorbance of right and left polarized lights results in an elliptically polarized light, and the molar ellipticity can be determined for optically active molecules (Greenfield, 2006). The protein samples of NDPK C and NDPK C with SanWie3 were used in the CD study at equimolar ratios of 10 µM each with a scan between 260 and 180 nm. The reading was taken at every 0.1 nm, and the CD units in mdeg were estimated. The resulting spectra from both NDPK C and NDPK C with SanWie3 were analyzed using CONTIN-LL and SELCON-3. The animated graphics were obtained by applying the spectral data into OrginLab software.

3.2.10 Nano Differential Scanning Fluorimetry

Real-time simultaneous monitoring of the intrinsic tryptophan fluorescence (ITF) at 330 nm and 350 nm was performed in Prometheus NT.48 instrument from NanoTemper Technologies with an excitation wavelength of 280 nm (Magnusson et al., 2019). Capillaries were filled with 10 µl suspension of 10 µM NDPK C or 10 µM SanWie3+10 µM NDPK C, placed into the sample holder, and the temperature was increased from 20 to 90°C at a ramp rate of 1°C/min, with one fluorescence measurement per 0.014°C. The recorded emission intensity ratio (350nm/330nm), representing the tryptophan fluorescence intensity and the shift of the emission maximum to higher wavelengths, or lower wavelengths, was plotted as a function of the temperature. The fluorescence intensity ratio and first derivative were calculated using the manufacturer's software (nanotemper).

3.2 11 cAMP assay

A direct cyclic AMP enzyme immunoassay was performed to measure the cAMP levels in neonatal rat cardiomyocytes (NRCM). NRCM were seeded on 12 well plates with ~1 million cells per well, at two different concentrations of SanWie3 (3 µM and 10 µM) and 1 µM isoproterenol in replicates. As NRCM have higher cAMP levels, acetylation protocol was not used. The cells were pre-incubated for 12 h with a serum-free medium. Cell lysis buffers containing SDS (>0.01%) are not entirely compatible with the kit. Therefore, acidified ice-cold 'sample diluent' from the kit was added to the cells and incubated at room temperature for 10 minutes to denature the proteins, mainly phosphodiesterases. The cells were scraped, and the lysates were collected in microcentrifuge tubes. They were centrifuged at 13,000 rpm for 15 min at 4°C. The supernatant was used to determine the cAMP level quantitatively through an ELISA kit, strictly following the manufacturer's instructions. The cAMP content was indirectly measured based on the OD obtained from the control cAMP binding in each sample, measured in pmol/ml. Using a four-parameter logistic curve-fitting method by applying cAMP measurements from the standard samples, the cAMP amount from the NRCM lysates was estimated through an online analysis software, 'myassays.com'. A predefined protocol for arbor assays Cyclic AMP Direct EIA Kit was used in the software.

3.2.12 Resazurin assay

Freshly isolated cells (NRCM/AMVCM) were seeded on 12 well plates. Two different concentrations of SanWie3, 3 µM, and 10 µM were used along with the untreated wells in both NRCM and AMVCM cell types at different time points, starting from 3 hours, up to 27 hours. During the end of each time point, the cell culture media was replaced with resazurin dye, dissolved in 1X HBSS at a final concentration of 44 µM (1X), and incubated at 37°C for 2 hours. Later, 100 µl of the supernatant was collected from each well at every time point from the untreated, and the SW3 treated cells for quantifying the resofurin levels as a fluorimetric measurement, using a predefined protocol on the multilabel reader.

3.2.13 Neonatal Rat Cardiomyocyte (NRCM) preparation

All the enzymes from the neonatal cardiomyocyte isolation kit were aliquoted and stored according to the instructions. 1-3 day old baby rats were collected from the animal house. They were decapitated, and the body was dissected at the thorax region to remove the heart. The isolated hearts were collected in a 1x ADS buffer. Before initiating the cardiomyocyte preparation, enzyme P and buffer Y (1 aliquot each for ten hearts) were added to a 15 ml centrifuge tube and placed in a 37°C water bath. All the hearts were transferred to a 10 cm cell culture dish with a small amount of 1X ADS buffer, were placed on ice. The atria were cut and discarded; the ventricles were collected into another 10 cm cell culture dish with 1X ADS buffer and minced using a stirrup-shaped blade until the tissue was cut into tiny pieces. The remaining

buffers for the heart digestion (enzyme A, enzyme D, and enzyme X- one aliquot each for ten hearts) were added to enzyme P and buffer Y containing solution. The minced tissue was transferred into a gentleMACS-C tube. The supernatant, without any tissue, was discarded, and the enzyme mixture was added to the C tube. A maximum of 20 heart tissue particles was added to a C tube. The 'neo-heart' program in gentleMACS dissociator was used with three alternate cycles each, 15 min incubation at 37°C and dissociation in gentleMACS. The dissociated heart tissue was filtered into a 50 ml centrifuge tube using a cell trap to remove the undigested tissue. Complete DMEM (DMEM with 1% Pen-Strep, 1% Glutamine (200 mM), 10% FCS) was added to the tube for enzyme deactivation. These tubes were centrifuged at 800 rpm for 15 minutes, and the cell pellet was dissolved in fresh c-DMEM to plate on 10 cm cell culture dishes with the cells from 10 hearts into one cell culture dish. The plates were incubated at 37°C for two 45-minute cycles; each time vigorously washed with 10 ml pipettes to dissociate the weakly bound cardiomyocytes, retaining the cardiac fibroblasts. The cardiomyocyte fraction was added with 5-BrdU at a final concentration of 1x and plated on the respective cell culture plates, coated with 1% collagen shortly before the cell seeding.

3.2.14 Adult mouse ventricular cardiomyocyte isolation

Langendorff method was used to isolate AMVCM from isolated adult mouse hearts. This method aims to supply the heart with oxygen and metabolites (perfusion buffer) via a single cannula inserted into the ascending aorta. The perfusion buffer with the liberase mix was perfused through the aorta towards the heart with the help of an external pump to digest the heart tissue. Before the isolation process, the water bath was heated up to 40°C, and the peristaltic pump was switched on with a flow rate of 3.5 ml/min. The Langendorff columns were rinsed with ultrapure water and perfusion buffer to clear all air bubbles in the hose system. The mice were intraperitoneally injected with heparin, 200 µl (1:50 diluted in 0.9%NaCl) before 30 minutes of isolation.

The mouse was anesthetized using isoflurane and euthanized by cervical dislocation. The heart was carefully dissected from the body and immediately placed into an ice-cold perfusion buffer. It was hung to a needle, using a clamp, and tightened with surgery suture, later rinsed with perfusion buffer for 1-2 minutes. The needle with the heart was transferred to the Langendorff system and perfused with trypsin and liberase containing perfusion buffer for 11 minutes, and 2.5 ml of which was collected in a 60 mm dish. Later the digested heart was collected into this dish and cut into small pieces for 30 seconds; immediately, 2.5 ml of stop buffer 1 (perfusion buffer with 1% BSA and 50 µM Ca^{2+}) was added and pipetted up and down for 3 minutes with a 1 ml pipette tip, cut at the end. The heart tissue was transferred into a 50 ml tube through a 100 µM mesh to allow the live cells to settle down for 11-15 minutes. The supernatant was discarded, and 5 ml of stop buffer 2 (perfusion buffer with 0.5% BSA and 38 µM Ca^{2+}) was added to the cells. Four minutes later, Ca^{2+} treatment was performed with

increasing Ca^{2+} concentrations (0.1 mM to 0.8 mM). Subsequently, the cells were incubated at 37°C for 15 minutes, later a-DMEM was added to suspend them. Eventually, the cells and seeded onto 12 well plates, previously coated with laminin.

3.2.15 Cardiomyocyte lysate preparation

The two different cardiomyocyte cell types (neonatal and adult) and the pulverized heart samples were added with 150-200 µl of Kranias buffer with protease (1:50) and phosphatase inhibitors (1:10). All the cell and tissue samples were added into microcentrifuge tubes with the already added metal beads. Tissue lyser was used to lyse the cells (1 cycle at 30 rpm for 30 seconds) and the tissue samples (3 cycles at 30 rpm for 30 seconds each). Then, the samples were centrifuged in a desktop centrifuge at room temperature at 13,000 rpm for 15 minutes. The supernatants were collected into new tubes; to these, 4X Laemmli buffer (without glycerol) was added to make a final concentration of 1X Laemmli buffer. The samples were heated at 95°C for 5 minutes. All the lysates were immediately used in the SDS-PAGE run or stored at -20°C for later use.

3.2.16 Hydrogen Deuterium eXchange Mass Spectroscopy (HDX-MS)

The HDX samples were prepared by LEAP robot-HDX, Marburg. Self-prepared Pepsin was used to digest the protein (NDPK C). HDX standard (1H/2D with 10 mM Tris-Cl, pH 8.0, 2 mM $MgCl_2$ 1% (v/v) DMSO) with NDPK C (50 µM) and ligand (100 µM) was run at 30 µl/min at 25°C. Quenching (400 mM KH_2PO_4, 2M Guanidine-HCl, pH 2.2) was at 1°C. HDX was performed for apoprotein with 198 µl 50 µM NDPK, and 2 µl DMSO and for ligand-bound protein with 198 µl 50 µM NDPK, and 2 µl SanWie3. Exchange times of HDX were read at the following time points: 00:00:00

00:00:10

00:01:35

00:16:40

02:46:40

A peptide coverage map of NDPK C was generated based on the deuterium incorporation. The relative deuterium exchange was mapped by estimating deuterium incorporation in NDPK C +/- SanWie3 bound NDPK C. The difference in the HDX on the crystal structure of NDPK C was eventually mapped.

3.2.17 Molecular docking studies using bioinformatics

The crystal structure of NDPK-C with co-crystallized ADP (PDB entry: 1ZS6) was used for docking experiments with GOLD Suite v.5.2 (Verdonk et al., 2003) and GoldScore as the primary scoring function. Before docking, water molecules were removed, and the protein was

protonated using the “Protonate 3D” application included in MOE2019 (Molecular Operating Environment, MOE2019, Chemical Computing Group, Montreal, QC, Canada). All binding models were minimized and further analyzed in LigandScout 4.4 (Inte:ligand, Vienna, Austria) (Wolber et al., 2006) by using a three-dimensional pharmacophore approach (Schaller et al., 2020). The prediction of metabolites was performed with the web tool GLORY by using the *MaxCoverage* model

3.2.18 FRET assays

FRET is a non-radiative energy transfer phenomenon of dipole-dipole coupling between two fluorophores. The transferred emission energy from the donor triggers fluorescence emission of the acceptor positioned typically within 1 to 10 nanometers (nm). Subcellular targeted fluorescence resonance energy transfer (FRET) sensors can precisely locate and measure compartmentalized cAMP, which helps in estimating the range of effector activation. Cells expressing the Epac1-camps sensor can be prepared by isolation of primary adult mouse left ventricular cardiomyocytes expressing Epac1-camps

Primary adult left ventricular cardiomyocytes expressing Epac1.cAMPs were isolated involving retrograde perfusion of the heart via the aorta (Lagendorff method-section-3.2.14). Glass bottomed dishes were used similar to the AMVCM isolation. One hour after plating, the culture media was replaced with DMEM supplemented with 2 mM L-glutamine and 0.1 mg/ml BSA. Later, FRET measurements were performed on these cells with or without SanWie3. FRET imaging of intracellular cAMP was performed using the steps, strictly following the FRET-cAMP imaging protocol (Borner et al., 2011). An unselective PDE inhibitor, IBMX, and forskolin were used to elevate the maximum cAMP response.

3.2.19 Calcium handling and cell contractility measurement

The adult mouse ventricular cardiomyocytes (AMVCM) isolated using Langendorff’s method were seeded on laminin-coated glass-bottomed dishes. Cells were allowed to attach to the coating for 30-120 min inside the incubator at 37°C, before using them for the experiments. IonOptix measurements are used for quantifying cellular ion levels and cardiomyocyte contractility using fluorescence indicators. The culture media from the cells was replaced with Ca^{2+} containing tyrode buffer before IonOptix measurements. For basal measurements, cells were loaded with 1 µM FURA 2 AM for 20 minutes. For SW3 treatment, cells were incubated with SW3 (10 µM) 10 minutes before FURA 2 AM loading, thus making a 30-minute incubation in SW3. The dishes were placed on an inverted epifluorescence microscope inside the IonOptix apparatus. Laser-mediated excitation at alternating wavelengths of 340/380 nm resulted in an emission detected with a photomultiplier at <515 nm for each excitation wavelength. The sarcomere length was recorded with a video camera and calculated by Fourier transformation of the intensity profile from the brightfield image. The cells were field

stimulated with platinum bath electrodes at 0.5 Hz, 10 volts to steady-state before Ca^{2+} and contractions were recorded simultaneously. The data are presented as the emission ratio of the alternating excitation wavelengths 340/380 and the sarcomere length as µm.

3.2.20 Ca^{2+} load measurements

Briefly, mice were anesthetized with isoflurane, and the hearts were quickly excised after cervical dislocation and subsequently mounted on a Langendorff perfusion system. The hearts were retrogradely perfused for 4 min (37 °C, pH 7.4) with nominally Ca^{2+}-free solution containing perfusion buffer, with added trypsin (0.6%), and $CaCl_2$ (0.125 mM) until they became flaccid. Ventricular tissue was collected in perfusion buffer containing 5% bovine calf serum to stop the digestion, cut into small pieces, dispersed, and filtered until no solid tissue was left. After calcium reintroduction by stepwise increasing Ca^{2+} from 0.1 mM to 0.8 mM, cardiomyocytes were plated on laminin-coated glass coverslips. Cells were allowed to settle and attach to the coating for 30 minutes at room temperature (RT) before using them for the experiments. For the Ca^{2+} measurements, cells were loaded with 2.5 µM Fura-2 acetoxymethyl ester (Invitrogen) and pluronic acid for 15 minutes in tyrode buffer at room temperature followed by a 15 min de-esterification period. The same protocol of IonOptix measurements (as mentioned in section 3.2.19) was followed. SR Ca^{2+} load was determined by rapid caffeine application (10 mM) after cells have been paced to a steady state at 0.5 Hz immediately after the last stimulus.

SR-Ca^{2+} leak measurements were performed at room temperature. Tetracaine solution (0 Na^+ and 0 Ca^{2+} with tetracaine at 1 mM) was used to block the resting Ca^{2+} leak. Cell culture media containing cardiomyocytes was replaced with tyrode buffer containing 2 mM Ca^{2+}. Cells were stimulated at 0.5 Hz for at least 20 minutes to bring the cellular Ca^{2+} to a steady-state. Immediately after the last pulse, tyrode was replaced with tetracaine solution to block the Na-Ca^{2+} exchange (primary Ca^{2+} influx and efflux mechanism at rest), was therefore blocked with little or no Ca^{2+} entering or leaving the resting cell. In control cells, tyrode buffer with 0 Na^+ and 0 Ca^{2+} and no tetracaine for 30 seconds, later 10 mM caffeine was added for SR Ca^{2+} release and to deplete the Ca^{2+} stores. The difference in levels of baseline Ca^{2+} with and without tetracaine was considered Ca^{2+} leak mediated by RyRs. To assess the effect of SanWie3, a subset of cells with 10µM of the inhibitor was incubated for 1 hr at RT before recording Ca^{2+} transients and SR-Ca^{2+} leak (Shannon et al., 2002).

3.2.21 Rat heart-muscle strip contractility measurement

Rats were anesthetized before isolating the hearts, which are dissected free of connective tissue and transferred to ice-cold 0.9% containing dish and weighed. The hearts were dissected to isolate papillary muscle strips. To measure the contractility of these papillary muscle strips, they were mounted onto the individual chambers in the organ bath chambers

containing a relaxing solution. After mounting, the strips were stretched to ~0.3 g diastolic tension, allowed to relax for ~5 minutes. Subsequently, the relaxing solution was replaced with a solution of the identical composition except for 1.8 mM $CaCl_2$ and 1.2 mM $MgSO_4$ concentrations. The muscle strips were field stimulated at 10-20 mA and a frequency of 1 Hz with impulses of 5 ms duration. The papillary muscle strips which are isometrically contracting were stretched to the maximum of their length-tension curve. Contraction–relaxation cycles were recorded and analyzed, and the basal contractility was expressed as a maximal developed force. Inotropic responses were expressed as changes in the maximal development of force (Skomedal et al., 1997). On average, 10-20 contraction-relaxation cycles were measured for each strip. Isoproterenol was used in a concentration gradient with increasing concentrations (0.1-300 nM). For SanWie3 treated, an equal number of muscle strips were used with preincubation of SanWie3 for 30 minutes at 10 µM. An antiarrhythmic drug, Lidocaine (10 µM), was used for both the control and SanWie3 treated strips.

3.2.22 Data quantification and statistical analysis

For immunoblot analysis, the images from protein visualization were used for quantification. Images were loaded in Image J software, and individual bands were selected using the 'Select tool'. The area of the select tool was adjusted to allow the maximum amountof the band and the minimum amount of the background to be selected. The 'measure' function was used to estimate the density of the selected band. By maintaining the 'Area' parameter identical, the successive bands on the same membrane were measured. 'Median' was measured for all the quantifications. The results were then analyzed for statistical significance using the GraphPad Prism 6 software. The data were presented as mean±SD. Statistical significance was established with paired/unpaired student's t-test or Analysis of Variance (ANOVA) with Tukey's post-test. p values < 0.05 were considered statistically significant.

4. Results

4.1 The small molecular compound SanWie3 is a preferential NDPK C inhibitor

4.1.1 *In vitro* validation of the NDPK C/G protein interaction

A recent report from our lab revealed that NDPK C is an essential component of the NDPK B/G proteins complex formation (Abu-Taha et al., 2017). Far western blot experiments indicated that with sufficient amounts of Gβγ, NDPK C shows a similar affinity to both G_s and G_i proteins. Here, we aimed to confirm this interaction through a pull-down assay using the soluble G_i family member transducin ($G_t\alpha\beta\gamma$). To this end, purified transducin and His-tagged NDPK C were incubated together and trapped over Ni-NTA agarose beads. The eluates were visualized on a fluorescent-stained acrylamide gel. In line with previous observations, the eluted fractions showed the presence of transducin along with NDPK C (Fig. 6, upper panel), indicating a direct interaction of transducin with the column-bound NDPK C. To exclude any unspecific binding of transducin to the agarose beads, flow-through and eluates in the absence of NDPK C were additionally collected but did not show significant amounts of protein in either of the fractions. The elution of Gα and Gβ subunits of transducin was confirmed by immunoblot using the respective antibodies (Fig. 6, lower panel).

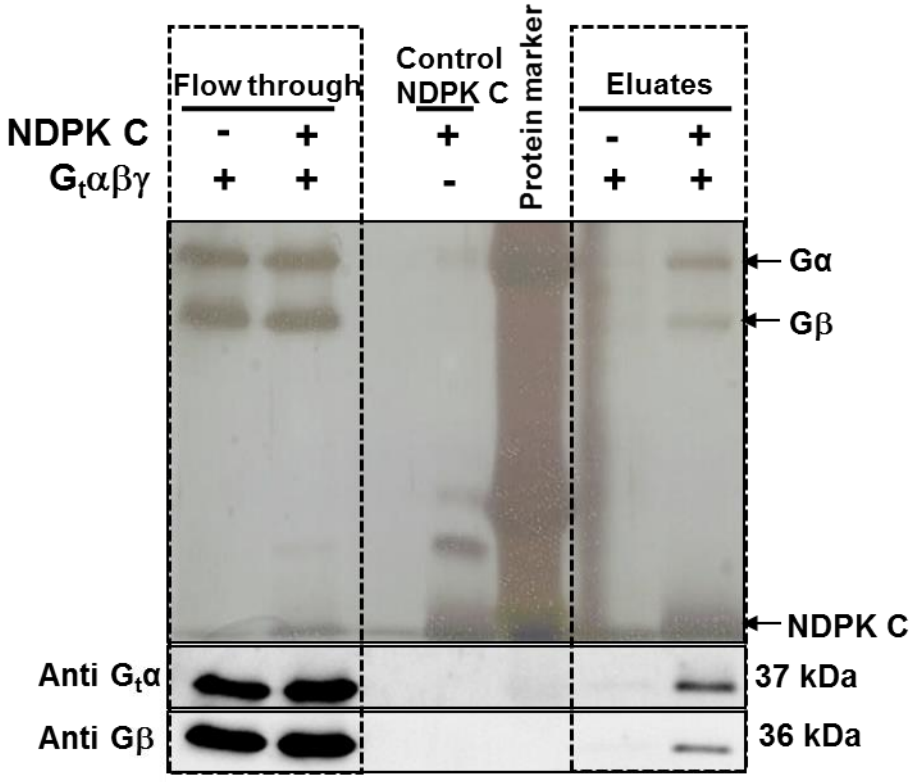

Fig 6: NDPK C directly interacts with transducin

Transducin and NDPK C together in equimolar ratios, and transducin alone were incubated at room temperature for 60 minutes. Ni-NTA beads were added to the protein-containing vials and further incubated for 45 minutes. The flow-through from the protein mixtures was collected separately (Fig 6,

left panel), the beads were vigorously washed with imidazole (10 mM) and NaCl (150 mM) containing buffer and subsequently eluted with the same buffer containing 200 mM imidazole. The upper panel represents a fluorescence stained (SYPRO Ruby) gel, showing the α- and β-subunits of transducin and the NDPK C. The lower panel is a representative immunoblot using $G_t\alpha$ and Gβ specific antibodies.

4.1.2 Confirmation of the catalytic activity of the purified NDPK isoforms

Knockdown of NDPK B or NDPK C in zebrafish embryos and NRCM resulted in a decrease of basal and isoproterenol-mediated cAMP levels, indicating an NDPK C/NDPK B complex formation that preferentially involves G_s proteins. In contrast, increased NDPKs levels at the plasma membrane of patients with end-stage heart failure (Lutz et al., 2001) are assumed to negatively influence cAMP levels by interacting with the highly abundant G_i proteins observed in these patients and thus further compromise contractility (Abu-Taha et al., 2017; Hippe et al., 2009). Therefore, in a therapeutic approach, we intended to validate and further develop first hit NDPK inhibitory compounds obtained from a kinase activity screen by using in vitro-purified recombinant human NDPK isoforms. To this end, hexahistidine-tagged NDPKs (NDPK A, B, and C) and their respective catalytically inactive mutants, with the catalytically required histidine replaced with alanine, were purified by affinity chromatography. WT NDPKs, which possess the catalytically active histidine residue (H118 in NDPK A/B, H135 in NDPK C), are intermediately phosphorylated while transferring the high-energy terminal phosphate from NTPs to NDPs. In the absence of an NDP as acceptor substrate, this intermediary state can be detected as autophosphorylation of NDPKs. To validate the concentration and purity of the recombinant proteins, similar amounts of the WT NDPK A/B/C and the catalytically inactive isoforms were separated on an SDS gel and visualized by a fluorescence dye (Fig. 7A-upper panel). Using MgATP as a substrate, the extent of autophosphorylation of the purified enzymes was detected by an N1-phosphohistidine specific antibody via immunoblot. A specific signal was detected only in the WT enzymes demonstrating the autophosphorylation of the catalytically active histidine residue. Protein samples without MgATP were used as negative controls (Fig. 7A, lower panel).

The phosphate transfer potential of NDPKs in transferring the high-energy phosphate from NTP to NDP was estimated by a ‘phosphotransfer’ assay (Fig. 7C). Applying ADP+GTP as substrates, NDPKs produce ATP, which the ATP-dependent firefly luciferase can use to produce a luminescence signal proportional to the amount of the generated ATP. Thus, by measuring the luminescence, the enzymatic activity of NDPK can be indirectly quantified. Only the WT NDPK isoforms were able to generate ATP, and therefore their ability to transfer high energy phosphate (Fig. 7B) could be confirmed.

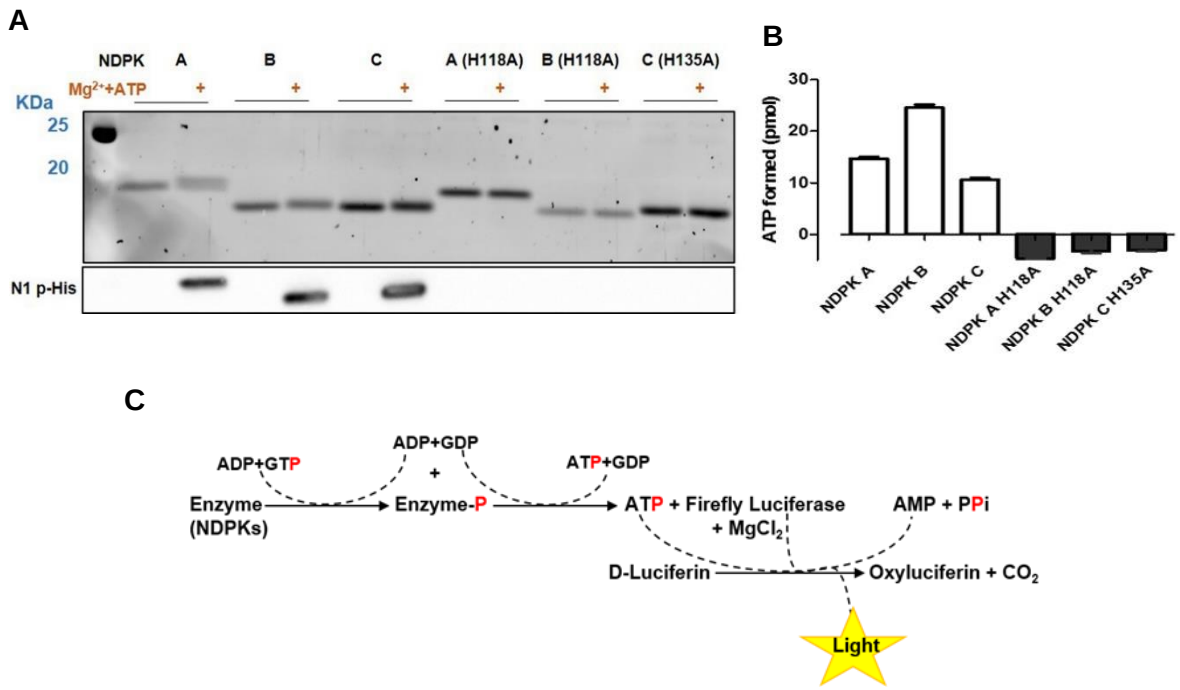

Figure 7: Purified wild type NDPK enzymes are enzymatic active compared to their respective catalytic-site inactive mutants

(A) Fluorescent stained (SYPRO Ruby) gel loaded with three different NDPK isoforms (NDPK A, B, and C) with their respective catalytically inactive mutants and full-length NDPK C. MgATP was present in every second lane (upper panel). Lower panel; a representative immunoblot, performed under identical conditions with the same set of proteins from the fluorescently stained gel, probed with an N1-phospho histidine specific antibody. (B) Phosphotransfer assay with the three wild-type isoforms and the respective catalytically inactive mutants. The enzymatic activity of NDPKs is given as the amount of ATP formed in pmol based on a standardization performed with increasing amounts of ATP.

4.1.3 Optimization of the phosphotransfer conditions for the comparison of potential inhibitors

The Michaelis Menten equation describes one substrate-one product enzyme kinetics. It links the enzymatic reaction rate to the substrate concentration, assuming that the concentration of the enzyme remains constant. A linear relationship of the enzymatic activity can be defined by substrate consumption over time and is an essential condition to estimate the efficacy of an enzyme inhibitor. At a fixed NTP concentration, NDPKs display a pseudo-Michaelis-Menten kinetic (Schnell, 2014). Thus, to determine the adequate concentration range for linear enzyme activity, different enzyme concentrations were applied using NDPK B as a representative for all NDPK isoforms in the presence of fixed concentrations of the substrates ADP and GTP. A linear increase in ATP formation was observed after a 30-minute incubation time in the range of 10 pM–1 nM of enzyme concentration (Fig. 8A). Subsequently, 120 pM NDPK B was used to measure the accumulation of the product ATP over time. A time-dependent linear increase in ATP formation was confirmed (Fig. 8B) over the initial chosen incubation time of 30 minutes. Finally, the enzyme-substrate dependence was tested with increasing concentrations of the

substrate ADP and three different concentrations of the phospho-donor GTP (50, 100, and 500 µM). A linear relationship between the substrate and product concentration was observed up to 30 µM ADP. This relation was independent of the chosen GTP concentrations. However, the enzyme-catalysed reaction was inhibited at higher ADP concentrations instead of reaching a steady-state equilibrium at maximum reaction speed. Higher ADP concentrations saturated NDPK B, resulting in the formation of a stable NDPK B-ADP complex. This process is called "abortive complex formation" and has been described for all NDPKs (Mourad & Parks, 1966a) (Fig. 8C). A double-reciprocal plot was generated by inverting the x- and y-axes to demonstrate the abortive complex formation at higher substrate concentrations. This approach visualizes the pseudo-Michaelis Menten kinetics at a fixed concentration of the first substrate GTP and altering the concentrations of the second substrate ADP. With increasing ADP concentrations, the enzymatic activity was decreased especially in the presence of lower GTP concentrations, showing the described abortive complex formation (Mourad & Parks, 1966b) (Fig. 8D). Therefore, the linear range concentrations of the substrate, 10 µM ADP with 100 µM of the phosphate donor GTP, were chosen for further investigations using 120 pM of the enzyme and an incubation time of 30 minutes.

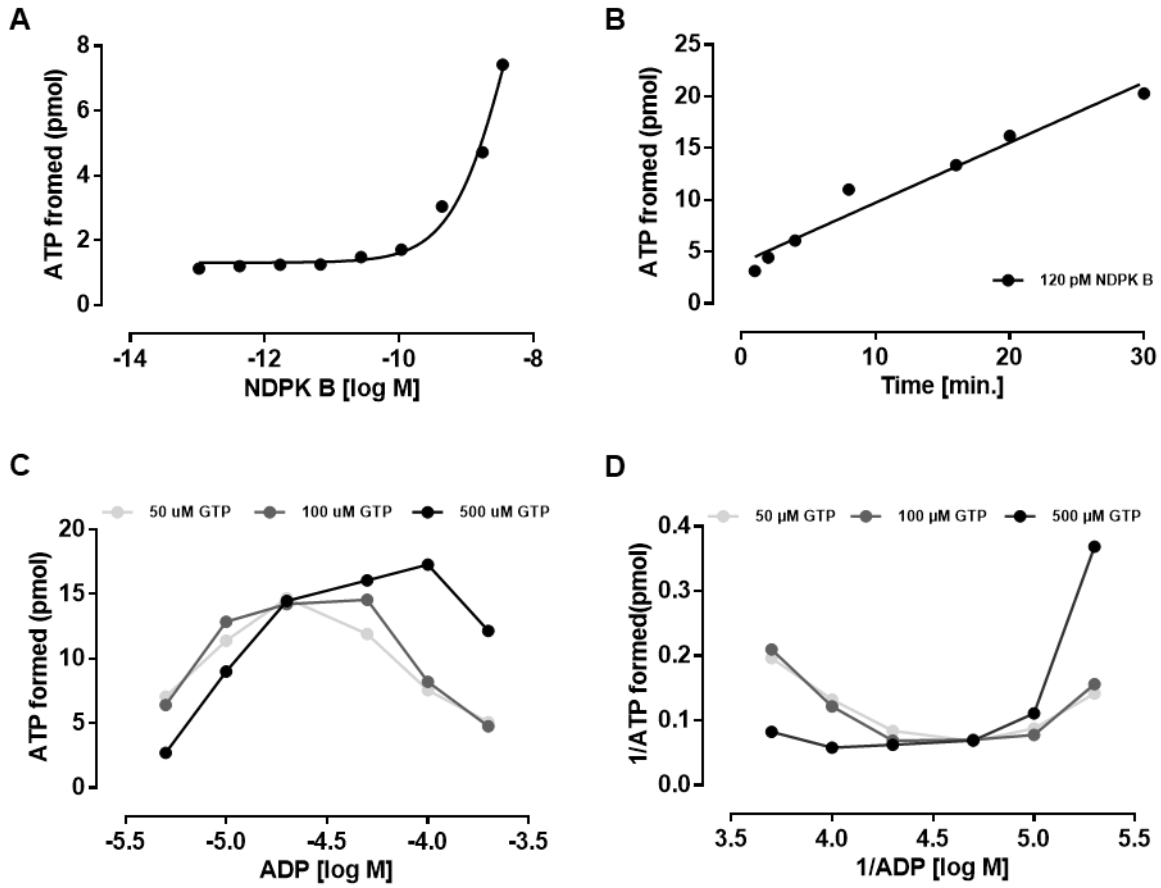

Figure 8: NDPK enzymatic activity had a linear relationship with time, enzyme, and substrate concentrations

(A, B, C, D) Phosphotransfer assays were used as a measure of enzymatic activity to determine the amount of ATP formed with: (A) Different concentrations (0.1 pM-10 nM) of the enzyme NDPK B. (B)

120 pM NDPK B was used at different time points (0-30 minutes). (C) Increasing ADP concentrations, used at 3 different GTP concentrations (50, 100, and 500 µM). (D) A double reciprocal plot of (C) with inversed 'ADP concentrations' and inversed 'ATP formed' values.

4.1.4 The small molecular compound, SanWie3 preferentially inhibits NDPK C

In collaboration with Dr. Aimo Kannt (Sanofi, Frankfurt), a small molecular compound screen was performed to investigate potential molecules that can inhibit the enzymatic activity of NDPKs. Three compounds (SanWie (SW) 1, 2, and 3) with an inhibitory potential were found in the screen. They, therefore, were validated for their inhibitory effect on the purified NDPK isoforms using the phosphotransfer assay. The enzyme kinetic parameters obtained from earlier experiments (Fig. 8) were applied to test SW1-3 on NDPK A, B, and C isoforms. SW1 and SW3 similarly inhibited NDPK A activity by 20% at 10 µM and 40% at 30 µM, whereas SW2 had only a minor inhibitory effect (approx. 10-15%) on this isoform at the maximal concentration of 30 µM (Fig. 9A). In contrast, NDPK B activity was affected by all three compounds, with SW3 being the most potent resulting in an inhibition of 40% at 10 µM and 60% at 30 µM (Fig. 9B). Surprisingly, NDPK C was the only isoform selectively inhibited by the compound SW3 (~90% inhibition) at concentrations higher than 10 µM, whereas SW1 and SW2 remained at an efficacy of 30-40% even at the highest concentration. The calculated IC_{50} value for SW3 was approximately 3 µM (Fig. 9C).

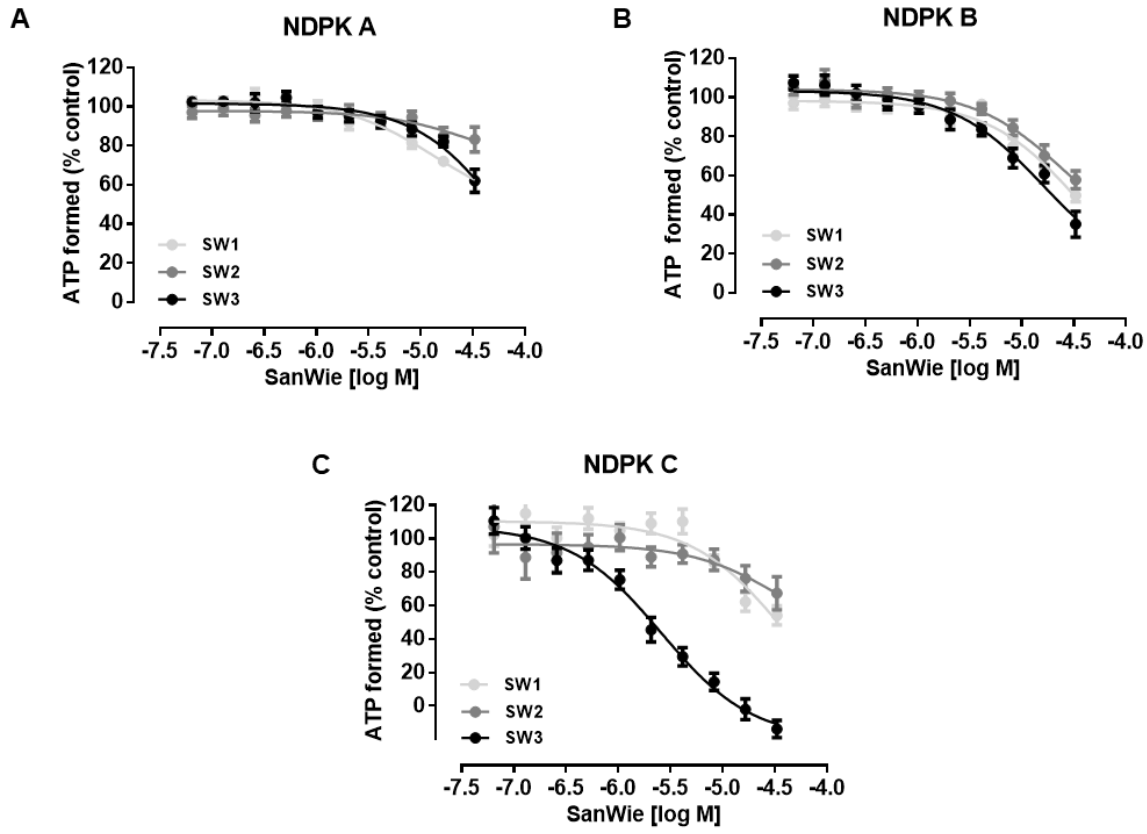

Figure 9: SanWie3 preferentially inhibited NDPK C

(A, B, C) Phosphotransfer assay with increasing concentrations of the inhibitors (SW1, 2, and 3). The amount of ATP formed by NDPK A (A), NDPK B (B), and NDPK C (C) was determined at 120 pM enzyme, 10 µM ADP, 100 µM GTP for 30 minutes at room temperature.

4.1.5 SanWie3 is an allosteric inhibitor of NDPK C

To study the mode of the inhibition of SW3 on NDPK C activity, a phosphotransfer assay with increasing concentrations of GTP was performed in the presence or absence of SW3. As expected, a linear increase in the enzymatic activity was observed with increased GTP concentrations under control conditions. However, in the presence of SW3, the enzymatic activity was reduced to a similar extent (about 50%) at all GTP concentrations, suggesting an allosteric inhibition mode of SW3 (Fig. 10A). In contrast to this observation, the degree of inhibition by a competitive inhibitor would have decreased at higher GTP concentrations due to the replacement of the inhibitor molecules at the active site by GTP. To further validate the allosteric inhibition by SW3, the enzymatic activity of NDPK C was determined at three different GTP concentrations (50, 100, and 500 µM), and the concentration-dependent effect of SW3 on ATP formation was assessed. SW3 inhibited the enzymatic activity at all GTP concentrations with similar efficacy, confirming the allosteric, non-competitive mode of inhibition (Fig. 10B).

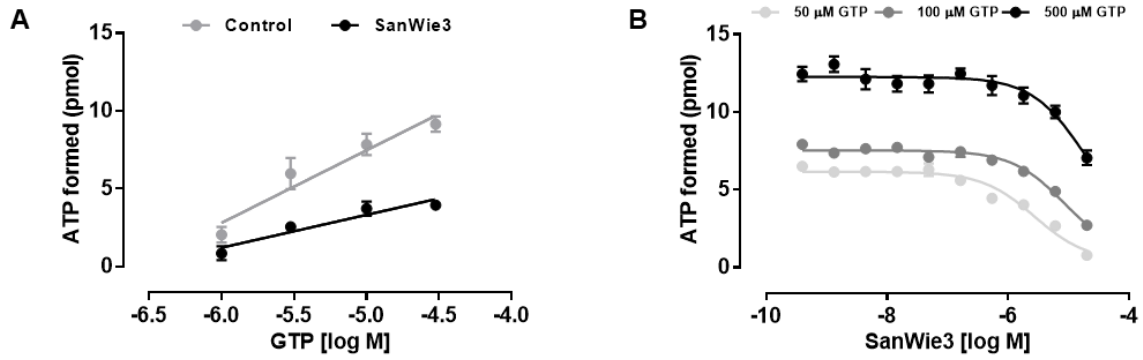

Figure 10: SanWie3 allosterically inhibited the NDPK isoform, NDPK C

Phosphotransfer assay analyzing the enzymatic activity of NDPK C in the absence and presence of SW3. (A) Increasing concentrations of GTP were used as a substrate in the absence and presence of 3µM SW3, and the amount of ATP formed was measured. (B) Increasing concentrations of SW3 were used to measure the amount of ATP formed in the presence of the three indicated concentrations of GTP.

4.1.6 SanWie3 binding causes a slight change in NDPK C structure

To monitor the potential changes in the structure of NDPK C due to SW3 binding, nano Differential Scanning Fluorimetry (nano DSF) and circular dichroism were performed in collaboration with Dr. Kathryn Perez from the biophysical core facility, EMBL, Heidelberg.

Nano DSF is a thermal unfolding assay based on tyrosine and tryptophan fluorescence to study the protein stability and melting temperature analysis at ultra-high resolution. In the presence of SW3, NDPK C exhibited a slight shift in the fluorescence intensity near the inflection point (64.6°C) at 350 nm, corresponding to a small change in the thermal stability compared to the control (only NDPK C). This shift confirmed that SW3 is indeed interacting with NDPK C (Fig. 11A). Circular dichroism was used to study if the binding of SW3 induces changes in the secondary structure of NDPK C. Therefore, the differential absorption of left and right circularly polarized light was measured. A slight decrease in the molar ellipticity of alpha-helices and a small increase in the molar ellipticity of β-sheets in the presence of SW3 was observed compared to NDPK C under control conditions (Fig. 11B). These data suggested that the interaction of SW3 causes small changes in the secondary structure of NDPK C.

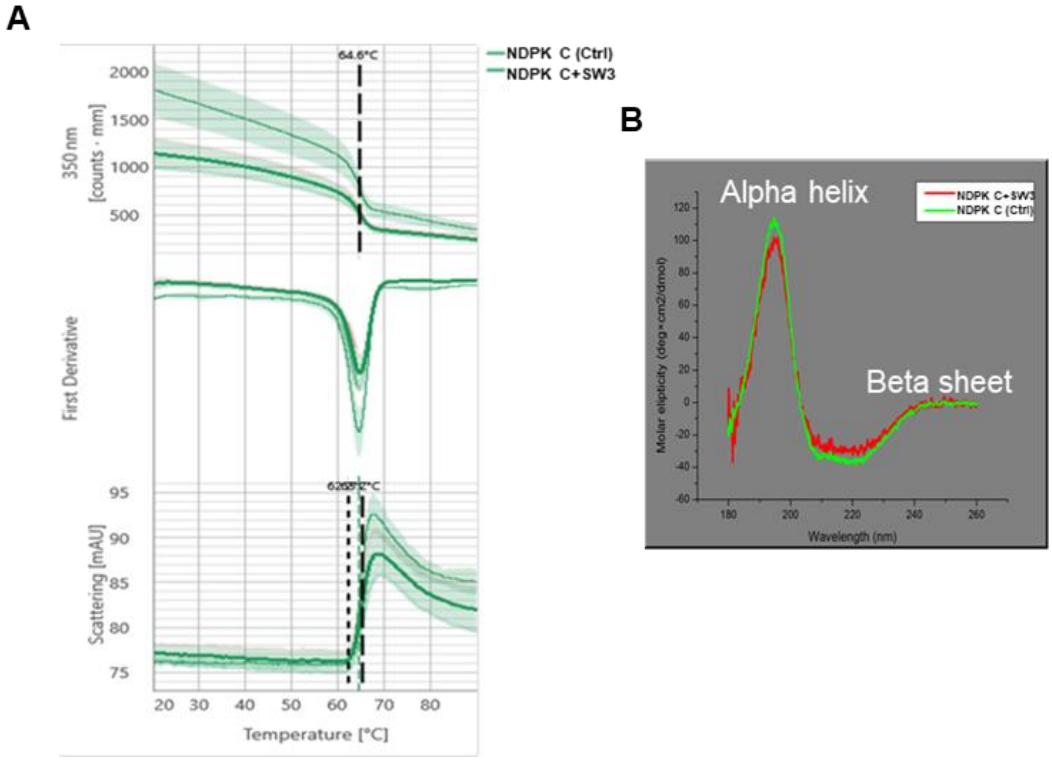

Figure 11: SanWie3 binding caused a slight change in the NDPK C structure

(A) NanoDSF of NDPK C with and without SW3. A scan of nanoDSF at 350 nm, with the plots showing a shift in the melting temperature (Tm) in the presence of SW3 compared to the control incubated with NDPK C (x-axis is representing the temperature used to distort the protein and the y-axis represents the fluorescence units). (B) Circular dichroism depicting the differences in the molar ellipticity of NDPK C in the presence and absence of SW3. The peak at about 190 nm represents the alpha-helical structure of NDPK C, and the trough at about 210-220 nm represents the molar ellipticity for the beta-sheets of NDPK C.

4.1.7 SanWie3 binds to a pocket near the active site of NDPK C

To better understand the interaction of NDPK C with SW3, we explored the SW3 binding site on NDPK C using Hydrogen-Deuterium eXchange Mass spectrometry (HDX-MS) in collaboration with Prof. Gert Bange from the synmikro facility at the University of Marburg. To this end, the NDPK C-SW3 complex was first subjected to deuterium exchange, followed by proteolytic fragmentation, the resulting peptides were subsequently analyzed by mass spectrometry. Peptides that still contain hydrogen atoms belong to the interface between NDPK C and SW3 within the complex. By comparing the superimposed peptides from only NDPK C and SW3 bound NDPK C, five different positions (1-5) were identified, where the hydrogen atoms were not exchanged with deuterium atoms (Fig. 12A). They are displayed on a ribbon structure of the NDPK C monomer with one binding site near the N terminus (1) and the other sites (2-4) near the NDP/NTP binding pocket (Fig. 12B). The embedded NDPK C monomer on the hexametric complex shows that SW3 is binding on the surface of the monomer, revealed by the exposed binding positions 1-5 on the surface, rather than the interface suggesting that SW3 does not interfere with the hexameric complex formation (Fig. 12C). The electrostatic potential mapped the structure of an NDPK C monomer (Fig. 12D) suggests that the potential binding site of SW3 on NDPK C in a small pocket, next to the catalytically active site (highlighted by a dashed circle).

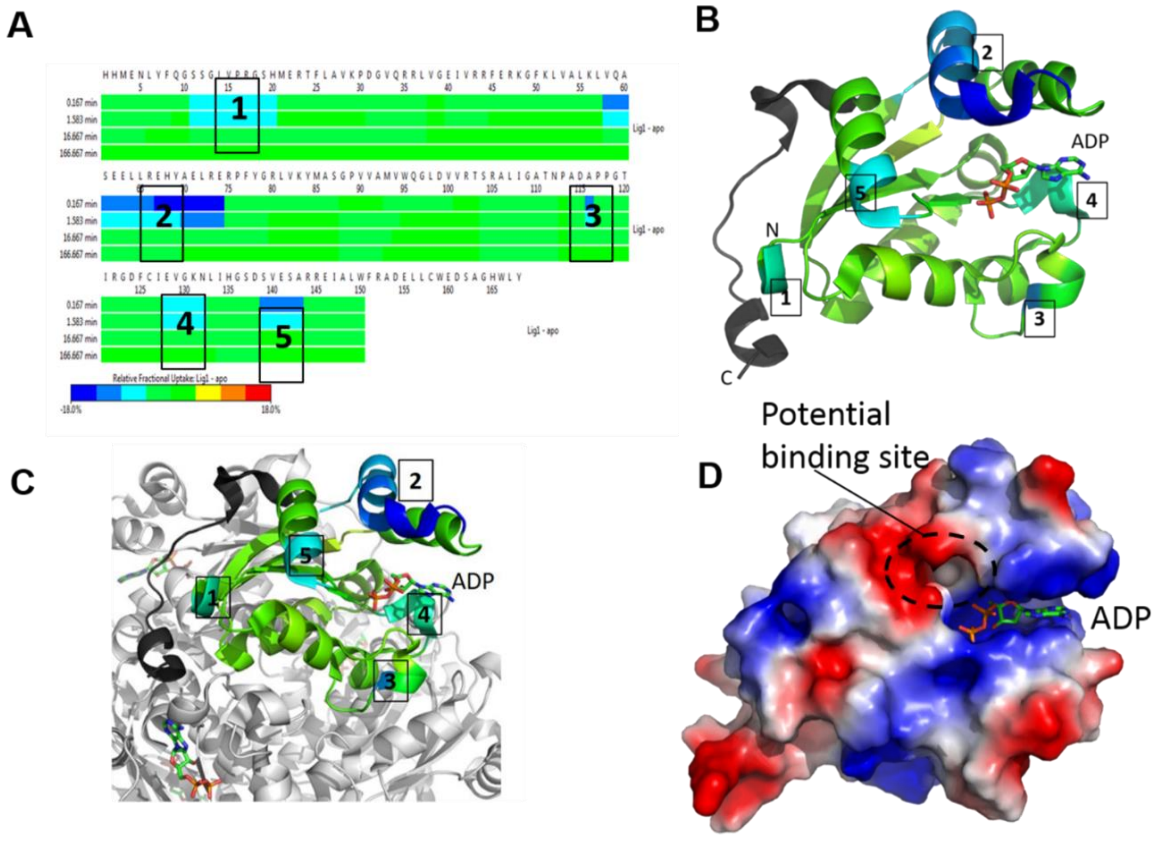

Figure 12: SanWie3 binds to a pocket near the active site of NDPK C

(A) Superimposed peptides of NDPK C with and without SW3, showing the five potential SW3 interaction sites on NDPK C by HDX. (B) The ribbon structure of a monomer of NDPK C is labeled with five interaction binding sites of SW3. (C) Overlay of figure 12B onto a hexamer, representing the interaction sites on the surface. (D) Electrostatic potential distribution on NDPK C showing the positive potentials in blue color and the negative potentials in red color, with the potential SW3 binding site near the active site.

4.1.8 SanWie3 interacts with several amino acids near the active site of NDPK C

To validate the interacting surface of SW3 and NDPK C, in-silico molecular modeling was performed in collaboration with Dr. Marcel Bermudaz and Prof. Gerhard Wolber from the Department of Molecular Drug Design, Free University of Berlin. Based on the crystal structure of human NDPK C (PDB entry: 1ZS6) and the results from the HDX experiments, we identified a shallow potential binding site of SW3 (Fig. 13C) near the co-crystallized ADP. From the deposited crystal structure of NDPK C-1ZS6, monomer-chain D showed an open conformation, exposing the side-chain of a glutamic acid residue, E71 (Fig. 13A, 13B). In silico-docking based on this conformation indicate a reliable binding probability of SW3 in the direct vicinity of the nucleotide-binding site occupied by ADP (Fig. 13D, E). Lipophilic contacts with A70 and L72 were observed, but most interactions are polar. The carboxyl group of SW3 forms a salt bridge with R75 and additionally allows for a hydrogen bond with that residue. The sulfur atom of the 1, 3-thiazolidine serves as a hydrogen bond acceptor for S142. Additional hydrogen bonds are formed with E71 and R145 (Fig. 13E).

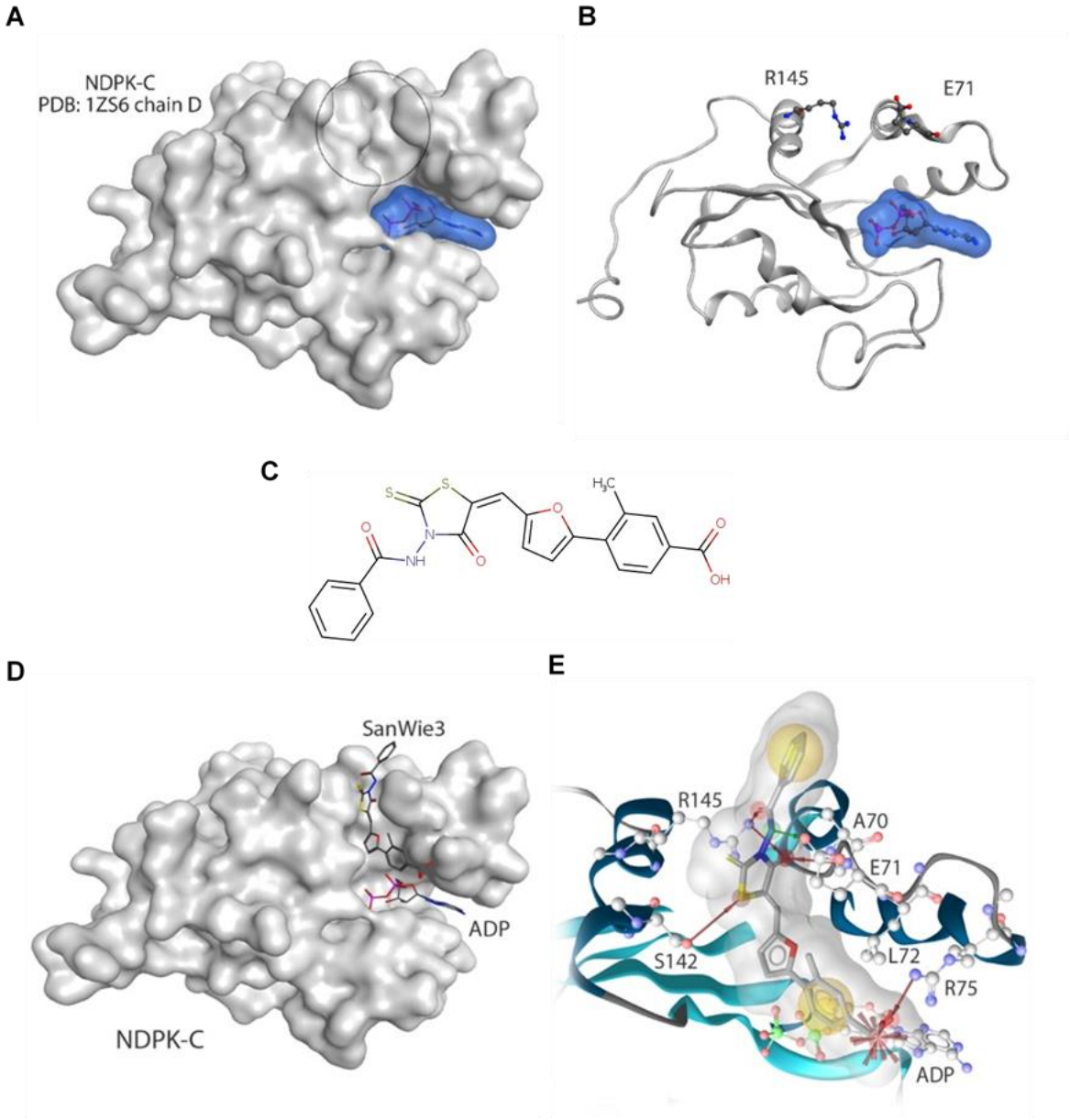

Figure 13: SanWie3 interacts with several amino acids near the active site of NDPK C

(A, B) The crystal structure of human NDPK C (PDB entry: 1ZS61) reports three monomer chain conformations, and only chain D is shown. The three conformations (not shown) are overall highly similar; however, they differ in a few sidechains. Chain D provided information about potential allosteric binding sites of SanWie3 in close vicinity to the co-crystallized ADP (E, black circle). (C) Molecular structure of SanWie3. (D, E) Potential binding mode of SanWie3 at human NDPK C showing a possible shallow binding site next to the co-crystallized ADP (PDB entry: 1ZS6). The three-dimensional interaction pattern indicates protein-ligand contacts with residues of region 2 (A70, E71, and L72) and region 5 (S142). Yellow spheres show lipophilic contacts, red and green arrows highlight hydrogen bond acceptors and donors, respectively, and the red star indicates a negative ionizable center.

4.2 Assessment of potential off-target effects of SanWie3

To assess the possible off-target effects of SW3, different protein kinases, receptors, and channels were screened regarding their potential interaction with SW3. This screening was performed in collaboration with Eurofins in Luxembourg, which revealed possible interactions within the subset serine/threonine kinases and GPCRs that were subsequently investigated in more detail.

4.2.1 AMPK2α is not a target of SanWie3

Two different concentrations of SW3 (1 µM, 10 µM) were tested on a panel of 60 different human kinases. The inhibitory effect of SW3 was calculated as a % inhibition of control enzyme activity. Kinases that showed more than 50% inhibition at 1 µM and 10 µM were considered potential interacting partners. At 1 µM, no inhibition greater than 50% was detected for any of the kinases. However, the 5'AMP-activated protein kinase catalytic subunit alpha 2 (AMPK2α) was inhibited up to 49%. At 10 µM, 8 out of the 60 kinases were inhibited by more than 50% (Fig. 14A). AMPK2α was the only kinase, which was inhibited at both SW3 concentrations. To verify the effect of SW3 on AMPK, an immunoblot was performed with NRCM lysates, treated with and without SW3 (3 µM and 10 µM). 5-aminoimidazole-4-carboxamide ribonucleotide (AICAR), a pharmacological activator of AMPK, was used at 1 µM to promote AMPK activation stably. The phosphorylation of Acetyl-CoA Carboxylase (ACC), an important substrate for AMPK kinase, and the autophosphorylation of AMPK were detected using the respective phospho-specific antibodies. No alteration of basal or stimulated phosphorylation of ACC and AMPK in response to AICAR was detected in the lysates of SW3 treated samples (Fig. 14B).

A

Kinase	%Inh (1 µM)	%Inh (10 µM)
AMPKα2(h)	**49**	**57**
Aurora-B(h)	19	80
c-RAF(h)	34	88
GSK3α(h)	23	65
MST2(h)	24	73
PEK(h)	18	66
Pim-2(h)	35	74
SAPK2a(h)	23	53

B

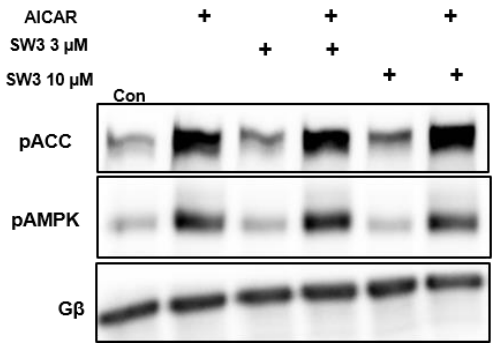

Figure 14: SanWie3 did not inhibit any other human kinases from the kinase screen

(A) The kinases that showed a potential inhibition (% of control) by SW3 (1 µM, 10 µM) from the screen. (B) A representative immunoblot from NRCM lysates, showing the phosphorylation of ACC and AMPK in the presence and absence of SW3 (3 µM, 10 µM), with and without stimulation of by 1 µM AICAR. Gβ expression was used as a loading control.

4.2.2 SanWie3 had no significant effect on α1-AR activity

To screen for other potential targets of SW3 such as channel's and receptor's interference with the ligand selectivity was calculated as the percent binding of a respective radioactively labeled ligand. Targets showing more than 50% reduction in ligand binding were considered as positive hits. Whereas most screens delivered no further hits, a subset of 18 pharmacologically relevant GPCRs suggested a potential agonistic activity of SW3 on the α_{1A}-adrenoceptor (α_{1A}-AR) and neuronal M1 (muscarinergic acetylcholine receptor-1), and an antagonistic effect on CB2 (cannabinoid receptor 2) (Fig. 15A). Because of the relevant expression of α1-AR in cardiomyocytes, we assessed the possible interaction of SW3 by comparing its effects with the α_{1A}-AR agonist A61603 in a reporter assay using enhanced green fluorescence protein (EGFP) production as readout. An adenovirus encoding EGFP under the control of a CMV promoter element was used in this reporter assay. The enhancer region of the CMV promoter comprises three NFκB binding sites and four CREB binding sites; hence transcriptional activity correlates with endogenous α_{1A}-AR activation in NRCM and can be visualized as an increase in EGFP fluorescence (Vettel et al., 2012). The extent of EGFP expression was measured as units of relative fluorescence. Consistently, the α_{1A}-AR agonist A61603 increased the EGFP expression up to 3-fold, whereas SW3 caused no increase in the EGFP expression, suggesting no agonistic effect on α_{1A}-AR (Fig. 15B). WB4101, an α_{1A}-AR specific antagonist, was used to verify A61603-dependent activity but remained unaffected in the presence of SW3.

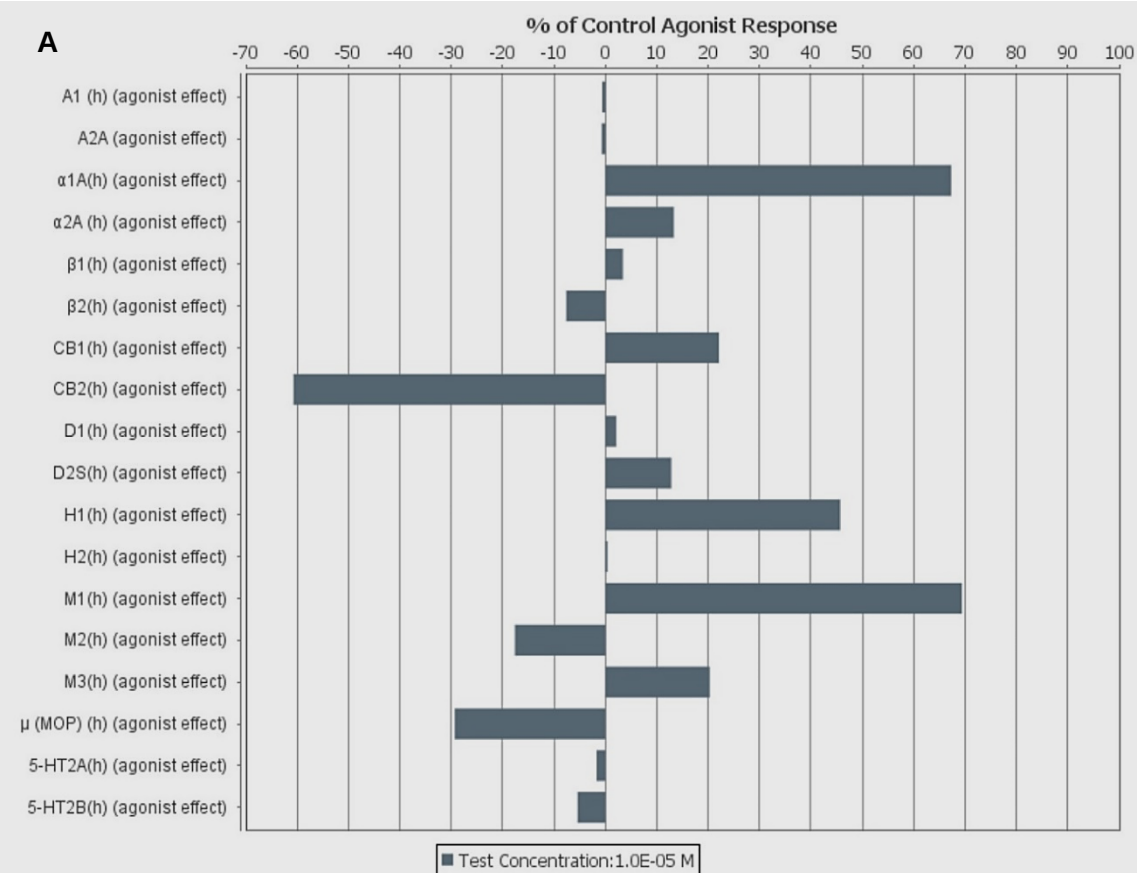

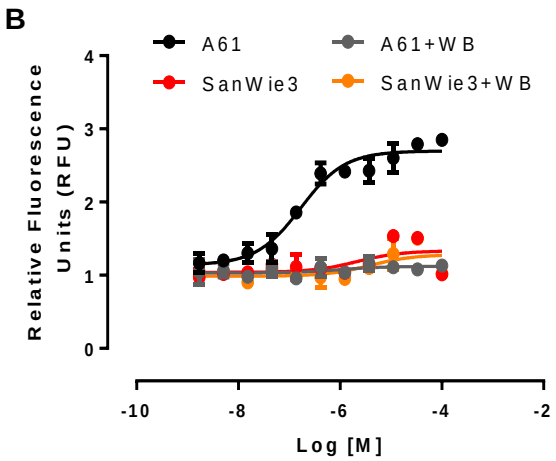

Figure 15: SanWie3 had no significant effect on GPCRs

(A) GPCRs showed a potential agonistic/antagonistic activity by 10 µM SW3 from the screen, showing the agonistic/antagonistic response compared to the percent of control. (B) GFP assay showing the GFP expression levels in relative fluorescence units; NRCM cultured on a 96 well plate were transduced with a control EGFP and EGFP-CMV promoter expressing adenovirus, incubated for 4 hours, later the cells were washed with PBS and exchanged with DMEM (high glucose). The next day, cells were verified for EGFP expression and treated with A61603, WB4104, and SW3 at increasing concentrations to measure the relative fluorescence.

4.3 Effects of SanWie3 on cell culture and tissue models

4.3.1 SanWie3 treatment did not affect the cell viability

To investigate the impact of SanWie3 on cell viability, a resazurin cell viability assay was performed in NRCM and adult mouse ventricular cardiomyocytes (AMVCM). Resazurin is an indicator dye used to determine cellular metabolic activity and mitochondrial viability through oxidation-reduction reactions in living cells. Metabolically active cells can effectively reduce the blue non-fluorescent resazurin dye to the fluorescent dye resofurin, emitting light in the red spectrum. Fluorescence was measured at different time points in the presence or absence of SW3, at 3 µM and 10 µM, for both NRCM (Fig. 16A) and AMVCM (Fig. 16B). No significant difference in the resofurin levels was observed in SW3 treated cells at different concentrations and time points compared to the control, indicating that SW3 had no significant effect on cell viability.

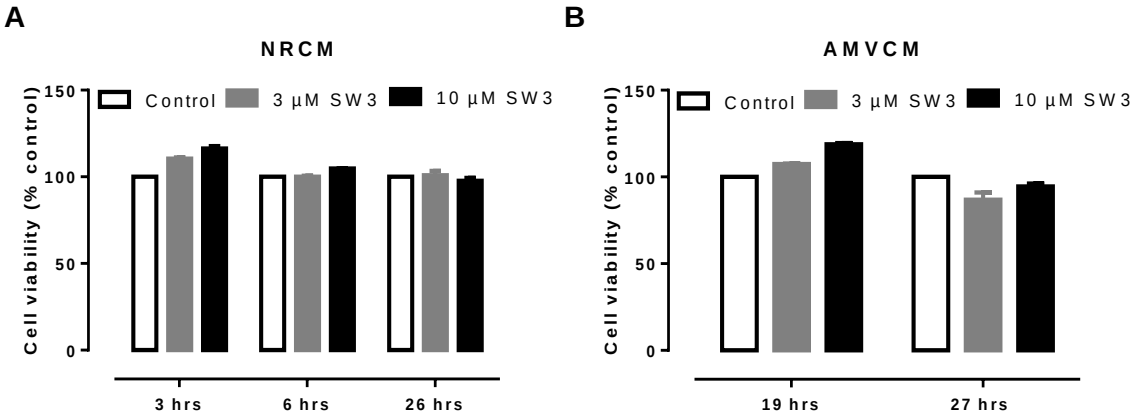

Figure 16: SanWie3 treatment did not affect the cell viability

(A, B) Resazurin assay showing the relative fluorescence levels in; (A) NRCM treated with SW3 (3 µM and 10 µM) for 3, 6, and 26 hours normalized to the control cells at the respective time points. (B) AMVCM treated with SW3 (3µM and 10 µM) for 19 and 27 hours normalized to the control cells at the respective time points. NRCM and AMVCM, each from one isolation, in technical replicates were added with the resazurin dye at a final concentration of 44 µM (1X) and incubated for 2-4 hours. 100 µl of the supernatant was collected after 2-4 hours from each well at every time point from the control, and the SW3 treated wells for quantifying the resofurin levels as a fluorimetric measurement to estimate the cell viability.

4.3.2 SanWie3 reduced isoproterenol-induced cAMP formation in NRCM

It is evident from previous reports (Cuello et al., 2003; Hippe et al., 2003) that NDPKs can mediate a receptor-independent activation of G_s. However, recent studies using siRNA-mediated knockdown or adenoviral overexpression implied a pivotal role of NDPK C in cAMP formation upon receptor stimulation (Abu-Taha et al., 2017). Following this data, the impact of SW3 on isoproterenol-induced cAMP formation was analyzed in NRCM. Consistently, SW3 significantly inhibited the receptor-induced increase in cAMP levels at the calculated IC_{50} of 3 µM, which were not further decreased in the presence of 10 µM SW3.

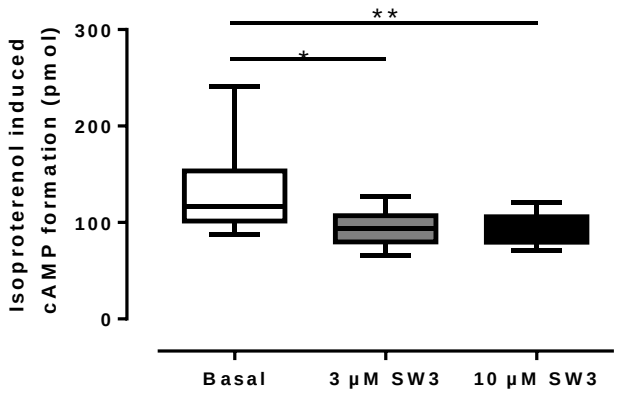

Figure 17: Isoproterenol induced cAMP levels were reduced by SanWie3 in NRCM

(A) Quantification of the cAMP levels from the basal and SW3 treated NRCM lysates. *P<0.05, **P<0.005 between Iso and SW3 treatment with ordinary one-way ANOVA, using Tukey's multiple comparison test. The cAMP levels were estimated by an indirect measure of an HRP-conjugated cAMP binding vs the cAMP binding from the samples binding to a cAMP antibody, determined by reading HRP activity at OD450 nm. The intensity of OD450 nm is inversely proportional to the concentration of cAMP from NRCM lysates. NRCM seeded on a 12 well plate were treated with two different concentrations of SW3 (3µM, 10 µM) for 60 minutes, along with the basal control. Cells were induced with 1µM Isoproterenol for 5 minutes and lysed in an acid-containing buffer. According to the user manual, the lysates were centrifuged to collect the supernatants, which were used in the cAMP assay.

4.3.3 SanWie3 reduced isoproterenol-dependent ser16 phosphorylation of phospholamban in NRCM

As SW3 decreased the cAMP levels in NRCM (Fig.17), the functional relevance of this reduction was studied by analyzing the phosphorylation of downstream cAMP/PKA targets in the presence or absence of SW3 (3 µM, 10 µM) in NRCM. Cardiac troponin I (ser23/24), myosin-binding protein C (ser282), and ser16 PLN phosphorylation levels were estimated by immunoblotting upon isoproterenol (1 µM) stimulation. In the presence of SW3, a significant decrease in the phosphorylation of ser16 PLN was observed in a concentration-dependent manner (Fig.18A), which was quantified by normalizing the pixel density of the p-ser16 PLN to calsequestrin (Fig. 18B). The other PKA targets showed no significant difference in their phosphorylation upon SW3 treatment, indicating that in immature NRCM, the endogenous NDPK C/G_s complex is not globally regulating cAMP levels but targeting specific cAMP pools

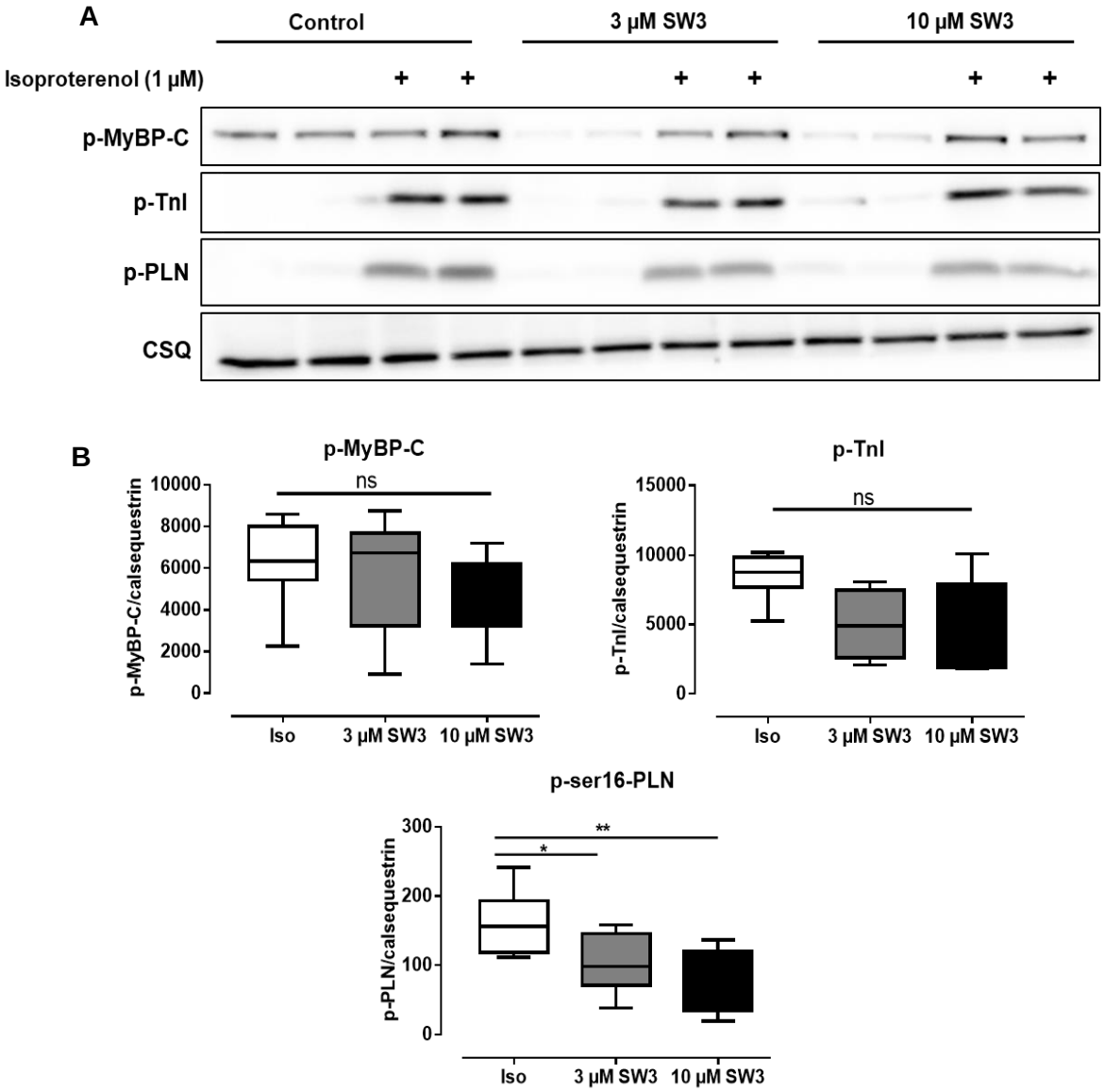

Figure 18: SanWie3 reduced PKA-dependent ser16 phosphorylation of phospholamban in NRCM

(A) A representative immunoblot with the control and SW3 treated NRCM lysates, probed with phosphospecific ser16 phospholamban and calsequestrin antibodies. NRCM were treated with or without SW3 (3 µM, 10 µM) for 60 minutes, followed by 1µM isoproterenol stimulation for 10 minutes, along with the respective controls. The cells were harvested in Kranias buffer (with protease and phosphatase inhibitors) and lysed using a tissue lyser. The supernatants were collected and run on a 15% PAGE, transferred on a nitrocellulose membrane, and probed with the respective phospho-specific antibodies. Calsequestrin was used as a loading control. (B) Quantification of bands from the immunoblot using an ImageJ analysis by applying linear regression. *P<0.05, **P<0.007 between Isoproterenol and SW3 treatment with ordinary one-way ANOVA, using Sidak's multiple comparison test.

4.3.4 SanWie3 treatment differentially affected cAMP pools in adult mouse cardiomyocytes:

Application of SW3 reduced isoproterenol-induced cAMP formation in NRCM, and as immunoblots indicated so far, the effect on PKA activity seemed to be restricted to the phosphorylation of PLN. (Fig. 18). Since the β_1-AR signal cascades are not yet fully matured in NRCM, especially regarding compartmentalization (Seki et al., 2003), we investigated local changes in the cAMP levels of SW3 treated AMVCM. To this end, the cAMP signals from different cardiomyocyte-microdomains were determined in collaboration with Prof. Viacheslav Nikolaev (Hamburg) by using compartment-specific FRET tools.

The binding of cAMP to the EPAC-based FRET sensor increases the distance between the attached donor and acceptor chromophore, thereby reducing the FRET signal. The change in the frequency of the emitted light is proportional to the cAMP concentrations. For normalization, each cell was finally treated with the global PDE-inhibitor, IMBX, combined with the AC activator forskolin to achieve the maximal cAMP response. To anchor the sensor to distinct compartments, fused proteins were generated comprising the 'pBs.cyt' sensor for the cytosol (Kaschubowski et al., 2020), pmEpac1 for plasma membrane (Perera et al., 2015), Epac1-JNC for the RYR (Borner et al., 2011), and Epac1-PLN for SERCA/PLN microdomains (Sprenger et al., 2015). All sensors were responsive to isoproterenol stimulation. SW3 treated cells did not change the FRET signal at cytosolic, RYR2, and plasma membrane microdomains (Fig. 19A, B, C). However, in contrast to NRCM, the presence of SW3 additionally decreased the FRET signal indicating higher cAMP levels in the SERCA/PLN microdomain (Fig. 19D). This data confirmed the SERCA/PLN domain as a critical target of NDPK C activity.

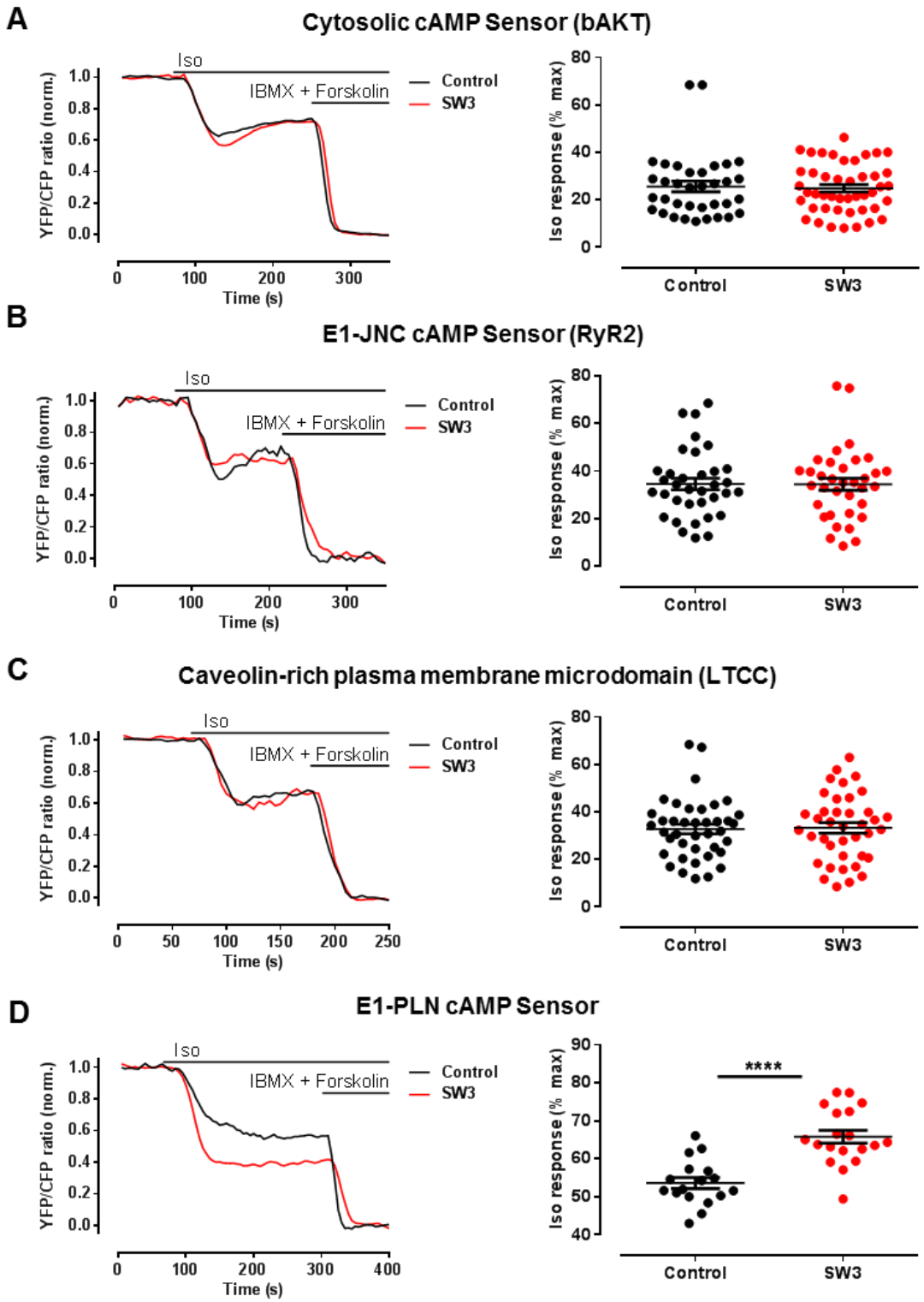

Figure 19: SanWie3 differentially regulated the cAMP pools in adult mouse cardiomyocytes

(A, B, C, D) FRET assay measurements in adult mouse cardiomyocytes. AMVCM expressing the specific cAMP biosensors were isolated using Langendorff's method from the genetically modified mice. FRET measurements were performed using an imaging protocol on AMVCM using CFP and YFP filter cubes for excitation and emission, respectively. SW3, Isoproterenol, IBMX, and forskolin were applied to the bath solution sequentially during the recording, using a pipette. The FRET ratio was measured after achieving a stable baseline. (A) Cytosolic cAMP Sensor (bAKT), (B) RyR2 cAMP sensor (E1-JNC),

(C) Caveolin-rich plasma membrane microdomain cAMP sensor (LTCC), (D) E1-PLN cAMP sensor. n=18, one-way-ANOVA with Mann Whitney post-test. *P<0.02 control vs SW3).

4.3.5 Both SanWie3 and G_i inhibition with pertussis toxin similarly increase ser16 phosphorylation in isoproterenol stimulated AMVCM

The FRET assays in the presence of SW3 demonstrated an increase in the SERCA/PLN cAMP pool in AMVCM (Fig. 19), which is contrasting to the NRCM data (Fig. 18). To study whether the cAMP level in the SERCA domain is under control of the NDPK C/G_i complex, PLN-phosphorylation in AMVCM was analyzed, and the effect of SW3 was compared to the G_i protein inhibition by pertussis toxin (PTX). In a pilot experiment, the efficacy of PTX was monitored by immunoblot in different cell types using different lysis buffers. Due to the ADP-ribosylation, PTX-modified $G\alpha_i$ proteins can be visualized by a shift towards higher molecular weight in an adapted SDS-PAGE compared to the native protein (Vega et al., 2020). Indeed, all treated samples showed a band shift of the $G\alpha_{i2,}$ the major isoform in cardiomyocytes, when cells were incubated for 12 h with 0.25 µg/µl PTX (Fig 20A).

In line with the FRET experiments, the immunoblot data confirmed that inhibiting NDPK C by SW3 induced an increase in PLN-Ser16 phosphorylation in isoproterenol treated AMVCM but had no additional effect on the phosphorylation of other PKA targets such as MyBPC or TnI. Similarly, the PTX treatment induced a comparable increase in PLN-Ser16 phosphorylation, whereas the other PKA targets remained unaffected. Additional application of SW3 after PTX treatment did not further enhance isoproterenol-induced PLN-phosphorylation (Fig. 20B, 20C). However, neither SW3 nor PTX exhibited a detectable effect on basal PLN-phosphorylation.

Taken together, this experimental setting indicated that, unlike in other cAMP compartments in adult cardiomyocytes, the extent of isoproterenol-induced, cAMP-PKA-mediated PLN-phosphorylation might be suppressed by G_i proteins which are likely activated by the complex formation with NDPK C.

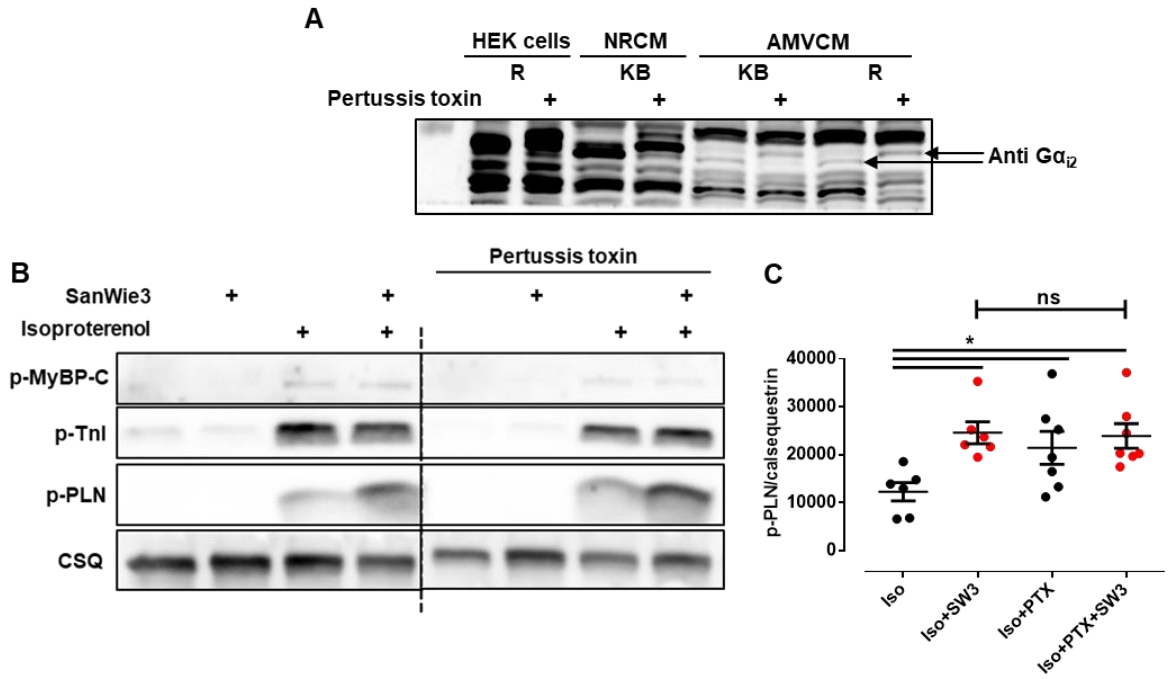

Figure 20: SanWie3 increased the ser16 phosphorylation of phospholamban comparable with pertussis toxin

(A) Representative immunoblot with of HEK cells, NRCM, and AMVCM lysed in either RIPA (R) or Kranias buffer (KB) with and without pertussis toxin treatment, probed with a $G\alpha_{i2}$ specific antibody. (B) Representative immunoblot and quantification of PLN-Ser16 phosphorylation in AMVCM, treated with PTX, SW3, or a combination of both. After stimulation with isoproterenol, as indicated, samples were probed with the phospho-specific antibodies against the PKA-phosphorylated forms of myosin binding protein, troponin-I, and PLN (ser16). Calsequestrin was used as a loading control. (C) Quantification of the band pixel density using ImageJ, $*P<0.05$ between Iso and the other treatments with one-way ANOVA, using Sidak's multiple comparison test.

4.3.6 SanWie3 treated adult cardiomyocytes exhibited higher basal Ca^{2+} amplitudes and accelerated basal Ca^{2+} reuptake and sarcomere relaxation

SERCA is responsible for removing Ca^{2+} from the cytosol into the SR at the end of the contraction cycle and is involved in cardiac muscle relaxation. To study the influence of SW3 on Ca^{2+} handling and cell contractility, calcium transients and sarcomere shortening of isolated paced cardiomyocytes were measured using the IonOptix video microscopy system.

In line with the effects of SW3 on SERCA activity in ISO-stimulated adult cardiomyocytes, a mild but significant increase in Ca^{2+}-reuptake velocity and sarcomere relaxation were observed under basal conditions (Fig. 21F, 21H). This effect was accompanied by a higher Ca^{2+} amplitude (Fig. 21A, 21B) during contraction, with a significant increase in diastolic Ca^{2+}-release indicated by the higher cytosolic Ca^{2+} levels. In addition, a higher baseline Ca^{2+} (Fig. 21E) was observed upon SW3 treatment, which suggested a higher pre-stimulation Ca^{2+} concentration than the basal conditions. No significant difference in the resting (diastolic)

sarcomere length was observed (Fig. 21G), indicated that SW3 did not over-stretch the sarcomere. These parameters, therefore, suggested a SERCA-mediated increase in SR Ca^{2+} load under basal conditions. However, the change in Ca^{2+} dynamics, which led to a significant acceleration of sarcomere relaxation, and higher systolic Ca^{2+} amplitudes did not translate into increased sarcomere shortening in SW3 treated AMVCM (Fig. 21C, 21D). Moreover, relaxation already occurred at around 40 ms, when there was only a minor reduction in cytosolic Ca^{2+} levels. Thus, both parameters indicate a potential change in the Ca^{2+} sensitivity of contractile proteins such as TnI under basal conditions.

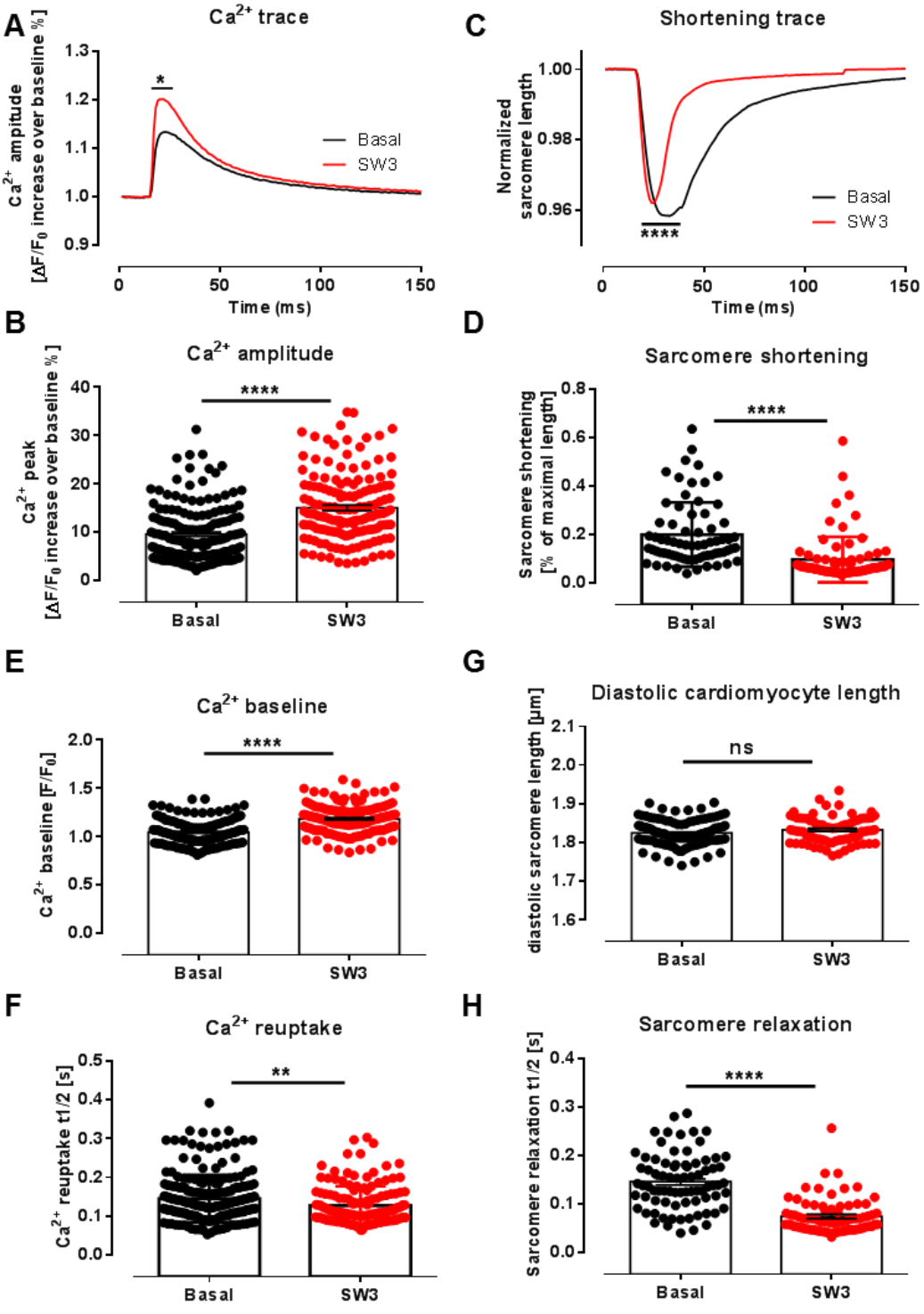

Figure 21: SW3 exhibited higher Ca^{2+} amplitudes in AMVCM

(A-H) The cells were incubated in 1 µM Fura-2 AM dye-containing buffer for 20 minutes before the measurements. The glass-bottomed petri dish containing cardiomyocytes was positioned parallel to the electrode in the measuring chamber of the IonOptix apparatus. The contractility of each cardiomyocyte was measured for 25 milliseconds at 0.5 Hz and 10 volts, separately at basal conditions in the presence of SW3 (10 µM). The following parameters were analyzed: (A, B) Baseline normalized calcium transient fluorescence ratio, with transient trace and Ca^{2+} peak. (C, D) Baseline normalized sarcomere length with shortening trace and shortening. (E, G) Baseline Ca^{2+} content and diastolic sarcomere length. (F, H) Ca^{2+} reuptake velocity of the cardiomyocytes measured as 50% time to baseline and sarcomere relaxation. For (A-H), mean ± SD is shown; ****P<0.0001, **<0.004, *<0.02, basal vs. SW3, two-tailed, unpaired t-test.

4.3.7 SanWie3 increased the sarcoplasmic reticulum Ca^{2+} load and spontaneous Ca^{2+} release

To further validate the effect of SW3 on the SERCA-PLN microdomain, SR Ca^{2+} load and the diastolic Ca^{2+} concentrations were measured in AMVCM in collaboration with Dr. Karin Hammer from the University Medical Center Regensburg. SR Ca^{2+} load of the cardiomyocytes was measured by rapidly applying caffeine at 10 mM to release SR Ca^{2+} via full RYR2 receptor activation. Consistent with our IonOptix measurements, SW3 treated cardiomyocytes showed a significant increase in basal SR Ca2+ load compared to the non-treated control (Fig. 22A). In line with the interdependence of SR Ca^{2+} load and spontaneous SR Ca^{2+} release (SCR), SW3 treated cells showed higher incidences of diastolic Ca^{2+} leak (Fig. 22C) (Shannon et al., 2002) and a corresponding tendency to higher diastolic Ca^{2+} levels as previously observed concentrations at basal conditions (Fig. 22B).

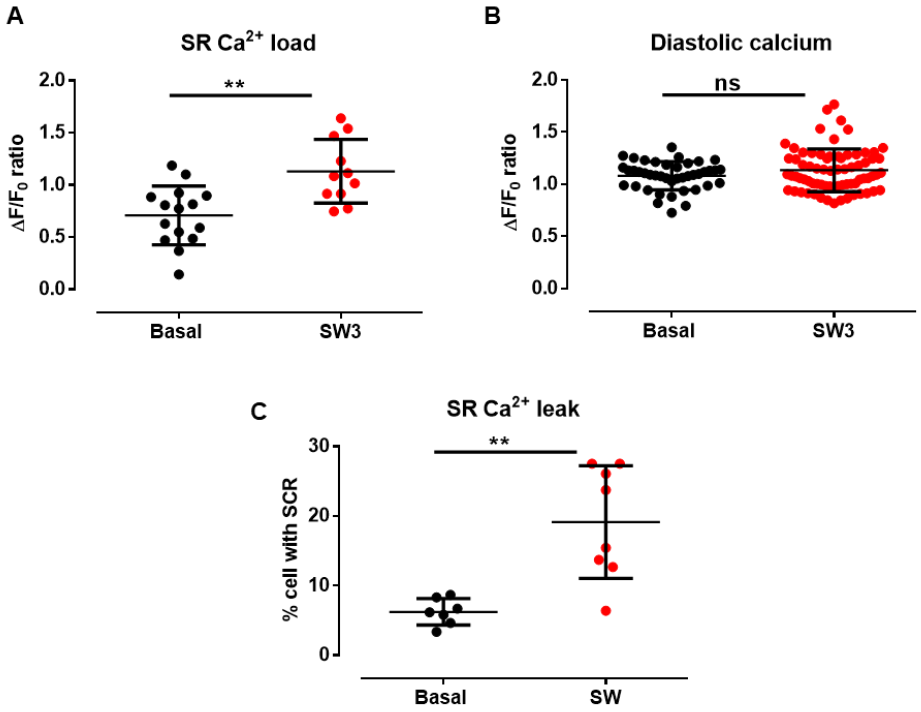

Figure 22: SanWie3 increased the sarcoplasmic reticulum Ca^{2+} load

(A) SR-Ca^{2+} load measurement with the non-treated and SW3 treated AMVCM. Mean ± SEM of the Ca^{2+} binding dye Fura-2 AM ratio, representing the unbound vs bound dye to Ca^{2+} ions. (B) A measurement of the diastolic Ca^{2+} concentration with the non-treated and SW3 treated AMVCM, with the y-axis showing the Fura-2 AM ratio. (C) Spontaneous calcium release (SCR) events were measured using confocal microscopy with isolated mouse ventricular cardiomyocytes, indicating the percentage of cells showing SCR. For (A), (C), mean ± SD is shown; ***P*<0.003 between basal vs SW3, two-tailed, unpaired t-test.

4.3.8 SanWie3 increased ser16 phosphorylation of PLN and contraction force in adult rat heart ventricular muscle strips

To study whether SW3 alters the contractility of cardiac tissue, organ bath experiments were performed with rat heart explants in collaboration with Dr. Magdolna Levay. Strips from the inner wall of the adult rat heart were prepared, and their contractility was studied with or without SW3 and increasing concentrations of isoproterenol (0.1-300 nM). Pre-incubation with 10 µM SW3 for 30 minutes significantly increased contractility on top of the isoproterenol stimulation (Fig. 23A), altering the maximal responsiveness of the muscle stripes. Thereafter, the muscle strips were analyzed for the phosphorylation of ser16 PLN and the other cAMP/PKA targets. The strips incubated with SW3 and treated with isoproterenol displayed a higher ser16 PLN phosphorylation than isoproterenol alone (Fig. 23B). There was no apparent difference in the phosphorylation of other PKA targets, troponin-I (ser23/24) and MBP (ser282) (Fig. 23B).

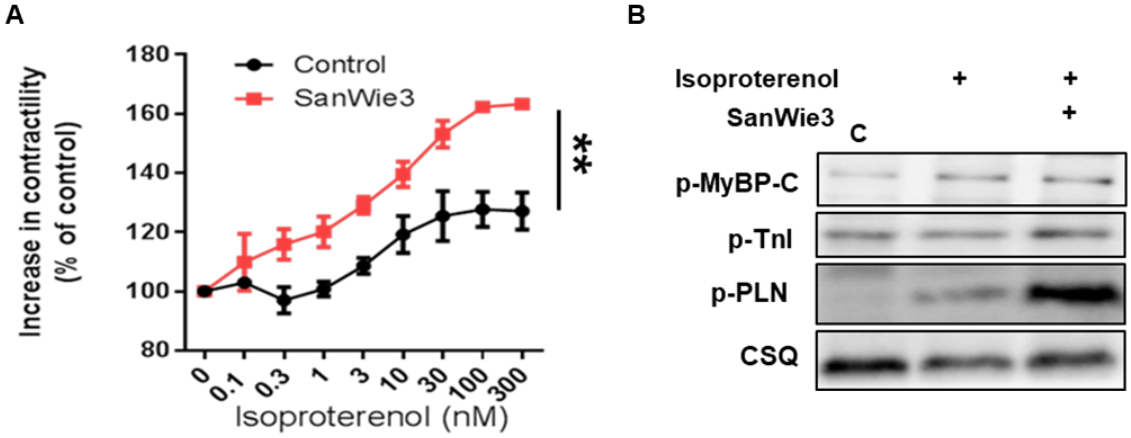

Figure 23: SanWie3 increased in ser16 phosphorylation of PLN in adult rat heart ventricular muscle strips

(A) Contractililty measurement of rat ventricular heart muscle strips with increasing concentrations of isoproterenol, with or without SW3. (B) Representative immunoblot from the lysates of rat ventricular heart muscle strips treated with isoproterenol alone or isoproterenol and SW3. The immunoblot was analyzed with the specific antibodies the phosphorylated forms of myosin binding protein, troponin-I, and PLN (ser16). Calsequestrin was used as a loading control.

4.3.9 SanWie3 treatment might slightly increase cardiac contractility in healthy mice

In a preliminary experiment, the influence of SW3 was tested on the survival of juvenile, healthy male mice in a small cohort (8-9 animals). 100 µl SW3 at a concentration of 100 µM dissolved in PBS (SW3) or control (PBS) was administered through daily intraperitoneal (IP) injections for seven days. Thereafter, potential changes in cardiac performance parameters were assessed in all the mice by echocardiography under anesthesia. In addition, blood samples were taken from the animals to measure serum levels of the inhibitor by mass spectroscopy (MS), in collaboration with Dr. Gegen Hagner from the metabolomics core facility, Heidelberg. Similar to the samples of pure dissolved SW3, the plasma of SW3 injected animals showed two distinct peaks at 13.24 and 13.38 minutes retention time in the MS analysis which was absent in control injected mice (Fig. 24A, B). Based on a standard curve, a concentration range of 1.35 - 2.57 µM was estimated for the mouse plasma levels, which is near the calculated IC_{50} value from the in vitro enzyme assays. To verify if SW3 was accumulated in the heart at sufficient concentrations, PLN phosphorylation of whole heart tissue was assessed by immunoblot. Indeed, in line with isolated cardiomyocytes treated in cell culture, p-PLN levels were significantly enhanced in the presence of SW3, with no difference in the extent of troponin I (ser23/24) phosphorylation (Fig. 25A, B). During echocardiography, no significant difference in the heart rate was observed (Fig. 26A). However, the analysis of the fractional shortening of the left ventricle during systole revealed an increase from 18.5 to 20.5% (Fig. 26B). This increase reached statistical significance ($p=0.0432$) in a one-tailed, unpaired t-test but not in the two-tailed analysis ($p=0.0864$).

Together, these analyses show that the application of SanWie3 in mice by daily IP injection reaches blood plasma levels which might already have biological effects in the heart but do not harm the animals within the studied seven day period.

24A

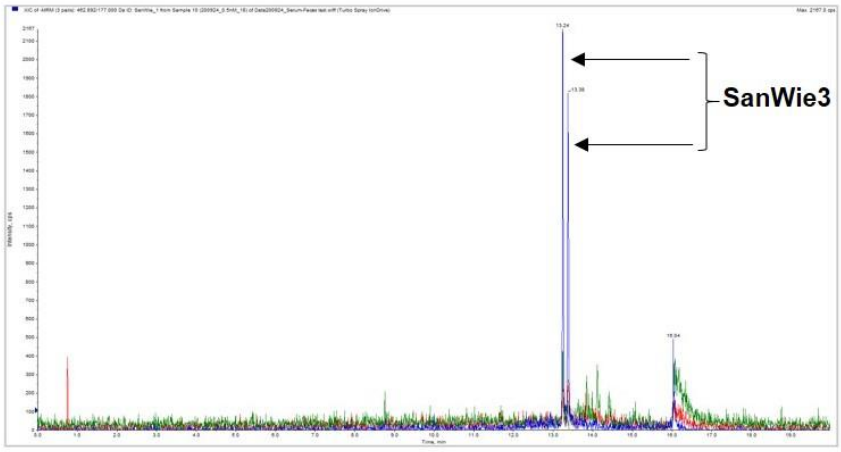

SanWie3-standard (500 pM)

24B

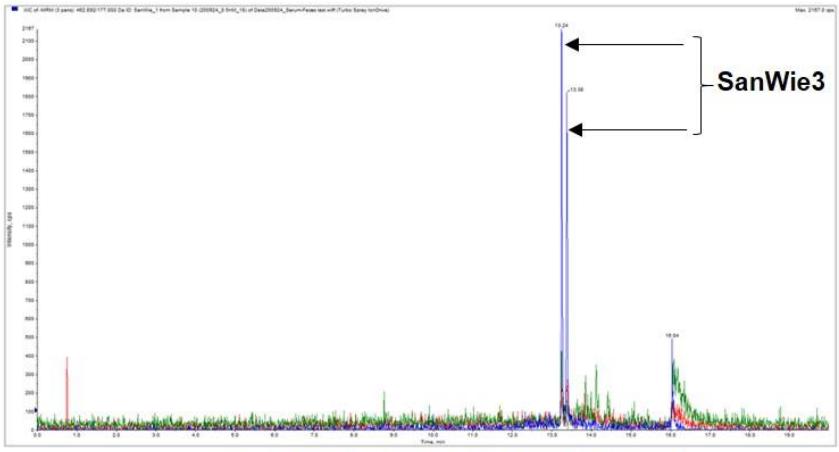

SanWie3-serum (1.35-2.57 µM)

25A

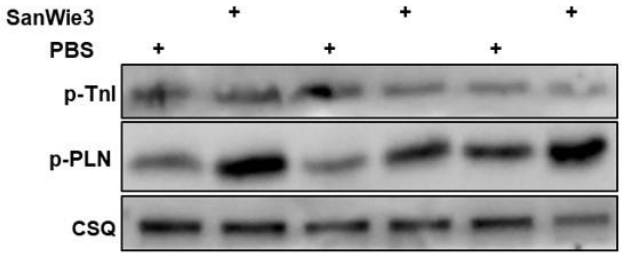

25B

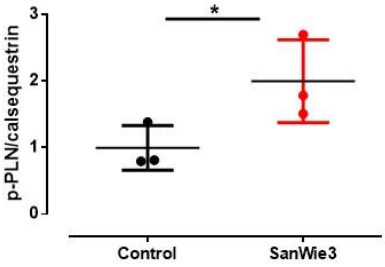

26A

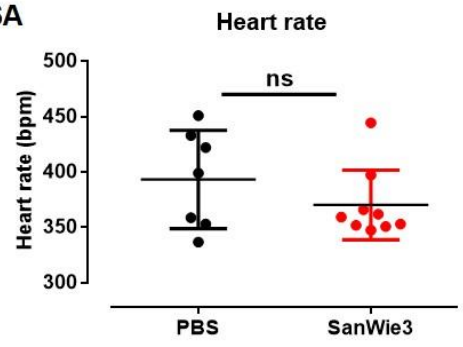

26B

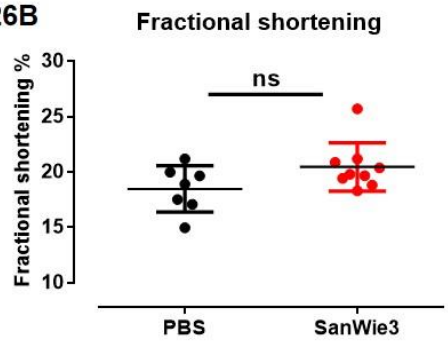

Figures 24, 25, and 26: SanWie3 might slightly increase cardiac contractility in healthy mice

(24A, B) The spectrum produced by a mass spectrophotometer, analyzed from pure DMSO dissolved and serum obtained SanWie3. (25A) Representative immunoblot from the lysates of the pulverized heart tissues from the SW3 treated and PBS injected mice. Phospho-specific of PLN and TnI were used for probing the blots. Calsequestrin was used as a loading control. (25B) Quantification of bands from the immunoblot using an ImageJ analysis by applying linear regression. *P=0.05, between PBS and SW3 treatment, using Mann Whitney test. (26A, B) Percent left ventricular ejection fraction and percent fractional shortening analysis from the PBS (n=6), and SW3 injected (n=8) animals using echocardiography. The animals were shortly shaved at the abdominal region for echocardiography analysis, using a continuous flow of 1-2% isoflurane mixed with 30-50% oxygen.

5. Discussion

This study aims to identify and characterize small-molecule compounds that could inhibit the enhanced NDPK activity in cardiovascular disorders, especially in end-stage heart failure. The results demonstrate that the small molecular inhibitor SanWie3 preferentially attenuates the enzymatic activity of NDPK C and modulates cAMP-dependent signaling in NRCM and AMVCM.

5.1 Preferential interaction of SanWie3 with NDPK C

Together with our collaborators, we developed a high-throughput screen including several thousand small molecule compounds. Although the screen initially aimed to identify putative inhibitors of NDPK B, follow-up studies performed in this study revealed that one of the three potential hits was a preferential inhibitor of the closely related isoform NDPK C. For the past three decades, the protein structure of NDPKs has been extensively investigated. Among group-I human NDPK isoforms, NDPK A and NDPK B are 80.8% homologous, whereas NDPK C shares 66.2% identity with NDPK A and 67% with NDPK B (Boissan et al., 2018). Even though all these isoforms share conserved amino acid residues, for example, within their catalytic site (K29, Y69, R105, T111, R122, H1135), the NDPK C isoform is relatively different at the N-terminal region with an additional 17 amino acids likely involved in membrane anchoring based on their lipophilicity (Abu-Taha et al., 2017). Apart from the active site, the significance of other amino acid residues in its vicinity has been shown. For example, introducing the point mutations of the adjacent amino acids P96S and S120G into the sequence of NDPK A altered its catalytic function (Freije et al., 1997), and all the point mutants with an exchange at the autophosphorylation from H118 to N118 lost their enzymatic activity, irrespective of the isoform (Zimmermann et al., 2012). Thus, considering the similarity within the catalytic domain, it seemed highly unlikely to identify an isoform-specific small molecule inhibitor directly interfering with the nucleotide-binding at the enzymatic center of NDPK C. However, the structural comparison analysis of the NDPK isoforms by superimposing the crystal structures revealed differences in a few amino acids within the proposed SW3 binding site of regions 2 and 5 (see Fig. 12). Region 5 included arginine (R145) and glutamic acid (E71) in NDPK C, corresponding to lysine and aspartate in NDPK A and B. Though lysine and arginine form electrostatic interactions, the guanidino group specific to arginine enables to form a more significant number of interactions compared to lysine (Sokalingam et al., 2012). Therefore, the hydrogen bonds formed by R145, with the carbonyl groups (see Fig. 12E), might determine the differential subtype affinity.

Moreover, region 2, closest to the active site, comprised the small, non-reactive amino acid A70 in NDPK C forming a potential lipophilic contact (see Fig. 12E) with the compound. In the two other isoforms, this position also constitutes a lipophilic residue, except that it is bulkier

(valine and isoleucine, respectively) and might interfere with the benzyl moiety of SW3. The significance of these amino acids could be determined by generating the NDPK C nucleotide substitution mutants (e.g., R145K at region 5 and/or A70V at region 2) and by analyzing their enzymatic activity in the presence of SW3. Similarly, generating NDPK A/B point mutants with the substitutions of V/I53A and/or K128R could also give insights into the importance of these amino acids and indicate whether a shift in their enzymatic activity would be possible comparable to NDPK C's reduced activity. Together, these data suggest that the differential amino acids might cause the isoform-specific structural differences and might contribute to the selectivity of SW3 towards NDPK C.

According to the phosphotransfer assays (see Fig. 9B, C), it is evident that even though SW3 preferentially inhibited NDPK C, the enzymatic activity of NDPK B was also reduced at higher concentrations. Taken the high homology between the NDPK isoforms into account, these data argue for a rather relative preference. Since the previous data have consistently demonstrated a contribution of NDPK B activity to the cellular cAMP formation and NDPK B/C heterooligomers are the most likely found in the complexes with heterotrimeric G proteins (Abu-Taha et al. 2017), combined inhibition of NDPK B and NDPK C by SW3 might be more desirable than an exclusive inhibition of NDPK C.

5.2 Potential mechanisms of SanWie3 mediated NDPK C-inhibition

Allosteric regulation controls protein function, where the effectors bind to regulatory sites distinct from the active site and subsequently induce conformational changes affecting the enzymatic activity (Kobe & Kemp, 1999). In contrast, competitive inhibitors bind to the active site and prevent the binding of protein's natural substrate. Therefore allosteric effectors most often bear no structural resemblance to their target protein's substrate, whereas a competitive inhibitor may be required to be chemically similar to the substrate to compete against it (Laskowski et al., 2009). Our results indicated that SW3 did not completely inhibit the enzymatic activity. Moreover, the extent of inhibition by SW3 was not decreased even at higher NTP substrate concentrations (see Fig.9). This result indicated that SW3 does not directly interfere with the nucleotide-binding site but instead binds to an allosteric site and induces conformational changes that affect the enzymatic activity of NDPK C.

Previous studies have established that the NDPK monomers assemble into stable tetramers or hexamers, which is essential to stabilize the catalytic site formation, while the monomeric subunits function independently from each other inside the NDPK complex (Georgescauld et al., 2020). Moreover, protein crystallization studies demonstrated that specific interactions between the monomeric NDPK subunits contribute to the organization of an oligomer. For example, in NDPK from *Mycobacterium tuberculosis,* it is shown that the amino acid residues R80 and D93 from each monomeric subunit form independent salt bridges between the

monomers for hexamer stabilization, and the mutants R80A/N and D93N exhibited less enzymatic activity and stability (Dautant et al., 2019). Additionally, two highly conserved structural motifs, the Kpn loop and the C-terminal segment, are critical in maintaining hexamer stability and assembly. The Kpn loop, which is specific to NDPKs, is an alpha helix motif positioned at monomers' interacting surface, promoting stabilization of the quaternary protein structure (Dautant et al., 2017). Our study identified that the carboxylic acid group of SW3 forms a salt bridge with R75, along with several other non-covalent interactions, revealed by the *in silico* prediction, characterization, and molecular docking analyses (see Fig. 13E). However, all these interaction sites are distinctly positioned away from the amino acid residues/domains necessary for oligomerization, and none of these structures was directly involved in SW3/NDPK C interaction. The influence of SW3 on NDPK C oligomerization was further validated in a preliminary experiment through size exclusion chromatography of NDPK C pre-incubated with SW3, which resulted in a similar outcome compared to NDPK C alone (data not shown). This result suggested that SW3 had no significant influence on the NDPK C hexamer and cannot disrupt the interaction of the NDPK C monomers.

Furthermore, the biophysical analyses performed to study the influence of SW3 on the secondary structure, and thermal stability of NDPK C indicated that SW3 binding causes only minor structural changes in the protein. The CD studies showed a 3% decrease in alpha-helix and a 4% increase in the beta-sheet structures (see Fig. 11B); additionally, nanoDSF showed a slight destabilization of NDPK C upon SW3 treatment (see Fig. 11A), which implicated the potential role of SW3 interfering with protein stability. These findings were further corroborated by the HDX-MS and *in silico* protein modeling analyses. The data obtained from HDX-MS suggested that SW3 potentially binds to a pocket-like structure by occupying a cavity close to the beta-phosphate of ADP, which has been co-crystallized in NDPK C (see Fig. 12). The remaining hydrogen atoms in this pocket indicated that SW3 directly interacts with region 2 near the active site-forming residues and region 5 near the catalytic histidine, which likely form the allosteric binding site. Thus, the allosteric mode of inhibition by SW3 most likely results from slight conformational changes in the NDPK C monomer. Although HDX-MS and the *in silico* molecular modeling analysis indicate how the ligand-binding pocket might look, the exact atomic interactions between the ligand and the protein cannot be deduced. Co-crystallization efforts of NDPK C with SW3 are therefore currently ongoing. The structural determination of the protein-ligand complex will provide the precise details of the atomic and molecular interactions and potentially reveal the SW3 inhibitory mechanism more clearly. This knowledge could further facilitate the optimization of the molecular structure of SW3 to obtain even more potent inhibitors.

5.3 Structural significance of SanWie3 as NDPK C inhibitor

Kinases regulate numerous signaling pathways and their deregulation effects, for example, the transcriptional profile and hence cell physiology and responsiveness to environmental stimuli. A wide range of different kinases can be targeted by kinase-specific inhibitors, with the majority of the kinase inhibitors competing with ATP at the catalytic site (Garuti et al., 2010). Because of the structural similarities with physiological ligands such as ATP, many kinase inhibitors exhibit potential off-target interactions with diverse protein kinase family members (Davis et al., 2011). Together, these reports imply the need for kinase inhibitors that do not compete with ATP, such as allosteric inhibitors but target distinct sites on a protein or a receptor. Along these lines, the structure of SW3 is significantly different from ATP or its analogs (see Fig. 13C). Our results showed that SW3 could be an effective allosteric pharmacological modulator without targeting the enzyme's active site, resulting in an uninterrupted NDT/NDP binding to NDPK C. Nevertheless, the in vitro kinase screen based on a panel of 60 different kinases to assess SW3 selectivity resulted in 8 other serine/threonine kinases, including AMPKα2 which might be affected in its activity (see Fig. 14). Since AMPKα2 was the only candidate inhibited at two different SW3 concentrations, we further validated this target in a cellular model but could not confirm any impact of SW3 on enzyme activity. Based on this result, we compared the structural resemblance between a potent ATP-competitive inhibitor of AMPK, dorsomorphin, and SW3, which indicated no significant similarity. Our preliminary data suggested that SW3 could not influence the phosphorylation state of AMPK and its substrate ACC in cardiomyocytes (see Fig. 14).

However, further validation of AMPK activity, such as AMPK regulation in different cell lines or measuring the activity of AMPK in an enzyme assay, is necessary to exclude the potential effects of SW3. Furthermore, considering the screen with only 60 different kinases, our study is limited because several other potential kinase panels need to be tested to prove SW3 specificity in blocking NDPK C. Another *in vitro* pharmacology screen of SW3 has resulted in an inverse agonistic effect on cannabinoid receptor (CB2) and an agonistic effect on αA1 and muscarinic (M1) receptors (see Fig. 15A). Among the GPCRs, αA1 adrenoceptors were of particular interest to this project because of their relevant and perhaps protective function during cardiac remodeling and failure (O'Connell et al., 2006). Our data in NRCM could not verify either agonistic or antagonistic actions of SW3 on αA1 adrenoceptors, whereas the known agonist A61603, as well as the antagonist WB4104, were both effective (see Fig. 15B). Although there is no structural similarity of SW3 with the respective agonists/antagonists of the targets identified from the screen, this does not exclude the actions of SW3 on these targets. Therefore further studies will be necessary to confirm the specificity of SW3.

The significance of allosteric enzyme activity and its subsequent regulation of cellular signaling can be corroborated by the diversity of evolved targets of protein kinases. For instance,

pyruvate kinase, the enzyme catalyzing the last step of glycolysis, transfers the phosphate group from phosphoenolpyruvate to ADP to form ATP and pyruvate. Herein, ATP allosterically binds to pyruvate kinase to slow glycolysis when the energy charge is high via feedback inhibition. The excessive ATP binds to the enzyme at an allosteric site, which causes a conformational change and alters the enzymatic activity (Jurica et al., 1998). Similarly, alanine can also allosterically inhibit pyruvate kinase, whereas fructose-1,6-bisphosphate allosterically activates pyruvate kinase by binding at a different allosteric site other than ATP binding, which causes feed-forward stimulation (Veith et al., 2013). Consequently, the existence of topographically distinct allosteric sites offers new paradigms for small molecular compounds to modulate enzymatic activity. Furthermore, the molecules targeting the allosteric sites may be less well conserved between enzyme subtypes than the orthosteric sites, offering a substantial advantage in terms of selectivity, which could potentially improve physicochemical properties (Wenthur et al., 2014).

5.4 Preference of NDPK C/G_i interaction in healthy adult cardiomyocytes

In previous studies, our lab has reported that NDPK B forms a complex with Gβγ dimers thereby, i) activates G proteins in a receptor-independent manner, and ii) targets G_s proteins to the plasma membrane, thus facilitating receptor-mediated cAMP formation (Hippe et al., 2011). However, in vitro experiments with purified proteins also revealed that NDPK B alone is insufficient to initiate complex formation (Cuello et al., 2003). Recently, we identified the isoform NDPK C as a possible missing link between NDPK B and heterotrimeric G protein interaction (Abu-Taha et al., 2017). Herein, we validated and confirmed the direct interaction of NDPK C with G_tβγ by performing in vitro pull-down assays with purified proteins (see Fig. 6). Moreover, immunoprecipitation and overexpression studies suggested that the selective NDPK C/G protein binding is not regulated by differential affinity to the Gα-subunit but instead depends on the abundance of the respective G proteins (Abu-Taha et al., 2017). It was therefore assumed that under physiological conditions, NDPK C promotes $Gα_s$ activity, thereby increasing cAMP production and contractility, whereas, in heart failure, NDPK C/G_i complex formation and thus cAMP deprivation prevails due to the increased expression levels of G_i (Abu-Taha et al., 2017; Feldman et al., 1988).

Indeed, initial experiments performed in NRCM and zebrafish embryos supported the hypothesis that NDPK B/C promotes global cAMP formation in response to βAR stimulation, by replenishing GTP pools to facilitate G_s activity and stabilizing complex formation. However, these studies were performed in cell lysates and immature cells systems, disregarding the impact of compartmentalization of adult cardiomyocytes on signalosome formation. It is well documented that proteins involved in the regulation of cAMP-dependent signaling are not equally distributed throughout the cell but organized in distinct microdomains. Proteins such as ACs, AKAPs/PKA, cAMP degrading phosphodiesterases, phosphatases, and caveolae-

localized G proteins are arranged in specialized signalosomes to control amplitude, duration, and specify the downstream target activation (Perera & Nikolaev, 2013; Steinberg & Brunton, 2001; Zaccolo, 2009). Thus, although not yet assessed, it seems feasible that the distribution of NDPK C may not be homogenous within the plasma membrane but associated with distinct signaling complexes. This hypothesis is further substantiated by the fact that NDPK C inhibition did not globally reduce the cAMP formation and thus PKA activity as initially expected, but instead, as demonstrated by subcellular FRET measurements, specifically increased cAMP levels in the SERCA2a/PLN subdomain as well as PKA-dependent PLN-phosphorylation (see Fig. 18, 19).

Interestingly, even though the NDPK/G protein interaction may differ between adult and less mature cardiomyocytes, the general spatial distribution of NDPK C seemed to be shared since the specificity regarding PLN regulation was also observed in NRCM. However, limited knowledge is available on the Spatio-temporal dynamics of the signalosome complexes and intracellular Ca^{2+} concentrations between neonatal and adult cardiomyocytes. The adult cardiomyocytes comprise a well-developed t-tubule network that forms functional junctions with the SR, whereas in neonatal cells, the t-tubule system is compensated with caveolae localized close to the SR (Jones et al., 2018; Seki et al., 2003). Thus, the difference in the functional organization between the cell types, including the compartmentalized G protein distribution, might be responsible for the differential effect of NDPK C inhibition on PLN phosphorylation.

Compared to previous data, it becomes evident that in contrast to the acute pharmacological intervention, neither overexpression nor depletion of NDPK C could fully recapitulate the endogenous enzyme function. Overexpression might disturb the spatial distribution and specific protein interaction (Abu-Taha et al., 2017), whereas a knockdown may lead to a complete loss of the signalosome, including its scaffold function for other signaling proteins. Previous data indicated that NDPK C may potentially enhance both receptor-dependent as well as receptor-independent G Protein activity. In our experimental settings (see Fig. 20), as we used the β_1/β_2AR agonist ISO instead of a β_1 or β_2AR specific agonist, it cannot yet be clearly deduced if NDPK C acts downstream of the G_i -coupled β_2AR to locally reduce cAMP levels or promotes the activation of local G_i pools receptor-independently. Moreover, neither PTX nor SW3 significantly affected basal PLN-phosphorylation, which might be allocated to the generally low basal cAMP in isolated cardiomyocytes, its rapid degradation by phosphodiesterase, or the tight control of PLN-phosphorylation by local phosphatase activity. Irrespective of the mechanism, the effects of PTX and SW3 revealed that, unlike other compartments, the SERCA2a/PLN microdomain is under the apparent control of a likely constitutive NDPK C-G_i signaling, as both interventions increased PLN phosphorylation in a

non-additive manner. How is this spatial organization affected during HF and if NDPK C inhibition would favor PLN-phosphorylation remains evaluated.

5.5 Significance of Ca^{2+} and the PLN/SERCA2a compartment in heart physiology and failure

Heart failure is associated with β_1AR desensitization and aberrant Ca^{2+} cycling. Early therapeutic attempts to reverse the subsequent low PKA activity and reduced contractile function by promoting the overall cellular cAMP levels clinically failed because of an arrhythmia-based increase in mortality (Packer et al., 1991). Over the last two decades, it became evident that the key to functional improvement may lay in the compartment-specific modulation of cAMP/PKA-dependent targets (Colombe & Pidoux, 2021). In this context, the Serca2a/PLN domain has gained particular interest. Serca2a activity is impaired by its protein downregulation and reduced PKA-dependent PLN-phosphorylation (Kranias & Hajjar, 2012). The consequences include higher diastolic Ca^{2+} levels, which are associated with an increase in arrhythmia susceptibility, a decreased Ca^{2+} load of the SR, and thus causes a reduced Ca^{2+} release during systole. The most recent strategy to remedy dysfunctional Ca^{2+} cycling in HF patients is via AAV-mediated overexpression of Serca2a, and still under investigation in clinical trials (Brittsan & Kranias, 2000). So far, the absolute levels of detectable transgene DNA of SERCA2a were low, with no beneficial effect on cardiac function (Lyon et al., 2020). On the other hand, concerning PLN activity modulation, several attempts have been made to increase PLN phosphorylation, reduce the PLN-SERCA2a interaction, or inhibit phosphatase 1, which dephosphorylates PLN. Many of these approaches have limitations for the over-stimulation that leads to Ca^{2+} leakage and arrhythmia (Chu & Kranias, 2006).

So far, it seems that the SW3 application might fulfill the requirements of a compartment-specific cAMP modulator. As expected, an increase in PLN-phosphorylation promoted higher SR load, Ca^{2+} reuptake, and relaxation velocities. However, in the absence of adrenergic stimulation, this was accompanied by an increase in diastolic Ca^{2+} levels and a higher SR leak (see Fig. 22). In contrast, sarcomere shortening remained unaffected and slightly lower than control conditions (see Fig. 21C). In addition, the relaxation dynamics indicated a potential loss in myofilament Ca^{2+} sensitivity. The mechanisms underlying this outcome under these rather artificial basal conditions remain unresolved, as basal cAMP levels and PKA target phosphorylation are challenging to assess in isolated cardiomyocytes. It will therefore be essential to re-evaluate these parameters under increasing βAR stimulation. In contrast, ISO-dependent force development in isolated cardiac muscle strips was increased in the presence of SW3, and preliminary data from SW3 injected mice showed a tendency toward higher fractional shortening (see Fig. 26B). Nevertheless, a potential increase in arrhythmia susceptibility, therapeutic relevance during chronic stress conditions and heart failure, and

long-term effects of NDPK C inhibition such as PKA/EPAC-dependent transcriptional regulation needs to be carefully evaluated in future research projects.

5.6 Strategies on optimizing the structure of SanWie3

Specifically targeting intracellular enzyme activity or protein/protein interactions remains a challenge in modern pharmacotherapy. Consequently, structure-based optimization studies are conventionally implemented to improve the potency and selectivity of lead compounds, which could potentially change the chemical nature of the molecule (Goldstein et al., 2008). Biochemical and cell-based studies such as site-directed mutagenesis and structure-activity relationship studies, along with structure-based design and advanced artificial intelligence-based tools, facilitate the target validation (Batool et al., 2019; Ferguson & Gray, 2018). The functional groups on the chemical molecules that interact with the biological targets can be altered to have a potential therapeutic benefit. For example, acetylcholine can non-selectively interact with both muscarinic and nicotinic receptors and is rapidly metabolized by acetylcholinesterase. However, bethanechol, a drug used for treating urinary retention, is structurally similar to acetylcholine, except for an additional methyl group, which slows its degradation by acetylcholinesterase (Gaitonde et al., 2019).

Compounds such as SW3 are lead structures that are usually further subjected to an optimization process to improve efficacy. Our in vitro enzymatic studies revealed that the approximate IC_{50} obtained for SW3 targeting NDPK C is ~3 µM, which is outside the range of clinically relevant target inhibition and prone to unwanted side effects (Paolini et al., 2010). Additionally, our *in silico* model-based docking studies revealed that one of the benzyl groups of SW3 enters the core of NDPK C near the active sites (see Fig. 13D). Thus, in a preliminary approach to identify SW3 similar molecules, the structure of SW3 was in principle compared to the commercially available small molecules with a similar carbon backbone chain, retaining the sulfanylidene-thiazolidine group and the benzyl groups at the ends (see Fig. 13C). Several SW3 similar molecules with diverse functional groups were screened for their inhibitory activity on the NDPK C. Among them, only an isomer of SW3 with the carboxylic acid side chain localized at the para position instead of the meta position exhibited a similar inhibitory effect compared to SW3 (data not included). However, it will be essential to have the expertise of a computational, structural biologist, and medicinal chemist in formulating a molecule that retains isoform-specific inhibitory activity and enhances the potency.

Further, elucidation of the crystal structure of NDPK C with bound SW3 will likely reveal opportunities for structural modifications of the ligand by locating the specific atomic interactions, which helps improve the affinity. Such a potent inhibitor molecule obtained from these studies can then be subjected to pharmacokinetic studies to assess absorption, distribution, metabolism, elimination, and its molecular, biochemical, and physiological effects.

The preliminary experiments on pharmacokinetics in mice revealed that serum concentrations of SW3 at ~2-3 µM (see Fig. 24), which is in the range of its IC_{50} value obtained from the in vitro enzyme assays (see Fig. 9C), can be obtained by daily repeated injections. In conclusion, the results demonstrate that the identified small molecular inhibitor preferentially attenuates the enzymatic activity of NDPK C and thus modulates cAMP-dependent signaling in NRCM and AMVCM. SanWie3 may therefore be a lead compound to design small molecules interfering with the effects of the detrimental cAMP suppression in specific cardiomyocyte compartments in heart failure.

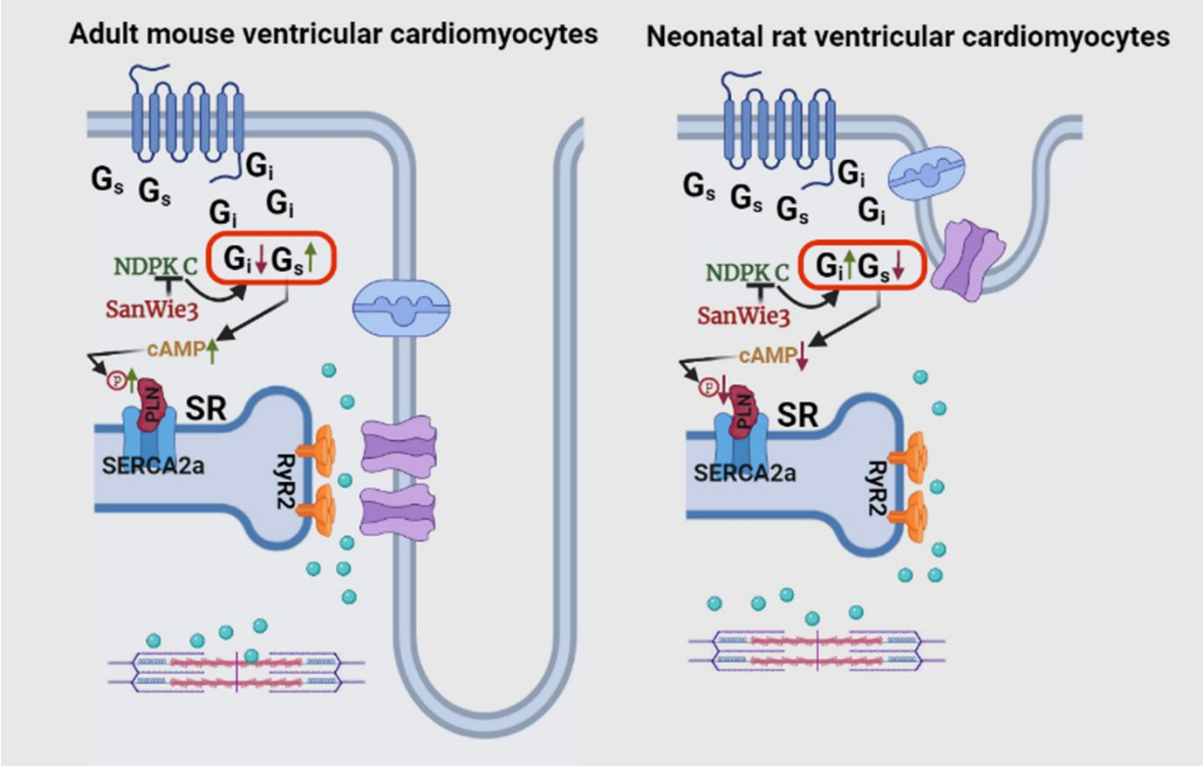

Figure 27: A scheme representing a potential, differential signaling between the immature and mature murine cardiomyocytes. In the left panel, the possibility of relatively higher G_i concentrations in an adult cardiomyocyte is shown. The presence of SW3 might inhibit NDPK C, thereby reducing the NDPK C mediated activation of G_i activity, leading to an increase in G_s induced activation of downstream signaling cascades at a specific signalosome, involving SERCA, resulting in increased contractility. On the contrary, the right panel represents an immature neonatal cardiomyocyte, with potential higher G_s concentrations, which could lead to the opposite effects compared to the adult cells, which might result in lower contractility.

6. References

Abu-Taha, I. H., Heijman, J., Feng, Y., Vettel, C., Dobrev, D., & Wieland, T. (2018). Regulation of heterotrimeric G-protein signaling by NDPK/NME proteins and caveolins: an update. *Lab Invest*, *98*(2), 190-197. https://doi.org/10.1038/labinvest.2017.103

Abu-Taha, I. H., Heijman, J., Hippe, H. J., Wolf, N. M., El-Armouche, A., Nikolaev, V. O., Schafer, M., Wurtz, C. M., Neef, S., Voigt, N., Baczko, I., Varro, A., Muller, M., Meder, B., Katus, H. A., Spiger, K., Vettel, C., Lehmann, L. H., Backs, J., Skolnik, E. Y., Lutz, S., Dobrev, D., & Wieland, T. (2017). Nucleoside Diphosphate Kinase-C Suppresses cAMP Formation in Human Heart Failure. *Circulation*, *135*(9), 881-897. https://doi.org/10.1161/CIRCULATIONAHA.116.022852

Aktories, K., Gierschik, P., Heringdorf, D. M. Z., Schmidt, M., Schultz, G., & Wieland, T. (2019). cAMP guided his way: a life for G protein-mediated signal transduction and molecular pharmacology-tribute to Karl H. Jakobs. *Naunyn Schmiedebergs Arch Pharmacol*, *392*(8), 887-911. https://doi.org/10.1007/s00210-019-01650-1

Anciaux, K., Van Dommelen, K., Willems, R., Roymans, D., & Slegers, H. (1997). Inhibition of nucleoside diphosphate kinase (NDPK/nm23) by cAMP analogues. *FEBS Lett*, *400*(1), 75-79. https://doi.org/10.1016/s0014-5793(96)01358-0

Attwood, P. V., & Muimo, R. (2018). The actions of NME1/NDPK-A and NME2/NDPK-B as protein kinases. *Lab Invest*, *98*(3), 283-290. https://doi.org/10.1038/labinvest.2017.125

Barclay, C. J. (2015). Energetics of contraction. *Compr Physiol*, *5*(2), 961-995. https://doi.org/10.1002/cphy.c140038

Batool, M., Ahmad, B., & Choi, S. (2019). A Structure-Based Drug Discovery Paradigm. *Int J Mol Sci*, *20*(11). https://doi.org/10.3390/ijms20112783

Beavo, J. A., & Brunton, L. L. (2002). Cyclic nucleotide research -- still expanding after half a century. *Nat Rev Mol Cell Biol*, *3*(9), 710-718. https://doi.org/10.1038/nrm911

Bers, D. M. (2014). Cardiac sarcoplasmic reticulum calcium leak: basis and roles in cardiac dysfunction. *Annu Rev Physiol*, *76*, 107-127. https://doi.org/10.1146/annurev-physiol-020911-153308

Besant, P. G., & Attwood, P. V. (2005). Mammalian histidine kinases. *Biochim Biophys Acta*, *1754*(1-2), 281-290. https://doi.org/10.1016/j.bbapap.2005.07.026

Besant, P. G., & Attwood, P. V. (2009). Detection and analysis of protein histidine phosphorylation. *Mol Cell Biochem*, *329*(1-2), 93-106. https://doi.org/10.1007/s11010-009-0117-2

Boissan, M., Dabernat, S., Peuchant, E., Schlattner, U., Lascu, I., & Lacombe, M. L. (2009). The mammalian Nm23/NDPK family: from metastasis control to cilia movement. *Mol Cell Biochem*, *329*(1-2), 51-62. https://doi.org/10.1007/s11010-009-0120-7

Boissan, M., Schlattner, U., & Lacombe, M. L. (2018). The NDPK/NME superfamily: state of the art. *Lab Invest*, *98*(2), 164-174. https://doi.org/10.1038/labinvest.2017.137

Borner, S., Schwede, F., Schlipp, A., Berisha, F., Calebiro, D., Lohse, M. J., & Nikolaev, V. O. (2011). FRET measurements of intracellular cAMP concentrations and cAMP analog permeability in intact cells. *Nat Protoc*, *6*(4), 427-438. https://doi.org/10.1038/nprot.2010.198

Bristow, M. R. (2011). Treatment of chronic heart failure with beta-adrenergic receptor antagonists: a convergence of receptor pharmacology and clinical cardiology. *Circ Res*, *109*(10), 1176-1194. https://doi.org/10.1161/CIRCRESAHA.111.245092

Bristow, M. R., Ginsburg, R., Umans, V., Fowler, M., Minobe, W., Rasmussen, R., Zera, P., Menlove, R., Shah, P., Jamieson, S., & et al. (1986). Beta 1- and beta 2-adrenergic-receptor subpopulations in nonfailing and failing human ventricular myocardium: coupling of both receptor subtypes to muscle contraction and selective beta 1-receptor down-regulation in heart failure. *Circ Res*, *59*(3), 297-309. https://doi.org/10.1161/01.res.59.3.297

Brittsan, A. G., & Kranias, E. G. (2000). Phospholamban and cardiac contractile function. *J Mol Cell Cardiol*, *32*(12), 2131-2139. https://doi.org/10.1006/jmcc.2000.1270

Buxton, I. L. (2008). Inhibition of Nm23H2 gene product (NDPK-B) by angiostatin, polyphenols and nucleoside analogs. *Proc West Pharmacol Soc*, *51*, 30-34. https://www.ncbi.nlm.nih.gov/pubmed/19544670

Cai, X., Srivastava, S., Surindran, S., Li, Z., & Skolnik, E. Y. (2014). Regulation of the epithelial Ca(2)(+) channel TRPV5 by reversible histidine phosphorylation mediated by NDPK-B and PHPT1. *Mol Biol Cell*, *25*(8), 1244-1250. https://doi.org/10.1091/mbc.E13-04-0180

Cheepala, S., Hulot, J. S., Morgan, J. A., Sassi, Y., Zhang, W., Naren, A. P., & Schuetz, J. D. (2013). Cyclic nucleotide compartmentalization: contributions of phosphodiesterases and ATP-binding cassette transporters. *Annu Rev Pharmacol Toxicol*, *53*, 231-253. https://doi.org/10.1146/annurev-pharmtox-010611-134609

Chen, C. W., Wang, H. L., Huang, C. W., Huang, C. Y., Lim, W. K., Tu, I. C., Koorapati, A., Hsieh, S. T., Kan, H. W., Tzeng, S. R., Liao, J. C., Chong, W. M., Naroditzky, I., Kidron, D., Eran, A., Nijim, Y., Sela, E., Feldman, H. B., Kalfon, L., Raveh-Barak, H., Falik-Zaccai, T. C., Elpeleg, O., Mandel, H., & Chang, Z. F. (2019). Two separate functions of NME3 critical for cell survival underlie a neurodegenerative disorder. *Proc Natl Acad Sci U S A*, *116*(2), 566-574. https://doi.org/10.1073/pnas.1818629116

Chiang, D. Y., Alsina, K. M., Corradini, E., Fitzpatrick, M., Ni, L., Lahiri, S. K., Reynolds, J. O., Pan, X., Scott, L., Jr., Heck, A. J. R., & Wehrens, X. H. T. (2018). Rearrangement of the Protein Phosphatase 1 Interactome During Heart Failure Progression. *Circulation*, *138*(15), 1569-1581. https://doi.org/10.1161/CIRCULATIONAHA.118.034361

Chu, G., & Kranias, E. G. (2006). Phospholamban as a therapeutic modality in heart failure. *Novartis Found Symp*, *274*, 156-171; discussion 172-155, 272-156. https://www.ncbi.nlm.nih.gov/pubmed/17019811

Colombe, A. S., & Pidoux, G. (2021). Cardiac cAMP-PKA Signaling Compartmentalization in Myocardial Infarction. *Cells*, *10*(4). https://doi.org/10.3390/cells10040922

Cuello, F., Schulze, R. A., Heemeyer, F., Meyer, H. E., Lutz, S., Jakobs, K. H., Niroomand, F., & Wieland, T. (2003). Activation of heterotrimeric G proteins by a high energy phosphate transfer via nucleoside diphosphate kinase (NDPK) B and Gbeta subunits. Complex formation of NDPK B with Gbeta gamma dimers and phosphorylation of His-266 IN Gbeta. *J Biol Chem*, *278*(9), 7220-7226. https://doi.org/10.1074/jbc.M210304200

Dautant, A., Henri, J., Wales, T. E., Meyer, P., Engen, J. R., & Georgescauld, F. (2019). Remodeling of the Binding Site of Nucleoside Diphosphate Kinase Revealed by X-ray Structure and H/D Exchange. *Biochemistry*, *58*(10), 1440-1449. https://doi.org/10.1021/acs.biochem.8b01308

Dautant, A., Meyer, P., & Georgescauld, F. (2017). Hydrogen/Deuterium Exchange Mass Spectrometry Reveals Mechanistic Details of Activation of Nucleoside Diphosphate Kinases by Oligomerization. *Biochemistry*, *56*(23), 2886-2896. https://doi.org/10.1021/acs.biochem.7b00282

Davis, M. I., Hunt, J. P., Herrgard, S., Ciceri, P., Wodicka, L. M., Pallares, G., Hocker, M., Treiber, D. K., & Zarrinkar, P. P. (2011). Comprehensive analysis of kinase inhibitor selectivity. *Nat Biotechnol*, *29*(11), 1046-1051. https://doi.org/10.1038/nbt.1990

de Lucia, C., Eguchi, A., & Koch, W. J. (2018). New Insights in Cardiac beta-Adrenergic Signaling During Heart Failure and Aging. *Front Pharmacol*, *9*, 904. https://doi.org/10.3389/fphar.2018.00904

Delaunay, M., Osman, H., Kaiser, S., & Diviani, D. (2019). The Role of Cyclic AMP Signaling in Cardiac Fibrosis. *Cells*, *9*(1). https://doi.org/10.3390/cells9010069

Desvignes, T., Pontarotti, P., Fauvel, C., & Bobe, J. (2009). Nme protein family evolutionary history, a vertebrate perspective. *BMC Evol Biol*, *9*, 256. https://doi.org/10.1186/1471-2148-9-256

Dexheimer, T. S., Carey, S. S., Zuohe, S., Gokhale, V. M., Hu, X., Murata, L. B., Maes, E. M., Weichsel, A., Sun, D., Meuillet, E. J., Montfort, W. R., & Hurley, L. H. (2009). NM23-H2 may play an indirect role in transcriptional activation of c-myc gene expression but does not cleave the nuclease hypersensitive element III(1). *Mol Cancer Ther*, *8*(5), 1363-1377. https://doi.org/10.1158/1535-7163.MCT-08-1093

Duc, N. M., Kim, H. R., & Chung, K. Y. (2017). Recent Progress in Understanding the Conformational Mechanism of Heterotrimeric G Protein Activation. *Biomol Ther (Seoul)*, *25*(1), 4-11. https://doi.org/10.4062/biomolther.2016.169

Eisner, D. A., Caldwell, J. L., Kistamas, K., & Trafford, A. W. (2017). Calcium and Excitation-Contraction Coupling in the Heart. *Circ Res*, *121*(2), 181-195. https://doi.org/10.1161/CIRCRESAHA.117.310230

El-Armouche, A., Zolk, O., Rau, T., & Eschenhagen, T. (2003). Inhibitory G-proteins and their role in desensitization of the adenylyl cyclase pathway in heart failure. *Cardiovasc Res*, *60*(3), 478-487. https://doi.org/10.1016/j.cardiores.2003.09.014

Engelhardt, S., Hein, L., Wiesmann, F., & Lohse, M. J. (1999). Progressive hypertrophy and heart failure in beta1-adrenergic receptor transgenic mice. *Proc Natl Acad Sci U S A*, *96*(12), 7059-7064. https://doi.org/10.1073/pnas.96.12.7059

Eschenhagen, T., Mende, U., Nose, M., Schmitz, W., Scholz, H., Haverich, A., Hirt, S., Doring, V., Kalmar, P., Hoppner, W., & et al. (1992). Increased messenger RNA level of the inhibitory G protein alpha subunit Gi alpha-2 in human end-stage heart failure. *Circ Res*, *70*(4), 688-696. https://doi.org/10.1161/01.res.70.4.688

Feldman, A. M., Cates, A. E., Veazey, W. B., Hershberger, R. E., Bristow, M. R., Baughman, K. L., Baumgartner, W. A., & Van Dop, C. (1988). Increase of the 40,000-mol wt pertussis toxin substrate (G protein) in the failing human heart. *J Clin Invest*, *82*(1), 189-197. https://doi.org/10.1172/JCI113569

Ferguson, F. M., & Gray, N. S. (2018). Kinase inhibitors: the road ahead. *Nat Rev Drug Discov*, *17*(5), 353-377. https://doi.org/10.1038/nrd.2018.21

Fischmeister, R., Castro, L. R., Abi-Gerges, A., Rochais, F., Jurevicius, J., Leroy, J., & Vandecasteele, G. (2006). Compartmentation of cyclic nucleotide signaling in the heart: the role of cyclic nucleotide phosphodiesterases. *Circ Res*, *99*(8), 816-828. https://doi.org/10.1161/01.RES.0000246118.98832.04

Fredriksson, R., Lagerstrom, M. C., Lundin, L. G., & Schioth, H. B. (2003). The G-protein-coupled receptors in the human genome form five main families. Phylogenetic analysis, paralogon groups, and fingerprints. *Mol Pharmacol*, *63*(6), 1256-1272. https://doi.org/10.1124/mol.63.6.1256

Freije, J. M., Blay, P., MacDonald, N. J., Manrow, R. E., & Steeg, P. S. (1997). Site-directed mutation of Nm23-H1. Mutations lacking motility suppressive capacity upon transfection are deficient in histidine-dependent protein phosphotransferase pathways in vitro. *J Biol Chem*, *272*(9), 5525-5532. https://doi.org/10.1074/jbc.272.9.5525

Gaitonde, S., Malik, R. D., Christie, A. L., & Zimmern, P. E. (2019). Bethanechol: Is it still being prescribed for bladder dysfunction in women? *Int J Clin Pract*, *73*(8), e13248. https://doi.org/10.1111/ijcp.13248

Garuti, L., Roberti, M., & Bottegoni, G. (2010). Non-ATP competitive protein kinase inhibitors. *Curr Med Chem*, *17*(25), 2804-2821. https://doi.org/10.2174/092986710791859333

Georgescauld, F., Song, Y., & Dautant, A. (2020). Structure, Folding and Stability of Nucleoside Diphosphate Kinases. *Int J Mol Sci*, *21*(18). https://doi.org/10.3390/ijms21186779

Ghigo, A., & Mika, D. (2019). cAMP/PKA signaling compartmentalization in cardiomyocytes: Lessons from FRET-based biosensors. *J Mol Cell Cardiol*, *131*, 112-121. https://doi.org/10.1016/j.yjmcc.2019.04.020

Gilles, A. M., Presecan, E., Vonica, A., & Lascu, I. (1991). Nucleoside diphosphate kinase from human erythrocytes. Structural characterization of the two polypeptide chains responsible for heterogeneity of the hexameric enzyme. *J Biol Chem*, *266*(14), 8784-8789. https://www.ncbi.nlm.nih.gov/pubmed/1851158

Goldstein, D. M., Gray, N. S., & Zarrinkar, P. P. (2008). High-throughput kinase profiling as a platform for drug discovery. *Nat Rev Drug Discov*, *7*(5), 391-397. https://doi.org/10.1038/nrd2541

Greenfield, N. J. (2006). Using circular dichroism spectra to estimate protein secondary structure. *Nat Protoc*, *1*(6), 2876-2890. https://doi.org/10.1038/nprot.2006.202

Guellich, A., Mehel, H., & Fischmeister, R. (2014). Cyclic AMP synthesis and hydrolysis in the normal and failing heart. *Pflugers Arch*, *466*(6), 1163-1175. https://doi.org/10.1007/s00424-014-1515-1

Hippe, H. J., Luedde, M., Lutz, S., Koehler, H., Eschenhagen, T., Frey, N., Katus, H. A., Wieland, T., & Niroomand, F. (2007). Regulation of cardiac cAMP synthesis and contractility by nucleoside diphosphate kinase B/G protein beta gamma dimer complexes. *Circ Res*, *100*(8), 1191-1199. https://doi.org/10.1161/01.RES.0000264058.28808.cc

Hippe, H. J., Lutz, S., Cuello, F., Knorr, K., Vogt, A., Jakobs, K. H., Wieland, T., & Niroomand, F. (2003). Activation of heterotrimeric G proteins by a high energy phosphate transfer via nucleoside diphosphate kinase (NDPK) B and Gbeta subunits. Specific activation of Gsalpha by an NDPK B.Gbetagamma complex in H10 cells. *J Biol Chem*, *278*(9), 7227-7233. https://doi.org/10.1074/jbc.M210305200

Hippe, H. J., Wolf, N. M., Abu-Taha, H. I., Lutz, S., Le Lay, S., Just, S., Rottbauer, W., Katus, H. A., & Wieland, T. (2011). Nucleoside diphosphate kinase B is required for the formation of heterotrimeric G protein containing caveolae. *Naunyn Schmiedebergs Arch Pharmacol*, *384*(4-5), 461-472. https://doi.org/10.1007/s00210-011-0618-x

Hippe, H. J., Wolf, N. M., Abu-Taha, I., Mehringer, R., Just, S., Lutz, S., Niroomand, F., Postel, E. H., Katus, H. A., Rottbauer, W., & Wieland, T. (2009). The interaction of nucleoside diphosphate kinase B with Gbetagamma dimers controls heterotrimeric G protein function. *Proc Natl Acad Sci U S A*, *106*(38), 16269-16274. https://doi.org/10.1073/pnas.0901679106

Honsho, M., Abe, Y., Imoto, Y., Chang, Z. F., Mandel, H., Falik-Zaccai, T. C., & Fujiki, Y. (2020). Mammalian Homologue NME3 of DYNAMO1 Regulates Peroxisome Division. *Int J Mol Sci*, *21*(21). https://doi.org/10.3390/ijms21218040

Houslay, M. D. (2010). Underpinning compartmentalised cAMP signalling through targeted cAMP breakdown. *Trends Biochem Sci*, *35*(2), 91-100. https://doi.org/10.1016/j.tibs.2009.09.007

Huser, J., Blatter, L. A., & Lipsius, S. L. (2000). Intracellular Ca2+ release contributes to automaticity in cat atrial pacemaker cells. *J Physiol*, *524 Pt 2*, 415-422. https://doi.org/10.1111/j.1469-7793.2000.00415.x

Iwatsubo, K., Minamisawa, S., Tsunematsu, T., Nakagome, M., Toya, Y., Tomlinson, J. E., Umemura, S., Scarborough, R. M., Levy, D. E., & Ishikawa, Y. (2004). Direct inhibition of type 5 adenylyl cyclase prevents myocardial apoptosis without functional deterioration. *J Biol Chem*, *279*(39), 40938-40945. https://doi.org/10.1074/jbc.M314238200

Janin, J., Dumas, C., Morera, S., Xu, Y., Meyer, P., Chiadmi, M., & Cherfils, J. (2000). Three-dimensional structure of nucleoside diphosphate kinase. *J Bioenerg Biomembr*, *32*(3), 215-225. https://doi.org/10.1023/a:1005528811303

Jones, P. P., MacQuaide, N., & Louch, W. E. (2018). Dyadic Plasticity in Cardiomyocytes. *Front Physiol*, *9*, 1773. https://doi.org/10.3389/fphys.2018.01773

Jurica, M. S., Mesecar, A., Heath, P. J., Shi, W., Nowak, T., & Stoddard, B. L. (1998). The allosteric regulation of pyruvate kinase by fructose-1,6-bisphosphate. *Structure*, *6*(2), 195-210. https://doi.org/10.1016/s0969-2126(98)00021-5

Kaetzel, D. M., Zhang, Q., Yang, M., McCorkle, J. R., Ma, D., & Craven, R. J. (2006). Potential roles of 3'-5' exonuclease activity of NM23-H1 in DNA repair and malignant progression. *J Bioenerg Biomembr*, *38*(3-4), 163-167. https://doi.org/10.1007/s10863-006-9040-3

Kamenetsky, M., Middelhaufe, S., Bank, E. M., Levin, L. R., Buck, J., & Steegborn, C. (2006). Molecular details of cAMP generation in mammalian cells: a tale of two systems. *J Mol Biol*, *362*(4), 623-639. https://doi.org/10.1016/j.jmb.2006.07.045

Kaschubowski, K. E., Kraft, A. E., Nikolaev, V. O., & Haag, F. (2020). Using FRET-Based Fluorescent Sensors to Monitor Cytosolic and Membrane-Proximal Extracellular ATP Levels. *Methods Mol Biol*, *2041*, 223-231. https://doi.org/10.1007/978-1-4939-9717-6_16

Kaumann, A. J., & Molenaar, P. (1997). Modulation of human cardiac function through 4 beta-adrenoceptor populations. *Naunyn Schmiedebergs Arch Pharmacol*, *355*(6), 667-681. https://doi.org/10.1007/pl00004999

Kee, J. M., Villani, B., Carpenter, L. R., & Muir, T. W. (2010). Development of stable phosphohistidine analogues. *J Am Chem Soc*, *132*(41), 14327-14329. https://doi.org/10.1021/ja104393t

Kilstrup, M., Hammer, K., Ruhdal Jensen, P., & Martinussen, J. (2005). Nucleotide metabolism and its control in lactic acid bacteria. *FEMS Microbiol Rev*, *29*(3), 555-590. https://doi.org/10.1016/j.femsre.2005.04.006

Kleczkowski, L. A., & Igamberdiev, A. U. (2021). Magnesium Signaling in Plants. *Int J Mol Sci*, *22*(3). https://doi.org/10.3390/ijms22031159

Kobe, B., & Kemp, B. E. (1999). Active site-directed protein regulation. *Nature*, *402*(6760), 373-376. https://doi.org/10.1038/46478

Kowshik, J., Giri, H., Kishore, T. K., Kesavan, R., Vankudavath, R. N., Reddy, G. B., Dixit, M., & Nagini, S. (2014). Ellagic acid inhibits VEGF/VEGFR2, PI3K/Akt and MAPK signaling cascades in the hamster cheek pouch carcinogenesis model. *Anticancer Agents Med Chem*, *14*(9), 1249-1260. https://doi.org/10.2174/1871520614666140723114217

Kranias, E. G., & Hajjar, R. J. (2012). Modulation of cardiac contractility by the phospholamban/SERCA2a regulatome. *Circ Res*, *110*(12), 1646-1660. https://doi.org/10.1161/CIRCRESAHA.111.259754

Lacombe, M. L., Milon, L., Munier, A., Mehus, J. G., & Lambeth, D. O. (2000). The human Nm23/nucleoside diphosphate kinases. *J Bioenerg Biomembr*, *32*(3), 247-258. https://doi.org/10.1023/a:1005584929050

Lane, A. N., & Fan, T. W. (2015). Regulation of mammalian nucleotide metabolism and biosynthesis. *Nucleic Acids Res*, *43*(4), 2466-2485. https://doi.org/10.1093/nar/gkv047

Lascu, I., & Gonin, P. (2000). The catalytic mechanism of nucleoside diphosphate kinases. *J Bioenerg Biomembr*, *32*(3), 237-246. https://doi.org/10.1023/a:1005532912212

Laskowski, R. A., Gerick, F., & Thornton, J. M. (2009). The structural basis of allosteric regulation in proteins. *FEBS Lett*, *583*(11), 1692-1698. https://doi.org/10.1016/j.febslet.2009.03.019

Lefkowitz, R. J., Rockman, H. A., & Koch, W. J. (2000). Catecholamines, cardiac beta-adrenergic receptors, and heart failure. *Circulation*, *101*(14), 1634-1637. https://doi.org/10.1161/01.cir.101.14.1634

Leroy, J., Vandecasteele, G., & Fischmeister, R. (2018). Cyclic AMP signaling in cardiac myocytes. *Current Opinion in Physiology*, *1*, 161-171. https://doi.org/10.1016/j.cophys.2017.11.004

Liu, Y., Chen, J., Fontes, S. K., Bautista, E. N., & Cheng, Z. (2021). Physiological And Pathological Roles Of Protein Kinase A In The Heart. *Cardiovasc Res*. https://doi.org/10.1093/cvr/cvab008

Lohse, M. J., Engelhardt, S., & Eschenhagen, T. (2003). What is the role of beta-adrenergic signaling in heart failure? *Circ Res*, *93*(10), 896-906. https://doi.org/10.1161/01.RES.0000102042.83024.CA

Lompre, A. M., Hajjar, R. J., Harding, S. E., Kranias, E. G., Lohse, M. J., & Marks, A. R. (2010). Ca2+ cycling and new therapeutic approaches for heart failure. *Circulation*, *121*(6), 822-830. https://doi.org/10.1161/CIRCULATIONAHA.109.890954

Lutz, S., Mura, R., Baltus, D., Movsesian, M., Kubler, W., & Niroomand, F. (2001). Increased activity of membrane-associated nucleoside diphosphate kinase and inhibition of cAMP synthesis in failing human myocardium. *Cardiovasc Res*, *49*(1), 48-55. https://doi.org/10.1016/s0008-6363(00)00222-4

Lutz, S., Mura, R. A., Hippe, H. J., Tiefenbacher, C., & Niroomand, F. (2003). Plasma membrane-associated nucleoside diphosphate kinase (nm23) in the heart is regulated by beta-adrenergic signaling. *Br J Pharmacol*, *140*(6), 1019-1026. https://doi.org/10.1038/sj.bjp.0705527

Lymperopoulos, A., Rengo, G., & Koch, W. J. (2013). Adrenergic nervous system in heart failure: pathophysiology and therapy. *Circ Res*, *113*(6), 739-753. https://doi.org/10.1161/CIRCRESAHA.113.300308

Lyon, A. R., Babalis, D., Morley-Smith, A. C., Hedger, M., Suarez Barrientos, A., Foldes, G., Couch, L. S., Chowdhury, R. A., Tzortzis, K. N., Peters, N. S., Rog-Zielinska, E. A., Yang, H. Y., Welch, S., Bowles, C. T., Rahman Haley, S., Bell, A. R., Rice, A., Sasikaran, T., Johnson, N. A., Falaschetti, E., Parameshwar, J., Lewis, C., Tsui, S., Simon, A., Pepper, J., Rudy, J. J., Zsebo, K. M., Macleod, K. T., Terracciano, C. M., Hajjar, R. J., Banner, N., & Harding, S. E. (2020). Investigation of the safety and feasibility of AAV1/SERCA2a gene transfer in patients with chronic heart failure

supported with a left ventricular assist device - the SERCA-LVAD TRIAL. *Gene Ther*, *27*(12), 579-590. https://doi.org/10.1038/s41434-020-0171-7

Ma, J., & Karplus, M. (1997). Molecular switch in signal transduction: reaction paths of the conformational changes in ras p21. *Proc Natl Acad Sci U S A*, *94*(22), 11905-11910. https://doi.org/10.1073/pnas.94.22.11905

MacLennan, D. H., & Kranias, E. G. (2003). Phospholamban: a crucial regulator of cardiac contractility. *Nat Rev Mol Cell Biol*, *4*(7), 566-577. https://doi.org/10.1038/nrm1151

Madamanchi, A. (2007). Beta-adrenergic receptor signaling in cardiac function and heart failure. *Mcgill J Med*, *10*(2), 99-104. https://www.ncbi.nlm.nih.gov/pubmed/18523538

Magnusson, A. O., Szekrenyi, A., Joosten, H. J., Finnigan, J., Charnock, S., & Fessner, W. D. (2019). nanoDSF as screening tool for enzyme libraries and biotechnology development. *FEBS J*, *286*(1), 184-204. https://doi.org/10.1111/febs.14696

Mangmool, S., & Kurose, H. (2011). G(i/o) protein-dependent and -independent actions of Pertussis Toxin (PTX). *Toxins (Basel)*, *3*(7), 884-899. https://doi.org/10.3390/toxins3070884

McCabe, K. J., & Rangamani, P. (2021). Computational modeling approaches to cAMP/PKA signaling in cardiomyocytes. *J Mol Cell Cardiol*, *154*, 32-40. https://doi.org/10.1016/j.yjmcc.2021.01.008

McFarlane, S. I., Winer, N., & Sowers, J. R. (2003). Role of the natriuretic peptide system in cardiorenal protection. *Arch Intern Med*, *163*(22), 2696-2704. https://doi.org/10.1001/archinte.163.22.2696

Milon, L., Meyer, P., Chiadmi, M., Munier, A., Johansson, M., Karlsson, A., Lascu, I., Capeau, J., Janin, J., & Lacombe, M. L. (2000). The human nm23-H4 gene product is a mitochondrial nucleoside diphosphate kinase. *J Biol Chem*, *275*(19), 14264-14272. https://doi.org/10.1074/jbc.275.19.14264

Mishra, N. S., Tuteja, R., & Tuteja, N. (2006). Signaling through MAP kinase networks in plants. *Arch Biochem Biophys*, *452*(1), 55-68. https://doi.org/10.1016/j.abb.2006.05.001

Mourad, N., & Parks, R. E., Jr. (1966a). Erythrocytic nucleoside diphosphokinase. 3. Studies with free and phosphorylated enzyme and evidence for an essential thiol group. *J Biol Chem*, *241*(16), 3838-3844. https://www.ncbi.nlm.nih.gov/pubmed/5916396

Mourad, N., & Parks, R. E., Jr. (1966b). Erythrocytic nucleoside diphosphokinase. II. Isolation and kinetics. *J Biol Chem*, *241*(2), 271-278. https://www.ncbi.nlm.nih.gov/pubmed/5903722

Myagmar, B. E., Flynn, J. M., Cowley, P. M., Swigart, P. M., Montgomery, M. D., Thai, K., Nair, D., Gupta, R., Deng, D. X., Hosoda, C., Melov, S., Baker, A. J., & Simpson, P. C. (2017). Adrenergic Receptors in Individual Ventricular Myocytes: The Beta-1 and Alpha-1B Are in All Cells, the Alpha-1A Is in a Subpopulation, and the Beta-2 and Beta-3 Are Mostly Absent. *Circ Res*, *120*(7), 1103-1115. https://doi.org/10.1161/CIRCRESAHA.117.310520

O'Connell, T. D., Swigart, P. M., Rodrigo, M. C., Ishizaka, S., Joho, S., Turnbull, L., Tecott, L. H., Baker, A. J., Foster, E., Grossman, W., & Simpson, P. C. (2006). Alpha1-adrenergic receptors prevent a maladaptive cardiac response to pressure overload. *J Clin Invest*, *116*(4), 1005-1015. https://doi.org/10.1172/JCI22811

Okumura, S., Takagi, G., Kawabe, J., Yang, G., Lee, M. C., Hong, C., Liu, J., Vatner, D. E., Sadoshima, J., Vatner, S. F., & Ishikawa, Y. (2003). Disruption of type 5 adenylyl cyclase gene preserves cardiac function against pressure overload. *Proc Natl Acad Sci U S A*, *100*(17), 9986-9990. https://doi.org/10.1073/pnas.1733772100

Packer, M., Carver, J. R., Rodeheffer, R. J., Ivanhoe, R. J., DiBianco, R., Zeldis, S. M., Hendrix, G. H., Bommer, W. J., Elkayam, U., Kukin, M. L., & et al. (1991). Effect of oral milrinone on mortality in severe chronic heart failure. The PROMISE Study Research Group. *N Engl J Med*, *325*(21), 1468-1475. https://doi.org/10.1056/NEJM199111213252103

Palacios, F., Schweitzer, J. K., Boshans, R. L., & D'Souza-Schorey, C. (2002). ARF6-GTP recruits Nm23-H1 to facilitate dynamin-mediated endocytosis during adherens junctions disassembly. *Nat Cell Biol*, *4*(12), 929-936. https://doi.org/10.1038/ncb881

Paolini, G. V., Lyons, R. A., & Laflin, P. (2010). How desirable are your IC50s? A way to enhance screening-based decision making. *J Biomol Screen*, *15*(10), 1183-1193. https://doi.org/10.1177/1087057110384402

Perera, R. K., & Nikolaev, V. O. (2013). Compartmentation of cAMP signalling in cardiomyocytes in health and disease. *Acta Physiol (Oxf)*, *207*(4), 650-662. https://doi.org/10.1111/apha.12077

Perera, R. K., Sprenger, J. U., Steinbrecher, J. H., Hubscher, D., Lehnart, S. E., Abesser, M., Schuh, K., El-Armouche, A., & Nikolaev, V. O. (2015). Microdomain switch of cGMP-regulated phosphodiesterases leads to ANP-induced augmentation of beta-adrenoceptor-stimulated contractility in early cardiac hypertrophy. *Circ Res*, *116*(8), 1304-1311. https://doi.org/10.1161/CIRCRESAHA.116.306082

Pollack, J. D., Myers, M. A., Dandekar, T., & Herrmann, R. (2002). Suspected utility of enzymes with multiple activities in the small genome Mycoplasma species: the replacement of the missing "household" nucleoside diphosphate kinase gene and activity by glycolytic kinases. *OMICS*, *6*(3), 247-258. https://doi.org/10.1089/15362310260256909

Postel, E. H., & Abramczyk, B. M. (2003). Escherichia coli nucleoside diphosphate kinase is a uracil-processing DNA repair nuclease. *Proc Natl Acad Sci U S A*, *100*(23), 13247-13252. https://doi.org/10.1073/pnas.2333230100

Preedy, M. E. J. (2020). Cardiac Cyclic Nucleotide Phosphodiesterases: Roles and Therapeutic Potential in Heart Failure. *Cardiovasc Drugs Ther*, *34*(3), 401-417. https://doi.org/10.1007/s10557-020-06959-1

Schaertl, S., Konrad, M., & Geeves, M. A. (1998). Substrate specificity of human nucleoside-diphosphate kinase revealed by transient kinetic analysis. *J Biol Chem*, *273*(10), 5662-5669. https://doi.org/10.1074/jbc.273.10.5662

Schaller, D., Šribar, D., Noonan, T., Deng, L., Nguyen, T. N., Pach, S., Machalz, D., Bermudez, M., & Wolber, G. (2020). Next generation 3D pharmacophore modeling. *WIREs Computational Molecular Science*, *10*(4). https://doi.org/10.1002/wcms.1468

Schaller, G. E., Shiu, S. H., & Armitage, J. P. (2011). Two-component systems and their co-option for eukaryotic signal transduction. *Curr Biol*, *21*(9), R320-330. https://doi.org/10.1016/j.cub.2011.02.045

Schnell, S. (2014). Validity of the Michaelis-Menten equation--steady-state or reactant stationary assumption: that is the question. *FEBS J*, *281*(2), 464-472. https://doi.org/10.1111/febs.12564

Schwede, F., Christensen, A., Liauw, S., Hippe, T., Kopperud, R., Jastorff, B., & Doskeland, S. O. (2000). 8-Substituted cAMP analogues reveal marked differences in adaptability, hydrogen bonding, and charge accommodation between homologous binding sites (AI/AII and BI/BII) in cAMP kinase I and II. *Biochemistry*, *39*(30), 8803-8812. https://doi.org/10.1021/bi000304y

Schwede, F., Maronde, E., Genieser, H., & Jastorff, B. (2000). Cyclic nucleotide analogs as biochemical tools and prospective drugs. *Pharmacol Ther*, *87*(2-3), 199-226. https://doi.org/10.1016/s0163-7258(00)00051-6

Sejersted, O. M. (2011). Calcium controls cardiac function--by all means! *J Physiol*, *589*(Pt 12), 2919-2920. https://doi.org/10.1113/jphysiol.2011.210989

Seki, S., Nagashima, M., Yamada, Y., Tsutsuura, M., Kobayashi, T., Namiki, A., & Tohse, N. (2003). Fetal and postnatal development of Ca2+ transients and Ca2+ sparks in rat cardiomyocytes. *Cardiovasc Res*, *58*(3), 535-548. https://doi.org/10.1016/s0008-6363(03)00255-4

Shannon, T. R., Ginsburg, K. S., & Bers, D. M. (2002). Quantitative assessment of the SR Ca2+ leak-load relationship. *Circ Res*, *91*(7), 594-600. https://doi.org/10.1161/01.res.0000036914.12686.28

Simon, M. I., Strathmann, M. P., & Gautam, N. (1991). Diversity of G proteins in signal transduction. *Science*, *252*(5007), 802-808. https://doi.org/10.1126/science.1902986

Sipido, K. R., & Vangheluwe, P. (2010). Targeting sarcoplasmic reticulum Ca2+ uptake to improve heart failure: hit or miss. *Circ Res*, *106*(2), 230-233. https://doi.org/10.1161/CIRCRESAHA.109.210740

Skomedal, T., Borthne, K., Aass, H., Geiran, O., & Osnes, J. B. (1997). Comparison between alpha-1 adrenoceptor-mediated and beta adrenoceptor-mediated inotropic components elicited by norepinephrine in failing human ventricular muscle. *J Pharmacol Exp Ther*, *280*(2), 721-729. https://www.ncbi.nlm.nih.gov/pubmed/9023284

Snider, N. T., Altshuler, P. J., & Omary, M. B. (2015). Modulation of cytoskeletal dynamics by mammalian nucleoside diphosphate kinase (NDPK) proteins. *Naunyn Schmiedebergs Arch Pharmacol*, *388*(2), 189-197. https://doi.org/10.1007/s00210-014-1046-5

Sokalingam, S., Raghunathan, G., Soundrarajan, N., & Lee, S. G. (2012). A study on the effect of surface lysine to arginine mutagenesis on protein stability and structure using green fluorescent protein. *PLoS One*, *7*(7), e40410. https://doi.org/10.1371/journal.pone.0040410

Sprenger, J. U., Perera, R. K., Steinbrecher, J. H., Lehnart, S. E., Maier, L. S., Hasenfuss, G., & Nikolaev, V. O. (2015). In vivo model with targeted cAMP biosensor reveals changes in receptor-microdomain communication in cardiac disease. *Nat Commun*, *6*, 6965. https://doi.org/10.1038/ncomms7965

Srivastava, S., Li, Z., Ko, K., Choudhury, P., Albaqumi, M., Johnson, A. K., Yan, Y., Backer, J. M., Unutmaz, D., Coetzee, W. A., & Skolnik, E. Y. (2006). Histidine phosphorylation of the potassium channel KCa3.1 by nucleoside diphosphate kinase B is required for activation of KCa3.1 and CD4 T cells. *Mol Cell*, *24*(5), 665-675. https://doi.org/10.1016/j.molcel.2006.11.012

Steinberg, S. F., & Brunton, L. L. (2001). Compartmentation of G protein-coupled signaling pathways in cardiac myocytes. *Annu Rev Pharmacol Toxicol*, *41*, 751-773. https://doi.org/10.1146/annurev.pharmtox.41.1.751

Stock, A. M., Robinson, V. L., & Goudreau, P. N. (2000). Two-component signal transduction. *Annu Rev Biochem*, *69*, 183-215. https://doi.org/10.1146/annurev.biochem.69.1.183

Surdo, N. C., Berrera, M., Koschinski, A., Brescia, M., Machado, M. R., Carr, C., Wright, P., Gorelik, J., Morotti, S., Grandi, E., Bers, D. M., Pantano, S., & Zaccolo, M. (2017). FRET biosensor uncovers cAMP nano-domains at beta-adrenergic targets that dictate precise tuning of cardiac contractility. *Nat Commun*, *8*, 15031. https://doi.org/10.1038/ncomms15031

Vega, S. C., Leiss, V., Piekorz, R., Calaminus, C., Pexa, K., Vuozzo, M., Schmid, A. M., Devanathan, V., Kesenheimer, C., Pichler, B. J., Beer-Hammer, S., & Nurnberg, B. (2020). Selective protection of murine cerebral Gi/o-proteins from inactivation by parenterally injected pertussis toxin. *J Mol Med (Berl)*, *98*(1), 97-110. https://doi.org/10.1007/s00109-019-01854-1

Veith, N., Feldman-Salit, A., Cojocaru, V., Henrich, S., Kummer, U., & Wade, R. C. (2013). Organism-adapted specificity of the allosteric regulation of pyruvate kinase in lactic acid bacteria. *PLoS Comput Biol*, *9*(7), e1003159. https://doi.org/10.1371/journal.pcbi.1003159

Verdonk, M. L., Cole, J. C., Hartshorn, M. J., Murray, C. W., & Taylor, R. D. (2003). Improved protein-ligand docking using GOLD. *Proteins*, *52*(4), 609-623. https://doi.org/10.1002/prot.10465

Vettel, C., Wittig, K., Vogt, A., Wuertz, C. M., El-Armouche, A., Lutz, S., & Wieland, T. (2012). A novel player in cellular hypertrophy: Gibetagamma/PI3K-dependent activation of the RacGEF TIAM-1 is required for alpha(1)-adrenoceptor induced hypertrophy in neonatal rat cardiomyocytes. *J Mol Cell Cardiol*, *53*(2), 165-175. https://doi.org/10.1016/j.yjmcc.2012.04.015

Wagner, P. D., & Vu, N. D. (2000). Histidine to aspartate phosphotransferase activity of nm23 proteins: phosphorylation of aldolase C on Asp-319. *Biochem J*, *346 Pt 3*, 623-630. https://www.ncbi.nlm.nih.gov/pubmed/10698688

Wang, J., Gareri, C., & Rockman, H. A. (2018). G-Protein-Coupled Receptors in Heart Disease. *Circ Res*, *123*(6), 716-735. https://doi.org/10.1161/CIRCRESAHA.118.311403

Weis, W. I., & Kobilka, B. K. (2018). The Molecular Basis of G Protein-Coupled Receptor Activation. *Annu Rev Biochem*, *87*, 897-919. https://doi.org/10.1146/annurev-biochem-060614-033910

Wenthur, C. J., Gentry, P. R., Mathews, T. P., & Lindsley, C. W. (2014). Drugs for allosteric sites on receptors. *Annu Rev Pharmacol Toxicol*, *54*, 165-184. https://doi.org/10.1146/annurev-pharmtox-010611-134525

Wieland, T. (2007). Interaction of nucleoside diphosphate kinase B with heterotrimeric G protein betagamma dimers: consequences on G protein activation and stability. *Naunyn Schmiedebergs Arch Pharmacol*, *374*(5-6), 373-383. https://doi.org/10.1007/s00210-006-0126-6

Wieland, T., Gierschik, P., & Jakobs, K. H. (1992). G protein-mediated receptor-receptor interaction: studies with chemotactic receptors in membranes of human leukemia (HL 60) cells. *Naunyn Schmiedebergs Arch Pharmacol*, *346*(5), 475-481. https://doi.org/10.1007/BF00168999

Wieland, T., Hippe, H. J., Ludwig, K., Zhou, X. B., Korth, M., & Klumpp, S. (2010). Reversible histidine phosphorylation in mammalian cells: a teeter-totter formed by nucleoside diphosphate kinase and protein histidine phosphatase 1. *Methods Enzymol*, *471*, 379-402. https://doi.org/10.1016/S0076-6879(10)71020-X

Wolber, G., Dornhofer, A. A., & Langer, T. (2006). Efficient overlay of small organic molecules using 3D pharmacophores. *J Comput Aided Mol Des*, *20*(12), 773-788. https://doi.org/10.1007/s10822-006-9078-7

Zaccolo, M. (2009). cAMP signal transduction in the heart: understanding spatial control for the development of novel therapeutic strategies. *Br J Pharmacol*, *158*(1), 50-60. https://doi.org/10.1111/j.1476-5381.2009.00185.x

Zaccolo, M., & Pozzan, T. (2002). Discrete microdomains with high concentration of cAMP in stimulated rat neonatal cardiac myocytes. *Science*, *295*(5560), 1711-1715. https://doi.org/10.1126/science.1069982

Zhou, X. B., Feng, Y. X., Sun, Q., Lukowski, R., Qiu, Y., Spiger, K., Li, Z., Ruth, P., Korth, M., Skolnik, E. Y., Borggrefe, M., Dobrev, D., & Wieland, T. (2015). Nucleoside diphosphate kinase B-activated intermediate conductance potassium channels are critical for neointima formation in mouse carotid arteries. *Arterioscler Thromb Vasc Biol*, *35*(8), 1852-1861. https://doi.org/10.1161/ATVBAHA.115.305881

Zhou, Y., & Artman, M. (2001). Nucleoside diphosphate kinase: a new player in heart failure? *Cardiovasc Res*, *49*(1), 7-10. https://doi.org/10.1016/s0008-6363(00)00273-x

Zimmermann, H., Zebisch, M., & Strater, N. (2012). Cellular function and molecular structure of ecto-nucleotidases. *Purinergic Signal*, *8*(3), 437-502. https://doi.org/10.1007/s11302-012-9309-4